UNIVERSITÄTSKLINIKUM HAMBURG-EPPENDORF

Zentrum für Molekulare Neurobiologie Hamburg

Prof Dr. rer. nat. Matthias Kneussel

Stable dynamics of synaptic and cellular networks in the hippocampus

Dissertation

zur Erlangung des Doktorgrades PhD
an der Medizinischen Fakultät der Universität Hamburg.

vorgelegt von:

Rais Cynthia
aus Bordeaux, France

Hamburg 2024

(wird von der Medizinischen Fakultät ausgefüllt)

Angenommen von der

Medizinischen Fakultät der Universität Hamburg am: 05.07.2024

Veröffentlicht mit Genehmigung der

Medizinischen Fakultät der Universität Hamburg.

Prüfungsausschuss, der/die Vorsitzende: Prof. Dr. Simon Wiegert

Prüfungsausschuss, zweite/r Gutachter/in: Dr. Sebastian Bitzenhofer

Table of contents

Abstract

During learning, experience-dependent activity triggers synaptic plasticity, modifying synaptic strength (Hayashi-Takagi et al., 2015; Whitlock et al., 2006; Xu et al., 2009). Most excitatory inputs form synapses on dendritic spines (Harris and Kater, 1994), and changes in synaptic strength result in structural modifications of spines (El-Boustani et al., 2018; Nägerl et al., 2004; Noguchi et al., 2011; Trachtenberg et al., 2002). Thus, memory traces formed during learning have been hypothesized to be stored at synapses (Greenough and Bailey, 1988; Squire, 1987) and therefore spines. Formation and consolidation of declarative, episodic memories require the hippocampus, and the Schaffer collateral synapse between areas CA3 and CA1 is considered one of the prototypical small glutamatergic synapses in the central nervous system. The formation of new memories implies a dynamic restructuration of the network (Holtmaat and Svoboda, 2009; Trachtenberg et al., 2002), which could conflict with the necessity for memory stability required to perform a task, at least on a short timescale. In CA1, the lifetime of dendritic spines has been followed for days, to determine the capacity for synapses to store memory traces. However, no consensus has been found between studies. So far only spine morphology has been investigated over multiple days in the hippocampus to assess spine lifetime and chronic analyses of synaptic function have been missing. Therefore, we are limited in our understanding of how structural changes relate to synaptic function *in vivo*.

On a first project, I combined chronic two-photon calcium imaging of ipsilateral CA1 spines with repeated optogenetic activation of presynaptic contralateral CA3 pyramidal neurons in the awake mouse. Using this approach, I induced local, synaptically evoked calcium responses at individual spines and assessed the stability of these functionally identified synapses over more than two weeks. These responding spines tend to form functional clusters of strongly connected spines and are more stable than non-responding spines on the same dendrites, suggesting that strong synaptic connectivity is associated with spine persistence. Taken together, this work suggests that spine lifetime in the hippocampus is related to synaptic weight, which may determine long-term synaptic connectivity.

Dynamic restructuration of the network has also been observed through the gradual remapping of spatial representation in the hippocampus. While the stability of the behavior of an animal navigating an environment has been shown, the representation of the environment is drifting over days. The cellular mechanism subtending this formation and elimination of place cells remains unclear. As the CA3 subdivision of the hippocampus exhibits a spatial representational drift, how this phenomenon accelerates the spatial code remapping in CA1 remains unclear. In this second project, I combined chronic two-photon calcium imaging of ipsilateral CA1 spines with optogenetic activation of presynaptic contralateral CA3 pyramidal neurons

in the mouse performing a spatial navigation task. Using this approach, I was able to induce a subset of place cells in CA1, whose place fields tend to form close to the reward zone rather than to the stimulation zone. Additionally, I show that this perturbation induced a change in the overall population code of already existing place cells, although only temporarily. This work suggests that, while the network is in a stable state, a modification of the inputs from presynaptic partners led to a remapping of the environment in CA1, suggesting that the network in CA1 is gradually pushed to a new state by presynaptic partners.

ZUSSAMENFASSUNG

Neuronale Aktivität während der Lernens löst erfahrungsabhängige synaptische Plastizität aus und verändert die synaptische Stärke (Hayashi-Takagi et al., 2015; Whitlock et al., 2006; Xu et al., 2009). Erregende Eingänge befinden sich meisten an exzitatorischen Synapsen an dendritischen Dornenfortsätzen (Harris und Kater, 1994), und Veränderungen der synaptischen Stärke führen zu strukturellen Veränderungen der Dornenfortsätze (El-Boustani et al., 2018; Nägerl et al., 2004; Noguchi et al., 2011; Trachtenberg et al., 2002). Daher wurde angenommen, dass Erinnerungsspuren, die während des Lernens gebildet werden, an Synapsen (Greenough und Bailey, 1988; Squire, 1987) und somit an Dornenfortsätzen gespeichert werden. Die Bildung und Konsolidierung von deklarativen, episodischen Erinnerungen erforderten den Hippocampus. Die sich dort befindliche Schaffer-Kollateralsynapse zwischen Neuronen in den Bereichen CA3 und CA1 gilt als eine der prototypischen glutamatergen Synapsen des zentralen Nervensystems. Die Bildung neuer Erinnerungen impliziert eine dynamische Umstrukturierung des Netzwerks (Holtmaat und Svoboda, 2009; Trachtenberg et al., 2002), was im Widerspruch zur Langzeitstabilität von Gedächtnisinhalten steht, zumindest auf einer kurzen Zeitskala. Verschiedene Studien haben die Lebensdauer dendritischer Dornenfortsätze an CA1 Neuronen über Tage hinweg verfolgt, um die Fähigkeit der Synapsen zur Speicherung von Gedächtnisspuren zu bestimmen. Allerdings gibt es keine einheitliche Meinung in den bisherigen Studien. Bislang wurde im Hippocampus nur die Morphologie der Dornenfortsätze über mehrere Tage hinweg untersucht, um die Lebensdauer der Dornenfortsätze zu bewerten, während chronische Analysen der synaptischen Übertragungsstärke fehlen. Daher wissen wir nur begrenzt, wie strukturelle Veränderungen mit der synaptischen Funktion in vivo zusammenhängen.

In einem ersten Projekt kombinierte ich chronische Zwei-Photonen-Kalzium-Mikroskopie von ipsilateralen CA1- Dornenfortsätzen mit wiederholter optogenetischer Aktivierung präsynaptischer kontralateraler CA3-Pyramidenneuronen in der wachen Maus. Mit diesem Ansatz konnte ich lokale, synaptisch hervorgerufene Kalziumantworten an einzelnen Dornenfortsätzen auslösen und die Stabilität dieser funktionell identifizierten Synapsen über mehr als zwei Wochen hinweg messen. Diese aktiven Dornenfortsätze neigen dazu, funktionelle Cluster stark verbundener Dornenfortsätze zu bilden und sind stabiler als nicht reagierende Dornenfortsätze an denselben Dendriten. Dies deutet darauf hin, dass eine hohe synaptische Verbindungsstärke die Persistenz der Dornenfortsätze fördert. Insgesamt legt diese Arbeit nahe, dass die Lebensdauer von Dornenfortsätze im Hippocampus mit der synaptischen Stärke zusammenhängt und diese somit möglicherweise die langfristige synaptische Konnektivität bestimmt.

Eine dynamische Umstrukturierung des Netzwerks wurde auch durch graduelle Neuordnung der räumlichen Repräsentation im Hippocampus beobachtet. Es wurde gezeigt, dass sich die neuronale Repräsentation der Umgebung im Hippocampus stetig ändert während das Bewegungsmuster eines Tieres in einem bestimmten Umfeld stabil bleibt. Der zelluläre Mechanismus, der dieser Dynamik von Ortszellen zugrunde liegt, bleibt unklar. Da die CA3- Region des Hippocampus eine räumliche Repräsentationsdrift aufweist, bleibt unklar, wie dieses Phänomen die Neuzuordnung des räumlichen Codes in CA1 beschleunigt. In einem zweiten Projekt kombinierte ich daher chronisches Zwei-Photonen-Kalzium-Imaging ipsilateraler CA1-Dornenfortsätze mit optogenetischer Aktivierung präsynaptischer kontralateraler CA3-Pyramidalneuronen in der Maus während der Durchführung einer räumlichen Navigationsaufgabe. Mit diesem Ansatz konnte ich eine Untergruppe von Ortszellen in CA1 optisch induzieren, deren Ortsfelder sich eher in der Nähe der Belohnungszone als in der Stimulationszone bilden. Darüber hinaus konnte ich zeigen, dass diese Manipulation zu einer Änderung des Gesamtpopulationscodes der bereits vorhandenen Ortszellen führte, wenn auch nur vorübergehend. Diese Arbeit deutet darauf hin, dass sich das Netzwerk zwar in einem stabilen Zustand befindet, dass aber eine Änderung der Signale von präsynaptischen Partnern zu einer vorübergehenden Neuordnung der Umgebung in CA1 führt, was darauf hindeutet, dass die funktionelle Netzwerkorganisation in CA1 durch präsynaptische Eingänge allmählich in einen neuen Zustand versetzt wird.

Introduction

1. Organization of the hippocampus

The hippocampus is a brain structure present in both hemispheres, located in the medial temporal lobe, and is a component of the limbic system. Each formation is divided into four distinct regions: the dentate gyrus, and the three *Cornu Ammoni* (CA1 to CA3) and is surrounded by the lateral ventricle (Figure 1). The hippocampus has been anatomically well characterized, already in the 19th century, in the mouse, and already in the 16th century in humans by Arantius (Bir et al., 2015; Engelhardt, 2016), due to its particular structure and functionally defined compartmentalization. Connections are well organized in layers along the dorsoventral axis as well as the anteroposterior axis. The hippocampus is a trisynaptic loop, with each part having a particular role in information processing (Andersen et al., 2007).

The dentate gyrus serves as the "entry" part of the hippocampus. It is composed of granule cells oriented in two laminar striates facing each other so that basal dendrites of granule cells are oriented towards the superficial part of the molecular layer. Diverse brain regions are projecting to the dentate gyrus, among which the entorhinal cortex through the perforant pathway, CA3, the septal nuclei, or the locus coeruleus (Pickel et al., 1974; Swanson and Hartman, 1975; Loughlin et al., 1986). In return, the dentate projects back to CA3, through bundles called mossy fibers. Its role in pattern separation has been notably hypothesized (Leutgeb et al., 2007; Madar et al., 2019).

CA3 is the most external part, forming the horn of the hippocampus. CA3 is mainly composed of pyramidal neurons, which are notably highly interconnected, forming a recurrent network (Miles et al., 2014). Thanks to its recurrent connections, CA3 is thought to be fundamental in maintaining memories at longer timescales. Except for projections from the dentate gyrus, CA3 receives inputs from the entorhinal cortex, but also from the amygdala, and the septum among other brain regions. CA3 neurons project to CA1 through Schaffer collaterals and make *en-passant* synapses on CA2 neurons. Schaffer collaterals originating from the contralateral hippocampi are also known as commissural projections. The same CA3 neurons give rise to projections to the ipsilateral and contralateral hippocampus (Swanson et al., 1980). They project to contralateral CA3, CA2, and CA1 (Blackstad, 1956; Fricke and Cowan, 1978). Worth noting, the number of commissural projections is different between species (van Groen and Wyss, 1988), they are less abundant in monkeys and potentially nonexistent in humans.

Although for long considered as an extension of CA3, CA2 is a small part of the hippocampus, probably the least well-described of the formation (Lorente de Nó, 1934). It is composed of large pyramidal neurons, as in CA3, and interneurons. It is

involved notably in social memories (Pronier et al., 2023; Tzakis and Holahan, 2019). Projections from the paraventricular nucleus, supramammillary nucleus, median raphe, and hypothalamus have been found only in CA2. CA2 neurons project to the supramammillary nucleus and the septal nuclei. Nonetheless, its primary output, as CA3, is CA1 (Dudek et al., 2016).

CA1 is the "output" part of the hippocampus. Composed of pyramidal neurons and interneurons, it receives inputs from CA2, CA3 neurons and from the entorhinal cortex through the temporoammonic pathway, as well as more distal regions such as amygdala, thalamus, ventral tegmental area (VTA) (Adeniyi et al., 2020), among others. CA1 is the part of the hippocampus that projects back to the entorhinal cortex (Naber et al., 2001). Moreover, CA1 projects to other brain regions such as the subiculum or the nucleus accumbens.
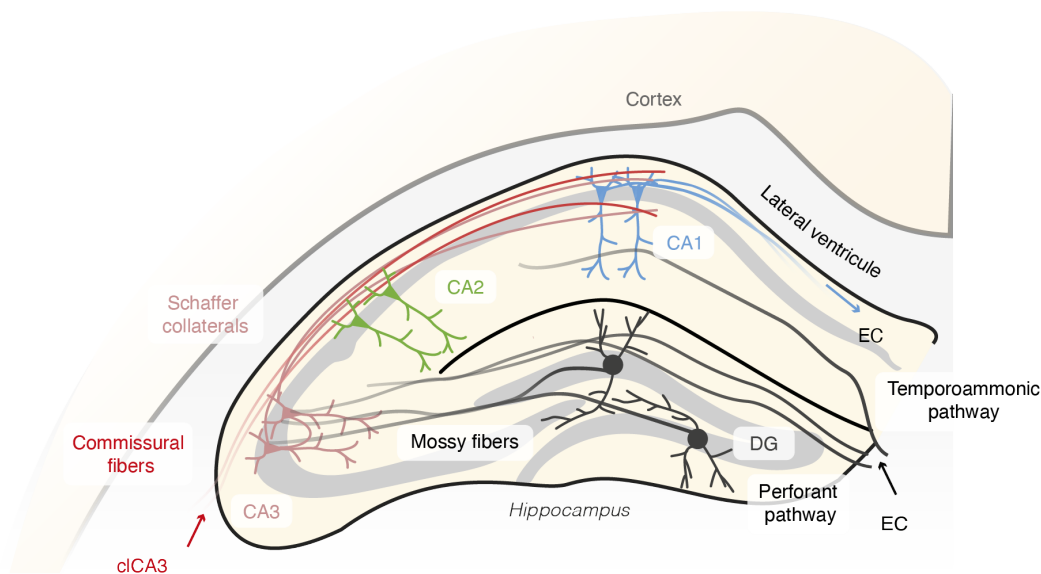
Figure 1. Organization of the hippocampal formation. The hippocampal formation is composed of the dentate gyrus (DG), the Cornu Ammonus 1 (CA1), 2 (CA2) and 3 (CA3). Five different pathways are present: the perforant pathway and the temporoammonic pathway originating from the entorhinal cortex (EC), the mossy fibers originating from the DG, the Schaffer collaterals originating from ipsilateral CA3 (ilCA3) and the commissural fibers originating from contralateral CA3 (clCA3). CA1 sends back projections to the EC.

The layers of the hippocampus starting from the most superficial are: the stratum *oriens*, stratum *pyramidale*, stratum *radiatum,* and stratum *lacunosum-moleculare*. Dendrites of CA1 neurons present in the different layers are respectively named: basal, oblique, and tuft dendrites (Figure 2). This denomination relates to different properties of these dendrites and can be recognized thanks to the order of the dendrite. CA1

11

inputs are organized differentially across its dendrites. Schaffer collaterals make synapses in CA1 both on apical dendrites, dendrites situated in stratum *radiatum*, and on basal dendrites, dendrites situated in stratum *oriens*.

As ipsilateral connections, commissural projections make synapses both on basal and apical dendrites, however with a higher fraction of synapses made on basal dendrites (Shinohara et al., 2012).
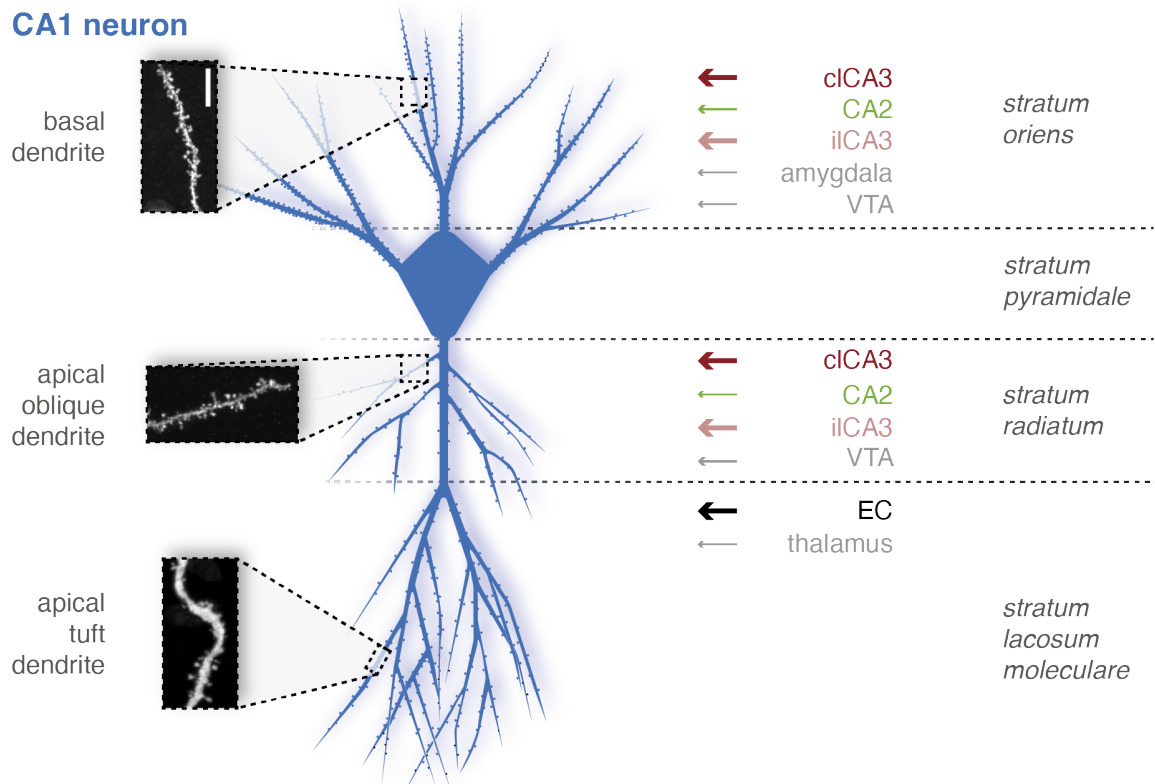
Figure 2. CA1 neuron morphology. External inputs to CA1 neurons are spatially organized on different dendrites, spanning from the stratum *oriens* to the stratum *lacunosum-moleculare*. clCA3: contralateral CA3, ilCA3: ipsilateral CA3, EC: entorhinal cortex. *Two-photon images of dendrites from Bloss et al 2016.*

As the Schaffer commissural collaterals are part of the main focus of this thesis, a more detailed description of the research on these connections is presented in the following point.

2. Neuronal transmission at the Schaffer collaterals

a. General foundation of synaptic transmission

Neurons are electrical units in the brain transmitting information. Although different types of transmission exist (chemical, electrical, and mechanical (Kasai et al., 2023; Ucar et al., 2021)), in the central nervous system (CNS), neurons mainly communicate through exchanges of chemicals. These neurotransmitters are conveyed at specialized sites called synapses. Synapses are composed of two parts, the presynaptic compartment, the bouton of the axon, and the postsynaptic compartment, both separated by the extracellular space, called the synaptic cleft. Upon voltage depolarization of the presynaptic neuron, vesicles are fused to the presynaptic membrane, releasing the neurotransmitters, such as glutamate for excitatory synapses. These neurotransmitters will spread in the synaptic cleft and bind to receptors in the postsynaptic compartment (Figure 3).
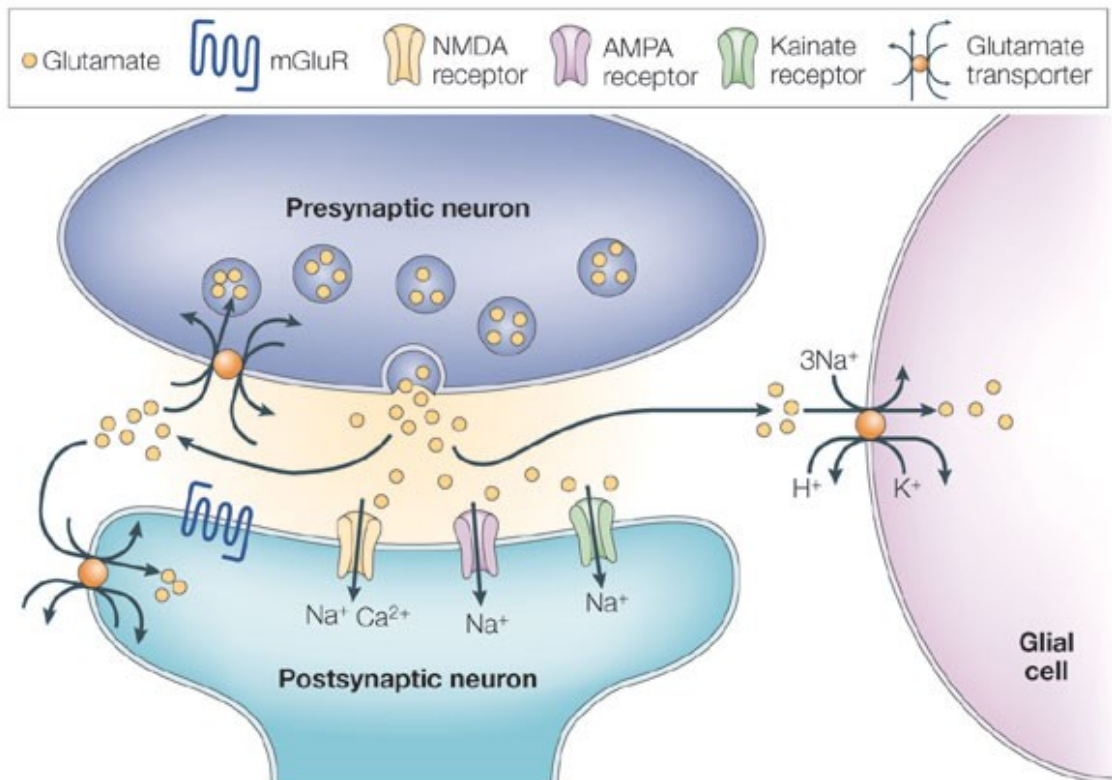
Figure 3. Chemical transmission at glutamatergic synapses. *Figure extracted from Attwell and Gibb 2005.*

The binding of glutamate on channels leads to their opening and exchanges of ions between the extracellular space and the intracellular environment, generating voltage depolarization of the postsynaptic partner. Under certain conditions (electrical isolation, concomitant depolarization at multiple synapses, etc.), depolarization of the postsynaptic cell will occur, and an action potential will be generated, propagating the signals to other cells (Lisman et al., 2007).

Glial cells can also be involved in synaptic transmission. Tripartite synapses have been found in the brain. In this case, astrocytes have been shown to regulate synaptic transmission (for review, see Perea, Navarrete, et Araque 2009) but are not discussed further as they are not the focus of this thesis.

More than 90% of excitatory synapses are located on small protrusions along dendrites emerging from the soma of neurons, known as dendritic spines (Robles et al., 2009). Inhibitory terminals both terminate on dendritic shafts and dendritic spines (DeFelipe and Fariñas, 1992). Spines can also be located directly at the axon hillock and soma.

Spines were first discovered by Santiago Ramón y Cajal (Figure 4A) (Ramón y Cajal, S. 1888, Yuste 2015). Electron microscopy studies, carried out years later, confirmed this discovery (Gray, 1959) and permitted elucidation of their detailed structure (Figure 4B) (Peters and Kaiserman-Abramof, 1969).

A: axon
c: synaptic cleft
d: postsynaptic densities
S : spine
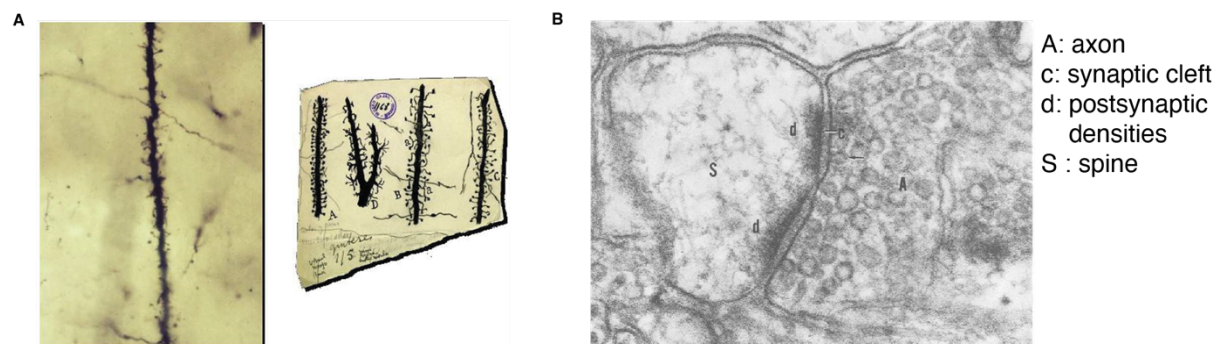
Figure 4. First description of dendritic spines. A. Discovery of spines prepared and illustrated by Cajal. *Figure from Yuste 2005.* **B.** Electron micrograph of a spine. *Modified figure from Peters and Kaiserman-Abramof 1969.*

Spines have been divided into four different categories (Figure 5) depending on head size, with volumes ranging from 0.01 to 0.03 μm^3, and neck size, with length ranging from 0.1 to 2.21 μm (Arellano et al., 2007; Bourne and Harris, 2008). However, this classification is still debated as the shape of spines is, at least partially, a continuum as spines are dynamic structures (Arellano et al., 2007; Pchitskaya and

Bezprozvanny, 2020). Densities of spines vary across regions, along dendritic arbors, developmental stages, and neuronal activity.
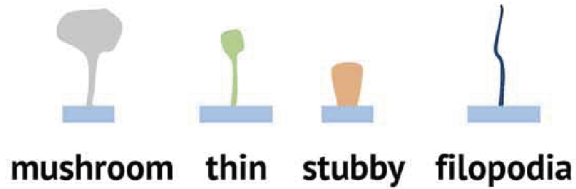
Figure 5. Classical view for spine categories. Mushroom spines are composed of a large head and long neck. Thin spines are composed of small head and long neck. Stubby spines lack a neck. Filopodia are long and thin spines. *Modified from Pchitskaya and Bezprozvanny 2020.*

b. Structure and function of dendritic spines

i. Composition of spines

Spines are composed of many actors (Figure 6). At the membrane, many different ionotropic glutamatergic receptors (iGluRs) are present on the postsynaptic cells, among which α-amino-3-hydroxy-5-methyl-4-isoxazolepropionic acid (AMPA), N-methyl-D-aspartate (NMDA) and kainate receptors. As ligand-gated, non-selective cation channels, positive charges can passively travel through, following an electrochemical gradient, when glutamate binds to the receptor. This process allows fast synaptic transmission. AMPARs are permeable to both Na^+ and K^+, and their permeability to Ca^{2+} depends on the subunit composition (Jane, 2007). The number of AMPARs at the synapse is correlated to synaptic strength (Huganir and Nicoll, 2013; Lee and Kirkwood, 2011; Lüscher and Malenka, 2012; Matsuzaki et al., 2001; Zhang et al., 2015). In comparison, NMDARs are permeable to Na^+, K^+, and Ca^{2+}, with Ca^{2+} representing ~15% of the total ion flux (Jahr and Stevens, 1993; Schneggenburger et al., 1993). However, to activate NMDARs, the binding of glutamate, glycine, and membrane depolarization via AMPAR activation are necessary. Depolarization enabled the removal of the magnesium block inserted in the channel pore, allowing cation flux. NMDARs are characterized by a slow kinetic and longer channel opening time.

Apart from these receptors, metabotropic glutamatergic receptors (mGluRs) are also present. These mGluRs are not channels but are coupled to G-proteins and can indirectly activate iGluRs upon glutamate binding. G-proteins are divided into different families, which can trigger either excitatory or inhibitory signaling cascades (Matozaki et al., 2000).

Cytoskeletal architecture, present in the spine, enables movement and anchoring of receptors. Actin and microtubule remodeling accompanies spine

morphogenesis (Korobova and Svitkina, 2010). Cytoskeletal proteins are also concentrated at postsynaptic densities (PSD), visible on electron microscopy images (Palay, 1956; Peters and Kaiserman-Abramof, 1969), along with a plethora of other proteins, including receptors, signaling, and scaffold proteins. The PSD is implicated in the regulation and trafficking of the ionotropic receptors and its area is correlated to synaptic strength (Harris and Stevens, 1989).
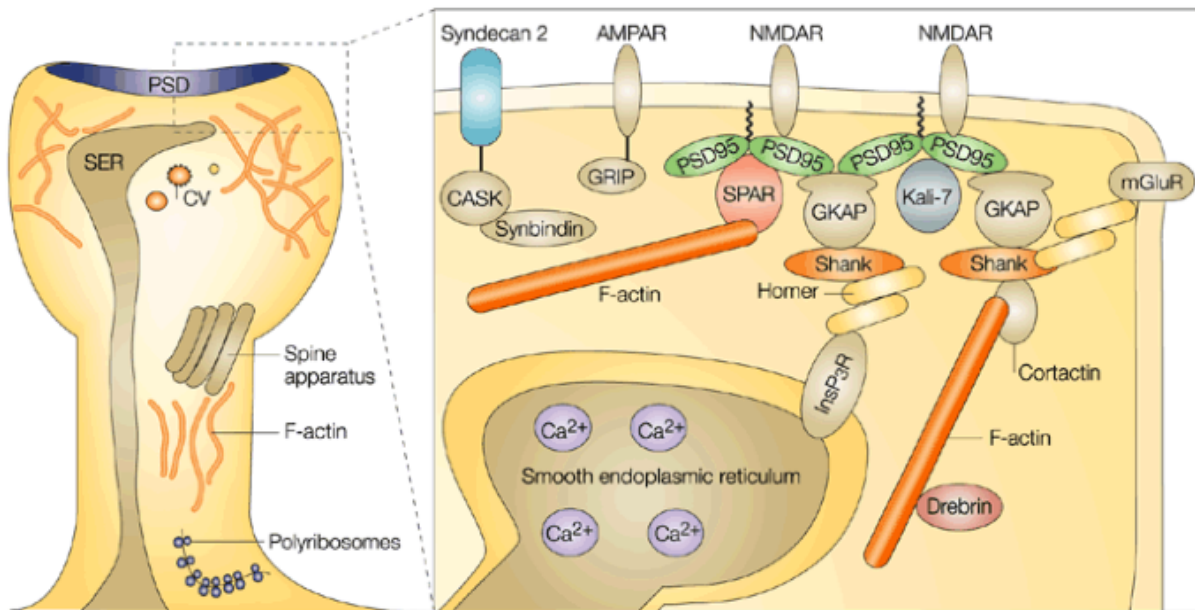
Figure 6. Organization of spines. Molecular organization of spines. SER: smooth endoplasmic reticulum; PSD: postsynaptic density; CV: coated vesicle; InsP3R: inositol-1,4,5-trisphosphate receptor; AMPAR: α-amino-3-hydroxy-5-methyl-4-isoxazolepropionic acid receptor; NMDAR: N-methyl-D-aspartate receptor; CASK: calcium/calmodulin-dependent serine protein kinase; F-actin: filamentous actin; GKAP, guanylate-kinase-associated protein; Kali-7, Kalirin-7; mGluR, metabotropic glutamate receptor; NMDAR, N-methyl-D-asparate receptor; SPAR, spine-associated RapGAP; GRIP: glutamate-receptor-interacting protein. *Figure extracted from Hering and Sheng 2001.*

Spines are biochemically and electrically compartmentalized units that can house their own molecular machinery (Araya et al., 2006; Cornejo et al., 2022). Indeed, a spine apparatus, a specialized endoplasmic reticulum compartment, is present in large spines. However, in smaller spines, only a single tubule of smooth endoplasmic reticulum has been observed (Perez-Alvarez et al., 2020b). Both endoplasmic reticulum can rapidly modulate calcium dynamics (Bell et al., 2019; Wu et al., 2017).

ii. Calcium in spines

Ca^{2+} is one of the main ions implicated in synaptic transmission, along with Na$^+$ and potassium K$^+$. Ca^{2+} is involved in neurotransmitter release through binding to the release machinery of vesicles, as well as in postsynaptic cascade signaling via activation of different proteins. Ca^{2+} acts as an important messenger in signal processing. Ca^{2+} enters the spine from the extracellular space through NMDARs, AMPARs, and voltage-sensitive calcium channels (VSCCs).
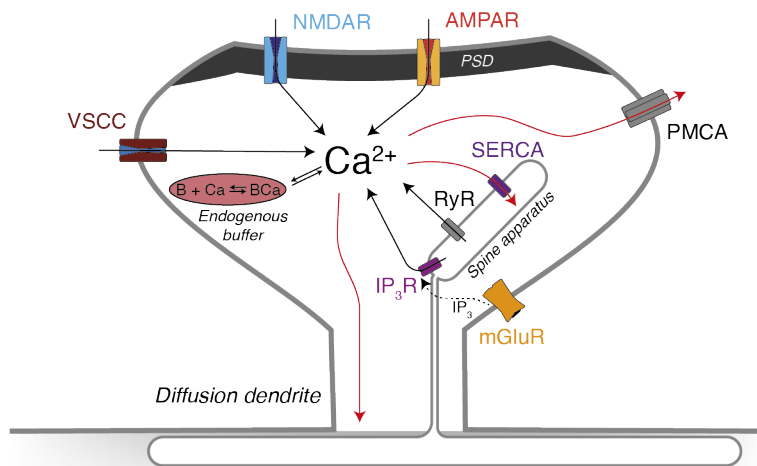
Figure 7. Calcium in dendritic spines. PMCA: plasma membrane calcium ATPase; VSCCs: voltage-sensitive calcium channels; RyR: ryanodine-receptor; IP$_3$R: inositol-1,4,5triphosphate receptor; SERCA: smooth ER calcium ATPase; B: calcium buffer. *Reproduced figure from Yuste et al 2000.*

However, internal sources of calcium also exist (Figure 7). Ca^{2+} is stored in the spine apparatus, which can release it through calcium-permeable channels; as a ryanodine-receptor or inositol-1,4,5triphosphate receptor (Kovalchuk et al., 2000; Oertner et al., 2002; Rochefort and Konnerth, 2012; Sabatini et al., 2002; Yuste et al., 2000, 1999). This release enables amplification of calcium signal, which can mediate synaptic plasticity (Yuste et al., 2000).

The spine neck structure permits the concentration of material, such as Ca^{2+}, by slowing down the diffusion of chemicals to dendrites (Bloodgood et al., 2009; Higley and Sabatini, 2012; Svoboda et al., 1996; Yuste and Denk, 1995). A high concentration of Ca^{2+} increases the probability of its binding to calcium-calmodulin-dependent protein kinase II (CaMKII), an important messenger for synaptic plasticity (Coultrap et al., 2014; Yasuda et al., 2022).

Optical imaging of calcium, notably using two-photon imaging, from cellular to organelles level has become a state-of-the-art technique for activity measurement (Chen et al., 2013; Dana et al., 2019; Miyawaki, 2011; Nakai et al., 2001; Palmer and Tsien, 2006; Yuste et al., 1999), although, so far, no calcium sensor has proven a linear

relationship between voltage and fluorescence changes upon calcium binding in the whole range of calcium concentrations (Evans et al., 2020; Wei et al., 2020; Zhang et al., 2023).

c. Measurement of synaptic transmission

Synaptic transmission has long been measured using electrophysiological methods. One of the first methods for studying monosynaptic connections has been the paired recording of neurons (Figure 8A). Using acute slices, structural and functional properties have been elucidated in microcircuits (Buhl et al., 1994; Debanne et al., 2008; Deuchars et al., 1994; Malinow, 1991; Qi et al., 2020). However, this method requires the identification of connected neurons for manipulation of the presynaptic partner. To circumvent this issue, later, patch-clamping combined with glutamate uncaging has been used to monitor parameters of transmission and receptor distribution at individual synapses (Ellis-Davies, 2019; Mitchell et al., 2019; Pettit et al., 1997; Vardalaki et al., 2022). This method does not require presynaptic partners and permits the stimulation of a unique synapse at a time (Figure 8B). Nevertheless, the method remains tedious, as only a few spines can be monitored at once and its use *in vivo* remains technically challenging (Noguchi et al., 2021, 2019).

Calcium imaging is the long-standing method of choice for activity measurement. Engineered calcium sensors are used as a proxy for cellular activity. As of today, the main class of calcium indicators used are jGCaMP sensors, genetically encoded calcium indicators (GECI) engineered by the fusion of a green fluorescent protein (GFP) and CaMKII (Lin and Schnitzer, 2016). The binding of Ca^{2+} leads to configuration changes in the protein chain and consequently, fluorescence emission increases. Different sensors have been produced over the last decade improving kinetics, fluorescence amplitude but also baseline fluorescence. The increased baseline fluorescence in jGCaMP7b (Dana et al., 2019) is a fundamental improvement as it unlocked fluorescence imaging at dendrites and spines (Figure 8C). Nonetheless, by releasing Ca^{2+} at a slower timescale, these sensors can act as buffers, interacting with native calcium signaling (McMahon and Jackson, 2018).

Two-photon microscopy is the state-of-the-art method for *in vivo* imaging, especially for deep structures, such as the hippocampus, located around 1mm from the cortical surface (Denk et al., 1990; Mizrahi et al., 2004; Zipfel et al., 2003). It allows deep penetration of light in highly scattering tissues, until around 400µm deep imaging, and focuses the light using scanning mirror for a low fluorescence excitation of tissue volume. However, most standard two-photon microscopes are limited to a scanning frequency of 30Hz (i.e., 33ms per frame) to allow for sufficient resolution in the case of spine imaging, limiting its power for studying synaptic transmission. This speed limitation is of importance to determine source inputs. Indeed, when a cell is firing, a

back-propagating action potential invades the dendrites in a few milliseconds, traveling from 250 to 500µm per second, which is faster than the time required for acquiring a single frame (Waters et al., 2005). This action potential will then hide the calcium transients from synaptic inputs in spines, prohibiting the identification of source inputs, unless dendritic events' contribution are later removed (Chen et al., 2013).
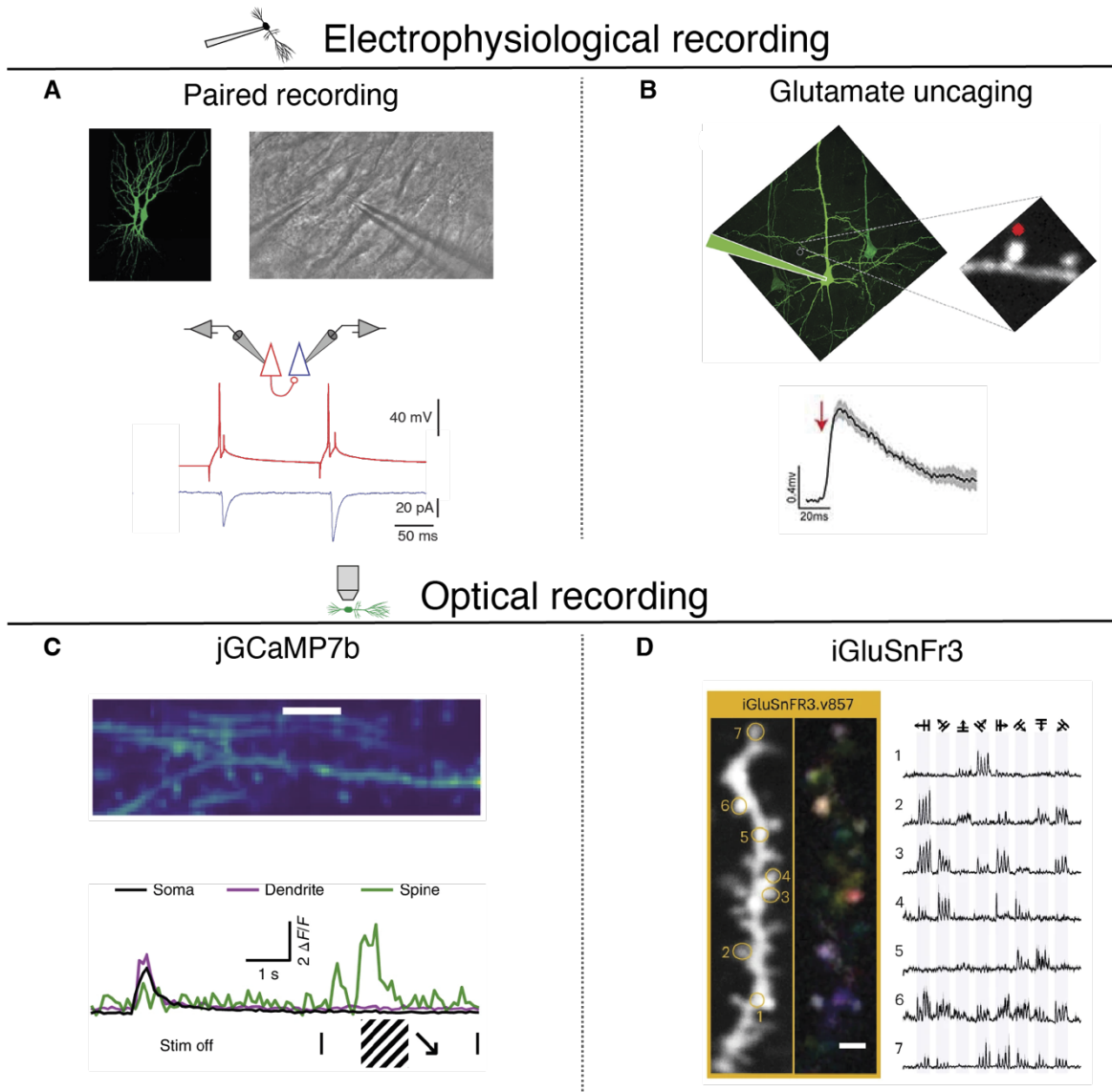
Figure 8. Techniques for measurement of synaptic transmission. A. Excitatory postsynaptic current recording from current clamp at the soma upon glutamate uncaging *in vitro. Figure from Mitchell et al 2019.* **B.** Recording of a pair of CA3 pyramidal neurons from a cultured hippocampal slice. *Figure from Debanne et al 2008.* **C.** Two-photon calcium imaging of jGCaMP7b of primary visual area (V1) spines in a mouse passively presented with drifting gratings. *Figure taken from Dana et al 2019.* **D.** Two-photon glutamate imaging of iGluSnFr3 of V1 spines in a mouse passively presented with visual motion stimuli. *Figure from Aggarwal 2023.*

A recent solution to circumvent the latter issue is the use of glutamate sensors (iGluSnFr) or GABAergic sensors in the case of inhibitory synapses (Marvin et al., 2019). *In vitro,* its use permitted the measure of release probabilities at individual synapses (Dürst et al., 2022; Jensen et al., 2019). So far, its use *in vivo* has been limited due to its low baseline fluorescence, making it difficult to identify spines (Marvin et al., 2018, 2013). However, a new version (iGluSnFr3) (Figure 8D), released last year, promises increased brightness and stability *in vivo* (Aggarwal et al., 2023).

d. Schaffer collaterals properties of synaptic transmission

The Schaffer collateral synapse is one of the most extensively investigated synapses of the brain. In 1892, Károly Schaffer was the first scientist to describe this circuit using a modified version of the Nissl staining, which was named after him (Szirmai et al., 2012). Since then, many scientists focused their work on Schaffer collaterals. In this circuit, synapses are glutamatergic and respond to the classical description as made before in this thesis. Yet, some particularities have been found.

Employing this particular circuit, plasticity has been described. Using electrophysiology, scientists discovered short-term and long-term potentiation. By delivering two short pulses (paired-pulse) within a short period, the amplitude of the second pulse increased. This paired-pulse facilitation is short-lasting and is the result of an increase in the probability of glutamate release (Schulz et al., 1995). Of now, this short-term plasticity protocol is a classical method for the evaluation of Schaffer collaterals synapses, especially for investigating the effect of long-term potentiation.

Long-term potentiation, a long-lasting form of plasticity, has also been extensively investigated using Schaffer collateral circuitry (Andersen et al., 1977; Bliss et al., 1983; Bliss, 1979; Lynch et al., 1977; Schwartzkroin and Wester, 1975; Wheal et al., 1983; Yamamoto et al., 1980). Interestingly, commissural afferents can independently support long-term potentiation (Andersen, 1960; Buzsáki, 1980; Wheal et al., 1983). Asymmetrical Schaffer and commissural capacity for long-term potentiation have been found in the mouse hippocampus. Electrophysiological studies found that left CA3 projections have a greater capacity for long-term potentiation, high-frequency stimulation strengthening only synapses with presynaptic input originating from left CA3 (Kohl et al., 2011; Shipton et al., 2014). This asymmetry is also observed in humans (Burgess et al., 2002), but not in rats (Martin et al., 2019).

This plasticity is the consequence of synaptic weight changes, resulting in potential structural changes in spines.

3. Plasticity of dendritic spines

a. Spine stability

Spines are dynamic structures. To understand the extent of spine remodeling in the hippocampus, spine lifetime has been estimated. Spine lifetime has been mostly investigated in the cortex. However, reported lifetimes have been divergent. For instance, in the neocortex, the spine survival fraction is up to 70% after 2 weeks in adulthood (Holtmaat et al., 2005). In the primary visual cortex and barrel cortex, spines have been also found stable with respectively 70% and 50% of spines persisting over a month (Grutzendler et al., 2002; Trachtenberg et al., 2002). A study even reported increased spine stability in the barrel cortex, with more than 70% of spines described at the same location 18 months after the first imaging session (Zuo et al., 2005). The extent of stability of these spines is still debated, yet, cortical spines are believed as rather unstable during development and reach a more stable state during adulthood (Yu and Zuo, 2011).

In contrast, reports of spine lifetime in CA1 are scarce. CA1 is a place of high synaptic plasticity, and therefore high spine turnover is expected. While many studies have attempted to determine CA1 spine lifetime, they differ in their estimates (Attardo et al., 2015a; Gu et al., 2014; Pfeiffer et al., 2018; Yang et al., 2021).

The first longitudinal study of spines appeared ten years ago (Gu et al., 2014). Gu et al used a mouse reporter line expressing a yellow fluorescent protein (YFP) in *Thy1* neurons (Feng et al., 2000). The *Thy1* lines are known for the sparse expression of the construct in CA1 pyramidal neurons. Because CA1 pyramidal neurons are densely packed, this sparse expression allows for the imaging of dendritic spines. For each session, the mice were anesthetized with a mix of ketamine and xylazine. Following the same spines on apical dendrites every four days over two weeks, they found that 96% of the spines present on the first day were still present at the end of the experiment, arguing for the high stability of spines in CA1 (Figure 9A).

However, a year later, a new study also investigated the spine lifetime in CA1 (Attardo et al., 2015b). Acknowledging the limits of two-photon imaging resolution, they compared the density of spines found using a classical two-photon microscope with the same density found using stimulated-emission depletion (STED) microscopy (Figure 9B). STED microscopy allows for a better resolution in all axes but is restricted in the depth one can image because this technique is highly sensitive to the light refraction of the tissue (Vicidomini et al., 2018). On the contrary to Gu et al, spines on basal dendrites of CA1 were then imaged on mice anesthetized with isoflurane. First, STED microscopy revealed that, because spines are closed together, one can easily merge spines and miss eliminated spines. This case could concern as high as 30% of the spines. Using a computational model taking into account the missed spines in a longitudinal dataset obtained by following the same spines over 80 days with two-

photon microscopy, they found that almost, if not all, spines would turn over in three to six weeks with a mean lifetime of nine days. This finding rather describes a high instability of spines in CA1.

In 2018, a new, and last, study was published on spine lifetime in CA1 (Pfeiffer et al., 2018). This study used STED microscopy to follow the same spines on basal dendrites of CA1 every two days for a total of four days (Figure 9C). They found that 40% of all spines present on the first day were eliminated. They notably found that large spines were more stable than smaller spines, arguing that, contrary to the claim of Attardo et al. for a single population of spines surviving nine days, different spine populations with varying lifetimes might coexist in CA1.

In conclusion, discrepancies in the turnover of CA1 spines have been found, from high stability to high instability. However, multiple differences can be noticed in these studies. First, the use of anesthetics was different across the studies: while Gu et al. used ketamine and xylazine, the other two used isoflurane. Secondly, the use of different microscopy techniques can explain the difference in survival fraction obtained from the three studies. As well described by Attardo et al., two-photon microscopy cannot accurately resolve individual spines, especially in CA1, where spines are densely packed. Already, electron microscopy reports have estimated a density of up to 3 spines/μm^2 (Harris and Stevens, 1989), while standard two-photon microscopy reports a density of up to 1 spine/μm^2. Finally, while Gu et al. studied spine turnover on apical dendrites, the other two focused on basal dendrites. These different branches receive different inputs (Figure 2) and may follow different synaptic plasticity rules, it seems plausible that different turnover rates are taking place depending on the branches, similar to what has been shown in the cortex (Yaeger et al., 2022).
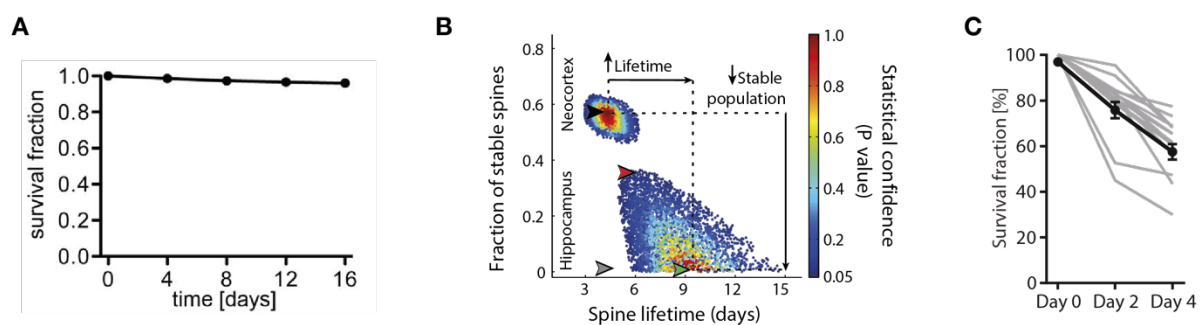
Figure 9. Reported stability of CA1 spines. A. High survival fraction of CA1 spines on apical dendrites after two weeks. *Figure from Gu et al 2014.* **B.** Strong instability of CA1 spines on basal dendrites. *Figure from Attardo et al 2015.* **C.** Low survival fraction of CA1 spines on basal dendrite over four days. *Figure from Pfeiffer et al 2018.*

Despite these differences, one common fact is that so far only spine morphology has been investigated over multiple days in the hippocampus to assert spine lifetime. Although morphological parameters have been correlated to the lifetime of different types of spines (Steffens et al., 2020) (filopodia vs mushroom spines), chronic analyses of synaptic function have been missing. Therefore, we are limited in our understanding of how structural changes relate to synaptic function *in vivo* while *in* vitro pieces of evidence have shown the functional influence on spine dynamics.

b. Long-term plasticity of spines

Synaptic plasticity is the mechanism by which the weight of inputs is modified. Synaptic modifications have been extensively studied over the years, unraveling different sets of rules one synapse can follow to change its strength (Bang et al., 2023; Citri and Malenka, 2008; Fröhlich, 2016; Magee and Grienberger, 2020).

i. Hebbian rules of synaptic plasticity

Already formulated in 1949, Hebb described long-term potentiation (LTP) and long-term depression (LTD), which are respectively the increase and decrease of synaptic strength (Hebb, 1949). Later, the expression "what fires together, wires together" became famous (Shatz, 1992). This form of plasticity relies on the correlative incidence of spikes in the presynaptic and postsynaptic neurons. While spiking of the postsynaptic neurons following the spiking of the presynaptic neurons triggers long-term potentiation, postsynaptic spiking preceding presynaptic activity induces long-term depression (Figure 10).

This form of plasticity was demonstrated in 1973 by Bliss and Lømo repetitively stimulating the perforant path of the hippocampus, inducing long-term potentiation at dentate gyrus synapses (Bliss and Lomo, 1973; Bragin et al., 1977; Douglas and Goddard, 1975; Lømo, 2003). Since then, the elucidation of cellular and molecular mechanisms taking place in the phenomenon has been a main research focus (Bliss and Collingridge, 1993; Fedorov et al., 1993; Malinow, 1994; Manabe and Nicoll, 1994; Stevens and Wang, 1994), but remains incomplete.

On the other hand, LTD was only reported in 1992, using the Schaffer collaterals microcircuit, demonstrating that the frequency and duration of stimulation are determinants of the direction of synaptic plasticity (Dudek and Bear, 1992).
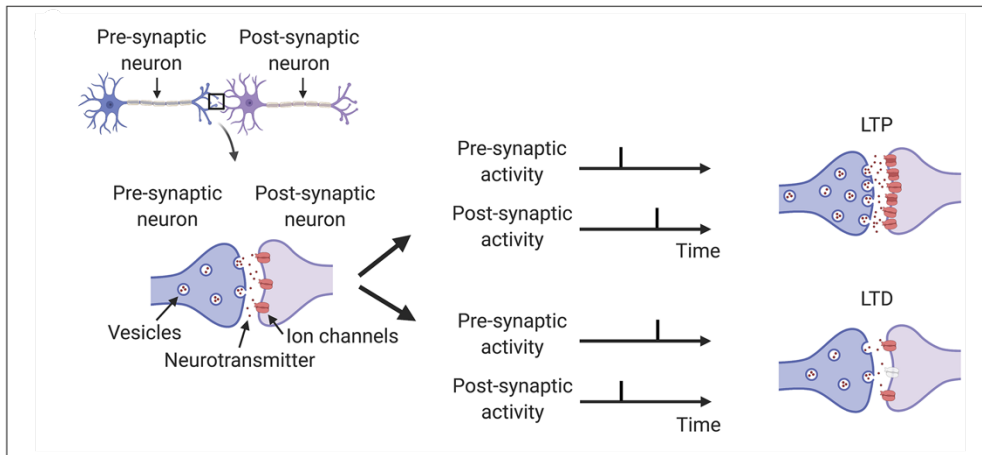
Figure 10. Hebbian rules of synaptic plasticity. The coincidence of presynaptic and postsynaptic spiking determines the direction of synaptic plasticity. *Modified figure from Bang et al 2023.*

Although both LTP and LTD can involve Ca^{2+} signaling and NMDARs, distinct signaling cascades are triggered, resulting in differences in the future response amplitudes due to the redistribution of AMPARs at the synapse (Bear and Malenka, 1994; Carroll et al., 1999; Choquet, 2018; Huganir and Nicoll, 2013; Lüscher and Malenka, 2012; Murakoshi et al., 2011; Zhang et al., 2021, 2015). Notably, the activity of CaMKII appears to be a key messenger in the expression of LTP at the synapse (Lisman et al., 2012). While LTP is mostly a postsynaptic mechanism, LTD, on the contrary, exhibits a presynaptic component, with a reduction in release probabilities (Wiegert and Oertner, 2013). Since it induces the production and trafficking of materials into or out of the synapse, LTD and LTP are correlated with the morphological changes of spines (Matsuzaki et al., 2004; Yang et al., 2008; Zhang et al., 2015).

Hebbian rules are a type of unsupervised synaptic plasticity (Figure 11A). A selectivity of inputs that are relevant to a particular task is not included. That's why modifications of Hebbian rules are envisioned.

ii. Modified Hebbian rules

Multiple changes have been tested, notably in computational networks, to account for the selectivity of inputs.

Already in the 40s, the dissociation between the network activity due to sensory experience and the associated but temporally delayed reward is identified as the distal reward problem (Hull, 1943). To circumvent this issue, an eligibility trace has been implemented in a computational neural network (Figure 11B). This eligibility trace consists of an internal signal localized at individual synapses as a sign of suitability to

modifications and, importantly, decaying over several seconds (Sutton and Barto, 1981).

Other modifications to the classical Hebbian rules have also been hypothesized. For instance, dopamine is one of the most investigated neuromodulators, involved in diverse tasks, primarily for its role in reward processing (Lewis et al., 2021; Schultz, 2007). Activation of dopamine receptors is associated with the expression of different types of synaptic plasticity and enhancement of long-term potentiation (Frey et al., 1993; Otmakhova and Lisman, 1996). Because of this, the concept of gating of Hebbian plasticity via specific neuromodulators has emerged (Figure 11C) (Brzosko et al., 2017; Gu, 2002; Nadim and Bucher, 2014; Ogelman et al., 2024). Because these signals are rather global in the brain and not specifically directed to individual synapses, an instructive signal has been added to the model, namely supervised synaptic plasticity (Wang and Naud, 2022).

In a model of supervised synaptic, an instructive signal, the difference between the predicted and actual signal named teaching signal, is used to optimize the model or performance in a task (Figure 11C) (Marblestone et al., 2016; Olshausen and Field, 1996; Roelfsema and Holtmaat, 2018).
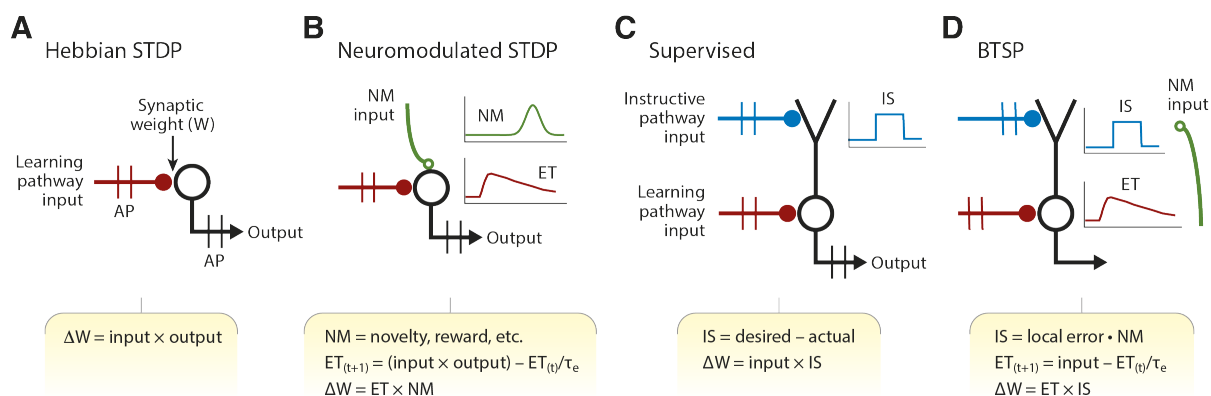
Figure 11. Synaptic plasticity models. **A.** Classical Hebbian rule. **B.** Modified Hebbian rule with an eligibility signal and a neuromodulatory signal. **C.** Supervised model including an instructive signal to classical Hebbian rules. **D.** BTSP as a combination of previous models. *Modified figure from Magee, Grienberger 2020.*

More recently, another model of plasticity at the junction of multiple of the above-introduced modifications has emerged from studies in the hippocampus. Behavioral timescale synaptic plasticity (BTSP) is a form of plasticity integrating signals over a seconds-long time window (Bittner et al., 2017; Grienberger et al., 2017). BTSP integrates an eligibility trace, an instructive signal and a neuromodulatory component

into its model (Figure 11D). This form of plasticity, discussed in more detail later, is notably involved in spatial selectivity firing of CA1 cells.

c. Structural plasticity at spines

i. Structural modifications of stimulated spines

Longitudinal investigations of spines revealed that spines are dynamic structures that continuously change in shape over time. These modifications are observed at different timescales, ranging from minutes to days after events.

In the 70s, the first electron microscopy studies showed that upon LTP induction, spines show a particular enlargement of their spine head when compared to controls (Fifková and Van Harreveld, 1977; Van Harreveld and Fifkova, 1975). Yet, it was only later, in the early 2000s, that a following study, using glutamate uncaging, showed a causal relationship between LTP induction and spine reshaping (Matsuzaki et al., 2004, 2001). The existence of this structural LTP (sLTP) has been further investigated in the following years and suggested that this enlargement particularly permitted the insertion of additional AMPARs (Harvey and Svoboda, 2007; Lamprecht and LeDoux, 2004; Lee et al., 2009; Noguchi et al., 2019; Okamoto et al., 2004). Eventually, this process is followed by an increase in the size of the PSD and presynaptic active zone (Figure 12A) (Bosch et al., 2014; Meyer et al., 2014; Nishiyama and Yasuda, 2015). Because spine head volume has been associated with correlates of synaptic strength, such as AMPARs density (Huganir and Nicoll, 2013; Lee and Kirkwood, 2011; Matsuzaki et al., 2001; Noguchi et al., 2011; Takumi et al., 1999), PSD area (Arellano et al., 2007; Harris and Stevens, 1989), and presynaptic active zone size (Schikorski and Stevens, 1997), spine structure has been used to estimate synaptic function. As so, large "mushroom" spines have been associated with strong synapses while small spines are considered as weak synapses. Similarly, filopodia are "silent" synapses, as they lack AMPARs. However, they show NMDAR-mediated currents and can be unsilenced via Hebbian plasticity (Vardalaki et al., 2022). These filopodia could be the precursors of larger spines (Fiala et al., 1998; Portera-Cailliau et al., 2003; Robles et al., 2009; Zuo et al., 2005).

Structural changes are also observed upon LTD induction (Figure 12B). However, compared to LTP structural modifications, shrinkage following LTD arises at longer timescales (Nägerl et al., 2004; Noguchi et al., 2019; Okamoto et al., 2004; Stein and Zito, 2019; Zhou et al., 2004). This event can also lead to spine elimination (Bastrikova et al., 2008). Yet, spine shrinkage is not always a consequence of synaptic depression (Nägerl et al., 2004; Wiegert and Oertner, 2013; Zhou et al., 2004), revealing a dissociation between functional and structural plasticity.
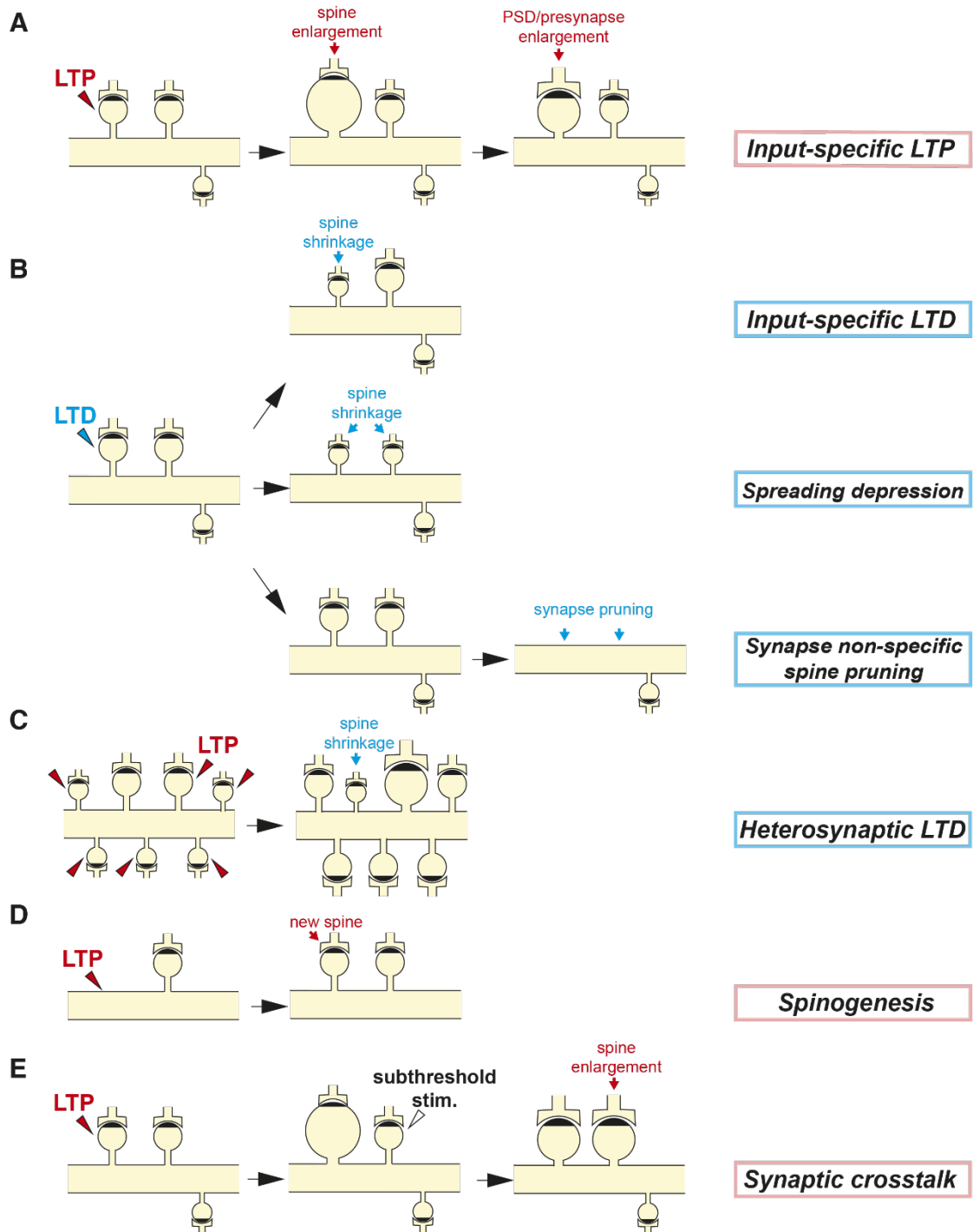
Figure 12. Spine structural plasticity. A. LTP induces the enlargement of the targeted spine. **B.** LTD can induce target-specific spine shrinkage (top), spread depression to neighboring untargeted spine (middle), or induce non-specific late spine pruning (bottom). **C.** Heterosynaptic plasticity is the induction of LTP at multiple neighboring spines, resulting in untargeted spine shrinkage. **D.** LTP can result in spinogenesis. **E.** Synaptic crosstalk is the facilitation of LTP induction of weakly stimulated spines due to previous LTP induction at a neighbor spine. *Figure from Nishiyama and Yasuda 2015.*

Additionally, it has been shown that spine neck structures are also altered following plasticity events, in correlation with spine head volume changes (Noguchi et al., 2005; Steffens et al., 2021). These changes can then change the spreading of signals to dendrites and spines.

ii. Evidence of propagation of plasticity signals

Since spine resources can traffic between spines along the same dendrites, long-term plasticity does not only affect structural fluctuations at targeted spines but can also result in functional and shape modifications of neighboring spines.

Observations have shown that LTD might induce synaptic depression at neighbor spines. In 2013, Hayama et al. used two-photon uncaging of GABA (an inhibitory neurotransmitter) at a single spine preceding standard LTD protocol. Not only did this experiment lead to spine shrinkage and even elimination of the stimulated spine, but it also resulted in the shrinkage of neighboring spines (Figure 12B). GABAergic signaling is shown to be responsible for the decrease in Ca^{2+} in the cytosol despite the increase in local Ca^{2+} near NMDARs (Hayama et al., 2013). This effect was notably reversed with the use of calcium chelators as ethylene glycol tetra-acetic acid (EGTA) and 1, 2-bis(o-amino-phenoxy)-ethane-N, N, N'N'-tetra-acetic acid (BAPTA). The spreading of synaptic depression is then dependent on LTD induction combined with GABAergic signaling.

Eventually, LTD can trigger non-specific synapses pruning around the stimulated spine. Using hippocampal organotypic slices, upon LTD induction, no shrinkage was observed either on the stimulated spine or neighboring spines (Wiegert and Oertner, 2013). Yet, a few days later, both the stimulated spines and neighboring spines were removed unspecifically (Figure 12B).

Unspecific induction of LTD on neighboring spines is not only triggered by LTD. Cases of synaptic depression after LTP induction on proximal spines have been observed (Figure 12C). In an experiment, LTP was induced on multiple nearby spines using glutamate uncaging (Oh et al., 2015). While these stimulated spines enlarged, neighboring unstimulated spines weakened and shrank. This process, namely heterosynaptic depression, is notably hypothesized as a way for dendrites to balance their total synaptic weights (Lynch et al., 1977; Scanziani et al., 1996).

LTP induction can also induce changes in neighboring spines, such as spinogenesis at nearby locations (Figure 12D). Such an event has been observed both *in vitro* (Kwon and Sabatini, 2011) and *in vivo*. Notably, *in* vivo, these new spines are relevant to the stimulus. Using optogenetic stimulation, El Boustani et al paired neurons to visual inputs. This manipulation led to the potentiation of multiple spines, estimated by an increase of spine head volume, that show tuning to the stimulus. In the next

days, they observed an increased rate of new spines, especially filopodia, appearing close to the identified responsive spines (El-Boustani et al., 2018). More recently, Hedrick et al followed spines in the motor cortex while mice were learning a lever press task. During learning, they show that spines form functional clusters and that new spines are more likely to appear next to responsive ones (Hedrick et al., 2022). However, so far, such *in vivo* investigations have mainly been led in the cortex.

Finally, a last case has been observed. The first induced potentiation can facilitate the LTP induction of neighboring spines (Figure 12E). Using glutamate uncaging, Harvey and Svoboda have shown that when inducing LTP at a target spine, even a weak stimulation of a neighboring spine can lead to long-term synaptic potentiation and spine enlargement (Harvey and Svoboda, 2007). Notably, it has been shown that the activation of Ras from potentiation is implicated in this synaptic crosstalk, as its activity has been recorded on spines and dendrites until ~10µm away from the stimulated spine (Harvey et al., 2008).

d. Other modulators of spine dynamics

Spine dynamics are also affected by other modulators which trigger potentiation or depression pathways.
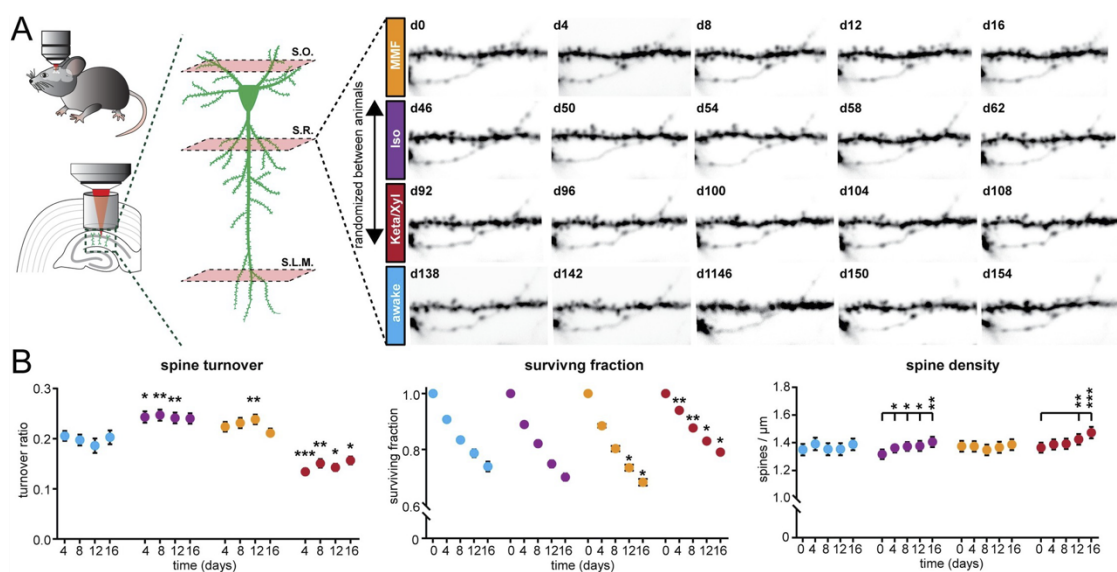
Figure 13. Spine dynamics upon repeated exposure of anesthetics. A. Schematic of two-photon imaging of spines in CA1 with example dendrite images. **B.** Spine turnover (left), surviving fraction (center) and spine density (right) under anesthesia and awake conditions. *Figure from Yang et al., 2021.*

As reported earlier, following the discrepancies between studies in studying CA1 spine turnover, we found that different anesthetics have been used, such as isoflurane (Attardo et al., 2015b; Pfeiffer et al., 2018) and a mix of ketamine and xylazine (Gu et al., 2014). As described in humans, sustained anesthesia can lead to cognitive impairment as, for instance, loss of memories (Monk et al., 2008). We hypothesized that the different anesthetics could trigger mechanisms influencing spine turnovers in the hippocampus. We then compared three commonly used anesthetics in rodents: isoflurane, a mix of ketamine and xylazine, and a mix of midazolam, medetomidine and fentanyl (MMF). We found different activity patterns depending on the different anesthetics compared to the awake condition using electrophysiological recordings and two-photon calcium imaging. Related, hippocampal-dependent memory was altered only following ketamine/xylazine and MMF exposure but not post-isoflurane exposure (Yang et al., 2021). Along the same line, spine dynamics were not significantly altered by isoflurane, but spines were more persistent when ketamine and xylazine were repeatedly applied, although to a lesser extent compared to the turnover found by Gu et al.

Synaptic potentiation has been mainly studied via a mechanism induced by NMDARs or mGluRs activation. However, neuromodulators, such as dopamine or serotonin, also act at the synapses modifying the gain of transmission and certainly can influence the synaptic strength and thus turnover (Maity et al., 2016; Speranza et al., 2021). A study shows that caffeine application on hippocampal slices can lead to the potentiation of synapses through the activation of adenosine receptors (Simons et al., 2011). Moreover, neuromodulator effects have been shown to have subsequent consequences on developmental (Ogelman et al., 2024) and behavioral outcomes (Lamanna et al., 2021; Speranza et al., 2021).

4. The role of the hippocampus in learning and memory

Evolving in a continuously fluctuating environment requires updates of the brain circuitry. Through rewiring, a phenomenon wherein neuronal connections are modified, the brain adapts to its surroundings and new associated stimuli. Notably, these modifications in synaptic strength facilitate the storage and formation of memories.

a. Memory trace storage

i. Relating long-term potentiation to memory formation

Still debated, how memory is stored and can be retrieved is a long-standing question (Lamprecht and LeDoux, 2004, 2004; Martin et al., 2000; O'Keefe et al., 1978; Takeuchi et al., 2014). Many scientists devoted years of research to finding the precise

location of a memory trace. Over the years, memory allocations have increasingly been attributed to numerous brain regions and substrates, spanning all scales from molecular to neuronal ensembles (Chaudhuri and Fiete, 2016; Davis and Squire, 1984; Dudai, 2002; Goelet et al., 1986; Holtmaat and Caroni, 2016; Kandel, 2001; Kandel et al., 2014) with no real ending consensus. Nonetheless, the hippocampus is still the most studied region for its involvement in memory formation, especially in spatial and episodic memory (Burgess et al., 2002; Squire, 1987).

The relationship between spine properties and learning was hypothesized years ago in humans. Indeed, patients suffering from different pathologies, such as epileptic seizure, stroke, ischemia, or mental retardation, displayed a reduced dendritic spines density as well as spine abnormal shapes (Harris and Kater, 1994). The hypothesis was that excessive calcium and other ions influx led to toxicity and possibly increased cell deaths. Yet, only far-fetched correlations were made and no proof of the implications of spines in learning in the hippocampus, although highly suspected (Bliss and Collingridge, 1993; Hebb, 1949; Konorski, 1948; Martin et al., 2000; Tsien, 2000), was given.

More than ten years later, the first *in vivo* study was published and established a clear link between LTP and learning in the hippocampus (Whitlock et al., 2006). Electrophysiological recordings were employed to capture activity in CA1 and stimulate Schaffer collaterals while rats performed an inhibitory avoidance task (IA). In this task, the rat can go from one illuminated to a dark chamber but receives a foot shock in the latter one. While an average response in CA1 remains unchanged after IA, multielectrode array recordings, which provide greater spatial precision, revealed that some synapses are potentiated while others are depressed, explaining the overall absence of difference. This study was then the first proof of a relationship between synaptic plasticity and learning, and thus memory storage in the hippocampus.

ii. Creating fear memories

A complementary proof of the involvement of LTP in memory formation in the hippocampus was the creation of fear memories using optogenetics.

Fear conditioning is one of the most straightforward tasks involving the hippocampus being used for investigating memories in labs (Cho et al., 2021; Choi et al., 2021; Ji and Maren, 2008; Johansen et al., 2010; Lai et al., 2018, 2012; Lovett-Barron et al., 2014; Sotres-Bayon et al., 2006, 2006). Notably, this behavior involves the amygdala, together with the hippocampus. Usually, a tone and a foot shock are associated with a specific context (information encoded in the hippocampus) in the amygdala, triggering a freezing response (Figure 14) (Kitamura et al., 2017; Sotres-Bayon et al., 2006).

The secret dream of many scientists is probably to localize a particular memory and to be able to manipulate it. One of the earliest, and perhaps most famous, studies of memory creation was published in 2013 by Ramirez et al. First, they expressed an optogenetic tool in a neuronal ensemble representing a fear memory of a foot shock in a given context in the dentate gyrus. When transferred to a new harmless context and upon reactivation of the described ensemble, mice specifically exhibit increased freezing behavior. This study demonstrated the possibility of associating a previous stimulus to a new context, creating "a false memory". This optogenetic manipulation recruited similar cascades of activation in different brain regions, especially the amygdala, that led to the expressed behavior (Liu et al., 2012; Ramirez et al., 2013).
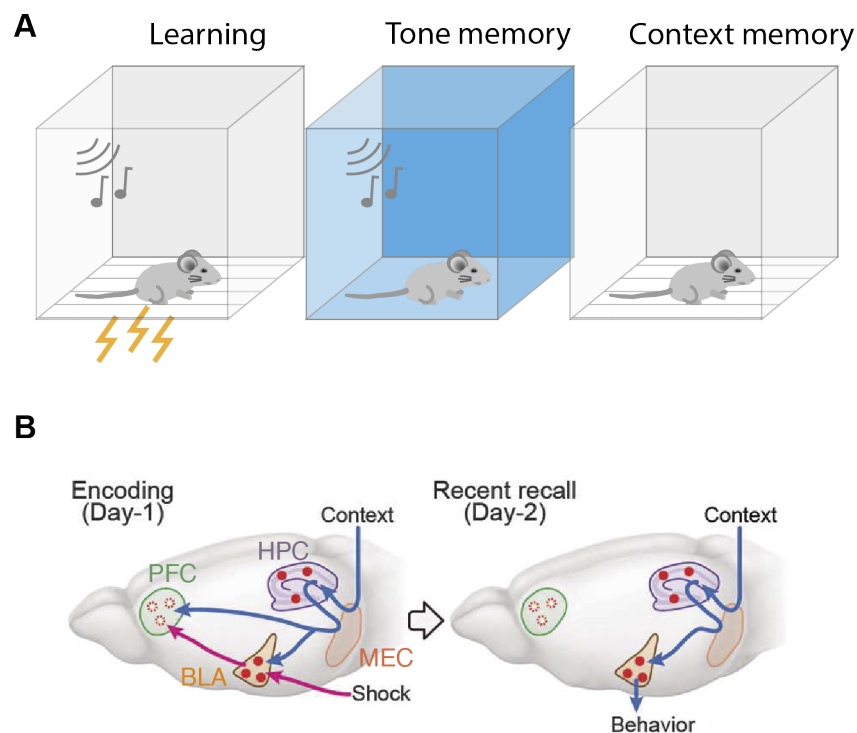
Figure 14. Fear conditioning. A. Schematic of fear conditioning task. An audio stimulus is paired with a foot shock in a conditioning box (left). The same audio stimulus is played in a new environment (middle). The mouse is placed in the conditioning box with no stimulus. **B.** Fear conditioning circuit involved the hippocampus and the amygdala. PFC: prefrontal cortex; BLA: basolateral amygdala; HPC: hippocampus; MEC: medial entorhinal cortex. *Figure from Kitamura et al., 2017.*

iii. Flexibility versus stability of memories

Yet, the question of how this memory is safely stored while new memories are formed, stability versus flexibility, is still unanswered (Abraham and Robins, 2005). As synapses are modified and formed during learning and thus memory is created, synapses have been considered the substrate of memory storage. Notably in the cortex, spiny synapses are maintained throughout life, and associated with lifelong memories (Yang et al., 2009). In the hippocampus, though, spines are found to have shorter lifetimes (Attardo et al., 2015b; Gu et al., 2014; Pfeiffer et al., 2018; Yang et al., 2021). Several explanations can be proposed.

On one hand, a small proportion of spines, underestimated by current studies, could be left unmodified, as resistant to LTP (Matsuzaki et al., 2004), and stored memories over longer periods before transfer to the cortex (Bontempi et al., 1999; Frankland and Bontempi, 2005; Marr and Brindley, 1997; McClelland et al., 1995; Squire, 1986; Teng and Squire, 1999). Yet, the choice of the synapses to modify and those to leave unmodified requires signaling to prevent the overwriting of old memories (Figure 15A). Simple Hebbian rules models do not allow for this choice, thus quickly saturating storage capacity and erasing old memories (Fusi, 2002; Fusi et al., 2005; Fusi and Abbott, 2007). New models of synaptic plasticity, can maintain memories at longer timescales (Magee and Grienberger, 2020).

On the other hand, spines could serve as the substrate for information transfer, while memories are rather integrated at the scale of dendrites. Various synaptic plasticity rules influence multiple spines at once, showing a relationship between synapses (Nishiyama and Yasuda, 2015). Additionally, the same axon has been shown to be connected to the same dendrite multiple times (Beniaguev et al., 2022; Knott et al., 2006; Markram et al., 1997). These synapses form functional clusters that support related information (El-Boustani et al., 2018; Frank et al., 2018; Hedrick et al., 2022). Relating multiple synapses to different information is challenging, especially if the axon transfers only one information, meaning that one dendrite receives identical information multiple times. Furthermore, the integration of inputs is dependent on the dendrites, inputs close to the soma are largely more influential on the neuron activity than inputs further away (Gulledge et al., 2005; Williams and Stuart, 2003). Diverse dendritic domains appeared to have different rules permitting input integration (Yaeger et al., 2022). This theory would mean that memory support resides in the pattern of connectivity more than in individual spines.

Finally, instead of storing memories at individual synapses through their weights, one could store information in the activity pattern between neurons (Figure 15B). This theory is notably highly supported by computational models. Maintenance of memories through fixed synaptic weight leads to "catastrophic forgetting" of previously stored information while creating new memories (Abraham and Robins, 2005; French, 1999; Robins, 2004; Sharkey and Sharkey, 1995). The introduction of

rehearsal permitted the reuse of approximated activity patterns, allowing both the stability of old memory traces and the integration of new ones (Robins, 2004; Robins and Frean, 1998).

Figure 15. Stability versus plasticity models for memory storage. A. Memory is stored in a defined circuit of fixed (top) or changing (bottom) synaptic weights (top). **B.** Memory is stored in the activity pattern of neurons. Darker dots indicate more active units and darker lines indicates stronger connection weights. *Figure taken from Abraham and Robins, 2005.*
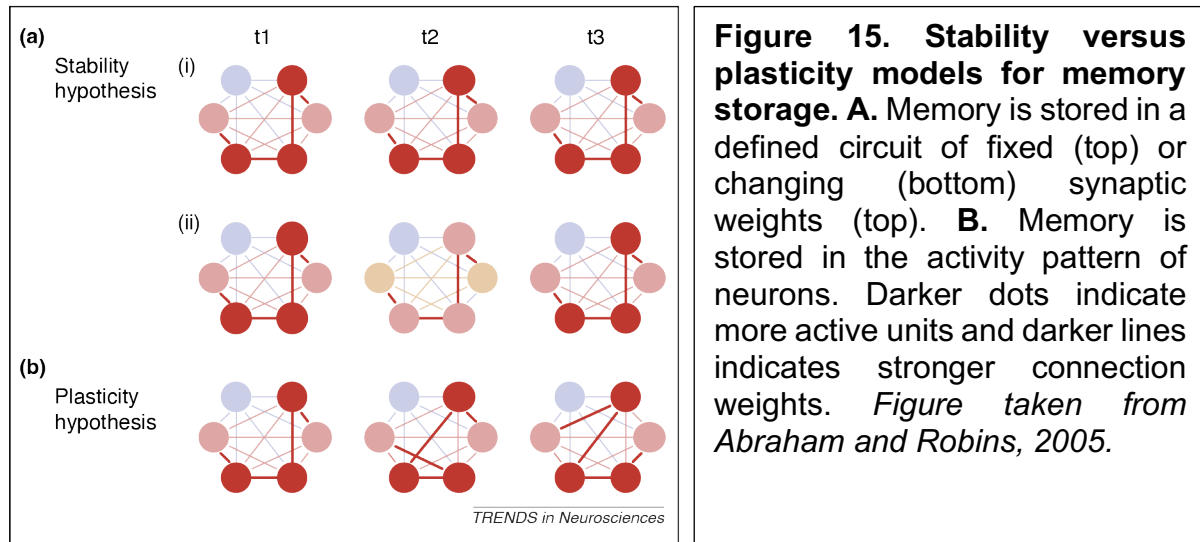
Despite various theories, no experimental proof has yet confirmed any of them. Nevertheless, experimental work on hippocampal spines suggests that the enhanced spine dynamics in the hippocampus are convincing as they correlate with the large drift in the representation of spatial memories observed in the hippocampus despite long-term storage of spatial memories.

b. Spatial navigation

i. Spatial tuning of cells in the hippocampus

The involvement of the hippocampus in spatial navigation was discovered using electrophysiological recordings in freely moving rats placed in an arena (O'Keefe and Dostrovsky, 1971). While recording those animals, 8 units showed increased firing rate specifically on precise spatial location and with precise head direction in the arena. These cells are thought to hold the information on the animal's position relative to its environment and are later called place cells.

Since this pioneering work, significant efforts have been devoted to understanding how place cells, cells exhibiting specific activity in particular spatial areas, are formed and maintained in the hippocampus, as well as investigating other types of cells associated with spatial navigation (Alme et al., 2014; Comrie et al., 2022; Kim et al., 2020; Moser et al., 2017, 2015; Nagelhus et al., 2023). Place cells are studied using different behavior apparatus (Eichenbaum et al., 1999), including mazes

(Grieves et al., 2016; Okada et al., 2017; Ormond and O'Keefe, 2022) and open arena (Kinsky et al., 2018).

Elucidating the circuit underpinning this behavior, two major inputs have been found for CA1 spatial representation. On one hand, the entorhinal cortex projecting to the dentate gyrus, CA3, and CA1 is known to convey information about the current sensory environment. On the other hand, CA3 is believed to play a role in maintaining the memory of the environment, representing its internal representation, and sending projections to CA1 in both hemispheres (Guan et al., 2021). By combining these inputs, CA1 represents the animal's position in its current environment (Martig and Mizumori, 2010; Otmakhova and Lisman, 1999). Additionally, CA1 receives other inputs such as dopaminergic inputs which are thought to be involved as reward prediction errors feedback when a reward is present in a task (Jang et al., 2019; Rouhani and Niv, 2021; Stanek et al., 2019).
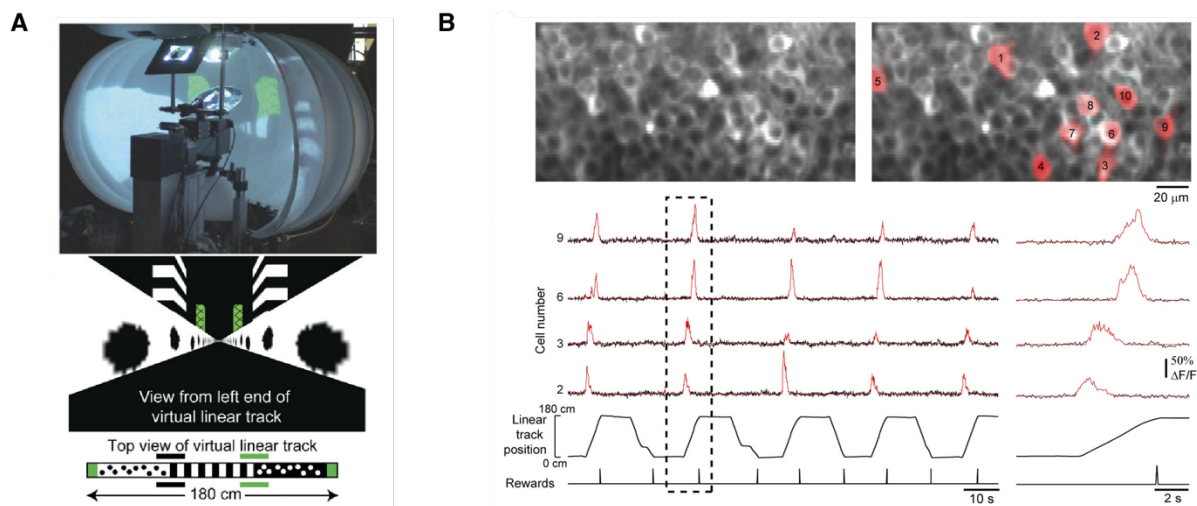
Figure 16. Two-photon imaging of CA1 place cells of a mouse running virtually along a linear track. A. Virtual environment setup (top) with a virtual linear track (bottom). **B.** Recordings on CA1 place cells using a calcium sensor. *Modified figure from Dombeck et al 2010.*

Besides place cells, reports mentioned the existence of head cells and reward cells in CA1, cells that are firing in the vicinity of a reward. When studied in the context of foraging or appetitive-goal-directed navigation, an overrepresentation of space around the reward location has been observed. This overrepresentation is constituted of "pure" place cells, "pure" reward cells but also of cells holding a mixed representation of reward and space, as shown when shifting the reward location in a virtual environment (Gauthier and Tank, 2018).

With the development of studies using calcium indicators, there arose a need for a head-fixed hippocampal-dependent behavioral task to facilitate two-photon

imaging. Two main ways were then used for recordings place cells in the hippocampus, although most labs use rewards as motivation for the mouse to navigate. One may use virtual reality and a floating ball on which a mouse can easily run (Figure 16). Conveniently, a virtual reality setup allows for consistency across runs but also rapid modifications of the virtual environment the mouse is navigating into (Adoff et al., 2021; Dombeck et al., 2010, 2007; Dupret et al., 2010; Gauthier and Tank, 2018; Go et al., 2021; Pettit et al., 2022). However, this method relies solely on visual inputs, which are believed to be less frequent sensory inputs used by mice. Instead, some labs, although a minority, use a linear treadmill with tactile or other types of cues (Geiller et al., 2022, 2017; Zemla et al., 2022). In both cases, calcium imaging enabled new ways to study spatial navigation in the hippocampus.

Once these place cells were discovered, the questions of how these place cells were formed, and more precisely by which plasticity mechanism, remain.

ii. Plasticity rules in place cell formation

While previously thought that induction of place cells was following Hebbian rules, meaning resulting from synchronous pre- and postsynaptic firing on a millisecond window, this plasticity window might appear physiologically not optimal. Recent studies have indicated that another type of synaptic plasticity might be responsible for induction at behaviorally relevant timescale, namely behavioral timescale synaptic plasticity (BTSP).

This process consists of a calcium plateau potential in dendritic processes, which increases synaptic weights during a several-second time window, representing a signal for plasticity induction, and a concomitant positional input that leads to the firing of the neuron. While this event is naturally occurring, it can also be triggered by generating a voltage ramp in CA1 neurons at a specific location during a single traversal, thus inducing a place cell (Bittner et al., 2017, 2015; Lee et al., 2012; Magee and Grienberger, 2020).

When exposed to a new environment, the plasticity window during which place cells can be easily induced is rather short, only consisting of a few traversals (Sheffield et al., 2017). Modifying already-formed place cells is even more challenging than inducing new ones. Indeed, it appears that after ~20 laps, there are almost no new place cells formed, suggesting that the plasticity window is then closed, preventing the formation of new place cells. This finding correlates with the increase in local inhibition in CA1 via somatostatin (SST) interneurons in the *stratum oriens*. Furthermore, hyperpolarization of interneurons in CA1 reduces the selectivity of spatial encoding (Grienberger et al., 2017). Both results suggest that local interneurons guide the formation of place cells and selectively increase inhibition to eliminate out-of-field

activity (Jeong and Singer, 2022; Manuel Valero et al., 2022). However, how this window is opened or closed is not clearly understood.
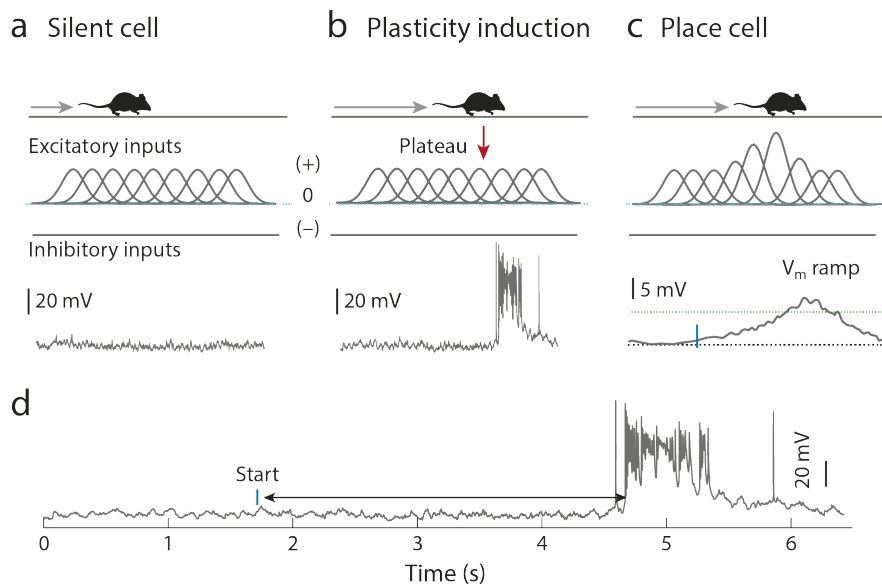
Figure 17. Formation of place cells through behavioral timescale synaptic plasticity. A. A silent cell receives excitatory inputs and balanced inhibitory activity. **B.** A plateau potential is initiated, leading to synaptic plasticity events. **C.** As a number of inputs increased in weight, a membrane potential (V_m) ramp is produced. **D.** Inputs are potentiated more than 4 seconds before producing a plateau. Green line: threshold for action potential. Blue line: Start of V_m ramp. *Figure and modified legend from Magee and Grienberger 2020.*

Since the creation of place cells was made plausible (Bittner et al., 2015), multiple studies have attempted to rewire place cells by manipulating CA1 cells' excitability (Diamantaki et al., 2018; Dudok and Szoboszlay, 2021; Fan et al., 2023; McKenzie et al., 2021; Robinson et al., 2020). Notably, using optogenetics and holographic stimulation, activating CA1 place cells that encode the reward zone led to a modification of the mouse behavior (Robinson et al., 2020). When investigated longitudinally, these methods consistently failed at inducing long-lasting place cells, as 4 out of 10 induced place cells were no longer present the following day (Fan et al., 2023).

To further understand the synaptic underpinning of place cells, the functional organization of spines and their relation to somatic activity has been recently published. While all place fields of an environment are represented at the synaptic level of an individual neuron, spines having the same place field as the somatic place field appear to be most likely clustered (Adoff et al., 2021). Whether and how these clusters are

changing over days and their relation to the place cell tuning switch remains to be determined.

iii. Stability of spatial representation in the hippocampus

The long-term representation of variables has been studied in various brain regions and has been a main research focus in recent years (Aitken et al., 2022; Aschauer et al., 2022; Bauer et al., 2024; Deitch et al., 2021; Driscoll et al., 2017; Felipe et al., 2020; Jensen et al., 2022; Margolis et al., 2012; Marks and Goard, 2021; Micou and O'Leary, 2023; Peron et al., 2015; Peters et al., 2014; Sadeh and Clopath, 2022; Wang et al., 2022; Ziv et al., 2013). So far, calcium imaging has shown that the hippocampus has been one of the brain regions with the higher drift in cellular representation with ~15% of CA1 cells being recurrently implicated in the same representation over a month in rodents (Ziv et al., 2013), while, for instance, little changes were reported in the motor cortex (Peron et al., 2015; Peters et al., 2014).
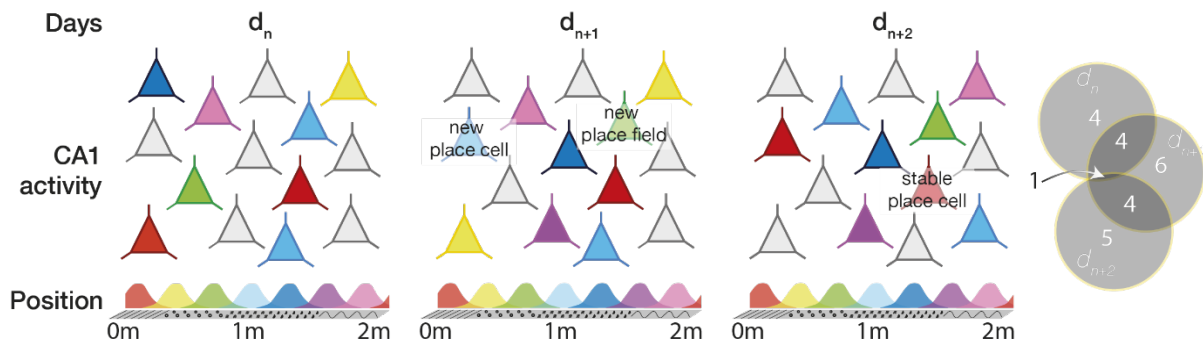
Figure 18. Fast remapping of CA1 place cells. New place cells are emerging on d_{n+1} and d_{n+2}. As well, place cells on d_n are changing place fields on d_{n+1} and d_{n+2}. Place cells on d_n are not engaged anymore on subsequent days. Overall, only a single place cell is stable over days.

Thus, the spatial representation of an environment appears unstable over days in the rodent hippocampus. Although exposed to the same environment over days, the neuronal representation is drifting. While recording CA1 in rats across days, Ziv et al. observed a drift in the representation despite a stable animal behavior performance. A fraction of neurons show place field remapping, although not necessarily randomly (Kinsky et al., 2018), while other neurons are being recruited into the representation (Figure 18). Since then, this result has been reproduced in different labs (Cholvin et al., 2021; Dong et al., 2021). Interestingly, an individual cell appears to have a recurrent innate activity level in different spatial tasks and across days (Hayashi et al., 2023).

Ensembles are not only dynamic in CA1 but also in other parts of the hippocampus. Yet, the overlap between days is different. In the dentate gyrus, little overlap has been reported between ensembles encoding the same behavioral task over days (Cholvin et al., 2021; Hainmueller and Bartos, 2018; Lamothe-Molina et al., 2022). Also, when comparing ensemble drifting between CA3 and CA1, it appears that representation in CA3 changes more slowly than in CA1 (Dong et al., 2021; Sheintuch et al., 2023).

One possible explanation is that the observed drift is due to intrinsic properties of CA1 cells. Still, this idea has been recently challenged by neuronal recording of hippocampal place cells in bats (Liberti et al., 2022). When trained to fly towards a reward, bats have much more reproducible flights than rodents running on a treadmill. Place cell ensembles, recorded in CA1, are minimally drifting over days, with map correlations higher than 0.6 after 10 days. Therefore, whether the cellular properties of the animals differ or the behavior is responsible for the drift is questioned.

Besides, older chronic electrophysiological recordings of freely moving rats reported little remapping in CA1 (O'Keefe et al., 1978; Thompson and Best, 1990; Tolman, 1948). Thus, a bias in the techniques (calcium imaging vs. electrophysiology) and the behavior (freely moving vs. head-fixed) used might be considered to understand the discrepancies.

While the cellular dynamics of hippocampal coding are being largely investigated in rodents, how information is encoded and preserved at the level of individual synapses during spatial navigation is less understood. Accordingly, the contribution of stochastic spine dynamics in representational drift in the hippocampus remains to be determined.

Aims of the studies

1. Project #1: Enhanced lifetime of Schaffer collaterals

The location of memory storage has long been the subject of debate. While studies have suggested that memories are stored in the dynamics of cellular activity, others have suggested that memories are stored in spines. To explore the latter possibility, the spine lifetime has been investigated in several brain areas, including in CA1, a key region implicated in memory formation and storage. So far, there has been no consensus among the studies. In particular, a recent study suggested that all spines eventually disappear with no distinction in the spine functionality. However, earlier *in vitro* studies identified the influence of synaptic strength on spine lifetime.

In this project, we asked the following questions:

1- Is there a relationship between morphology and function of CA1 spines *in vivo*?
2- Does connectivity strength influence spine turnover *in vivo*?

2. Project #2: Place cell remapping in the hippocampus

While place-specific activity has been found in different parts of the brain, the CA1 region of the hippocampus represents a central brain region for the encoding of space thanks to the existence of single cells that respond to fixed and precise locations in the environment, often called place cells. However, the precise cellular mechanisms governing the formation, stabilization and loss of place cell activity remain unclear. One key feature of place coding in the brain is the significant degree of place code remapping which occurs over days despite constant environment and stable animal behavior, a phenomenon often referred to as representational drift. While presynaptic regions to CA1, such as the nearby CA3 subdivision of the hippocampus, have been postulated to be possible drivers for place-code remapping, empirical evidence is still lacking.

Here, we thus asked two questions:

1- Is the drift of CA1 place cell representations accelerated by CA3 inputs?
2- Are CA3 inputs sufficient to generate novel place cells?

RESULTS

1. Project #1: Enhanced lifetime of Schaffer collaterals

a. Identification of postsynaptic CA1 neurons by optogenetic stimulation of presynaptic CA3 neurons.

To identify ipsilateral CA1 (ilCA1) spines connected to contralateral CA3 (clCA3) neurons, we sparsely labeled ilCA1 pyramidal neurons in adult mice with a cre-dependent calcium sensor, jGCaMP7b, and implanted a chronic hippocampal window. To elicit presynaptic action potentials, we implanted an optic fiber above clCA3 pyramidal neurons densely expressing the red light-activated optogenetic actuator ChrimsonR (Figure 19a, 20a-b). Next, mice were habituated to the microscope to enable head-fixed two-photon imaging during wakefulness. During the spine imaging sessions, the motion of the mice was recorded using a passive treadmill for closed-loop automated optogenetic stimulation in the absence of locomotion, thus minimizing motion artifacts (Figure 19b).

To maximize the number of spines we can record from, we first identified ilCA1 neurons receiving synaptic input from clCA3 neurons. Upon strong optogenetic stimulation in clCA3, a subset of ilCA1 neurons showed large, invariant calcium transients, while the remaining ilCA1 did not show detectable suprathreshold calcium events (Figure 19d-e). The robust and reproducible responses suggest reliable synaptic input from optogenetically activated clCA3 neurons without triggering global activation of CA1.
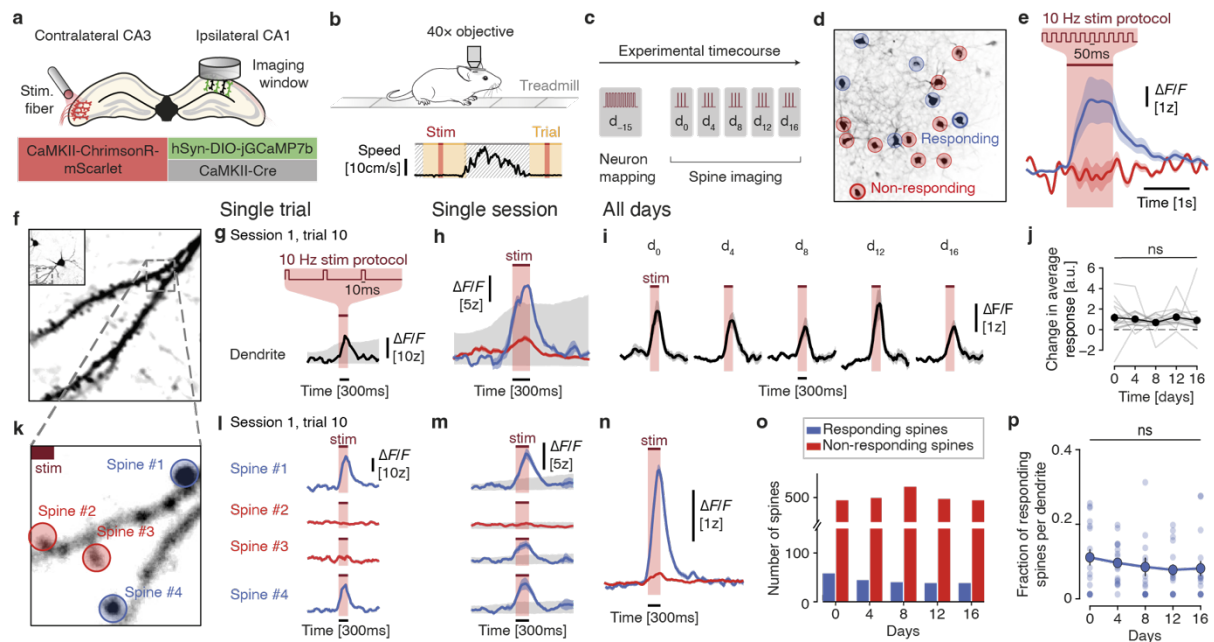
Figure 19. Identification of synaptically connected CA1 neurons by optogenetic stimulation of presynaptic CA3 neurons. a Schematic depicting injection in clCA3 and ilCA1 for sparse labeling and chronic implants. **b** Schematic depicting a treadmill recording motion from the mouse for closed-loop experiments under the two-photon microscope. **c** Experimental time-course of the experiment. **d** Example of a field of view with neurons responding (blue) and non-responding (red) to optogenetic stimulation. **e** Mean EPSCaTs from responding (blue) and non-responding (red) neurons in (d). Mean ± s.e.m. **f** Example of a field of view showing a dendrite from the neuron on inset. **g** Example of a trial of EPSCaTs in the dendrite upon subthreshold optogenetic stimulation. **h** Average responses from successful (blue) and unsuccessful (red) EPSCaTs in the dendrite during the session of (b). Mean ± s.e.m. **i** Averages of dendritic EPSCaTs across time of all dendrites. Mean ± s.e.m. **j** Changes in the average amplitudes of EPSCaTs in all dendrites. Repeated measures ANOVA. Mean ± s.e.m. **k** Zoom from (a) during the optogenetic trial in (b). **l** Calcium traces of four spines, as indicated in (f), during a single trial as in (b). Spines #1 and #3 show EPSCaTs, contrary to spines #2 and #4. **m** Average EPSCaTs from the four spines in (f) and (g). Three spines are classified as responding and one as non-responding during this session. Mean ± s.e.m. **n** Average EPSCaTs of daily-assessed responding spines (blue) and daily-assessed non-responding spines (red). **o** Number of daily-assessed responding (blue) and non-responding (red) spines over time. **p** Fraction of daily-assessed responding spines per dendrite over time. ANOVA with repeated measures. ns: non-significative.
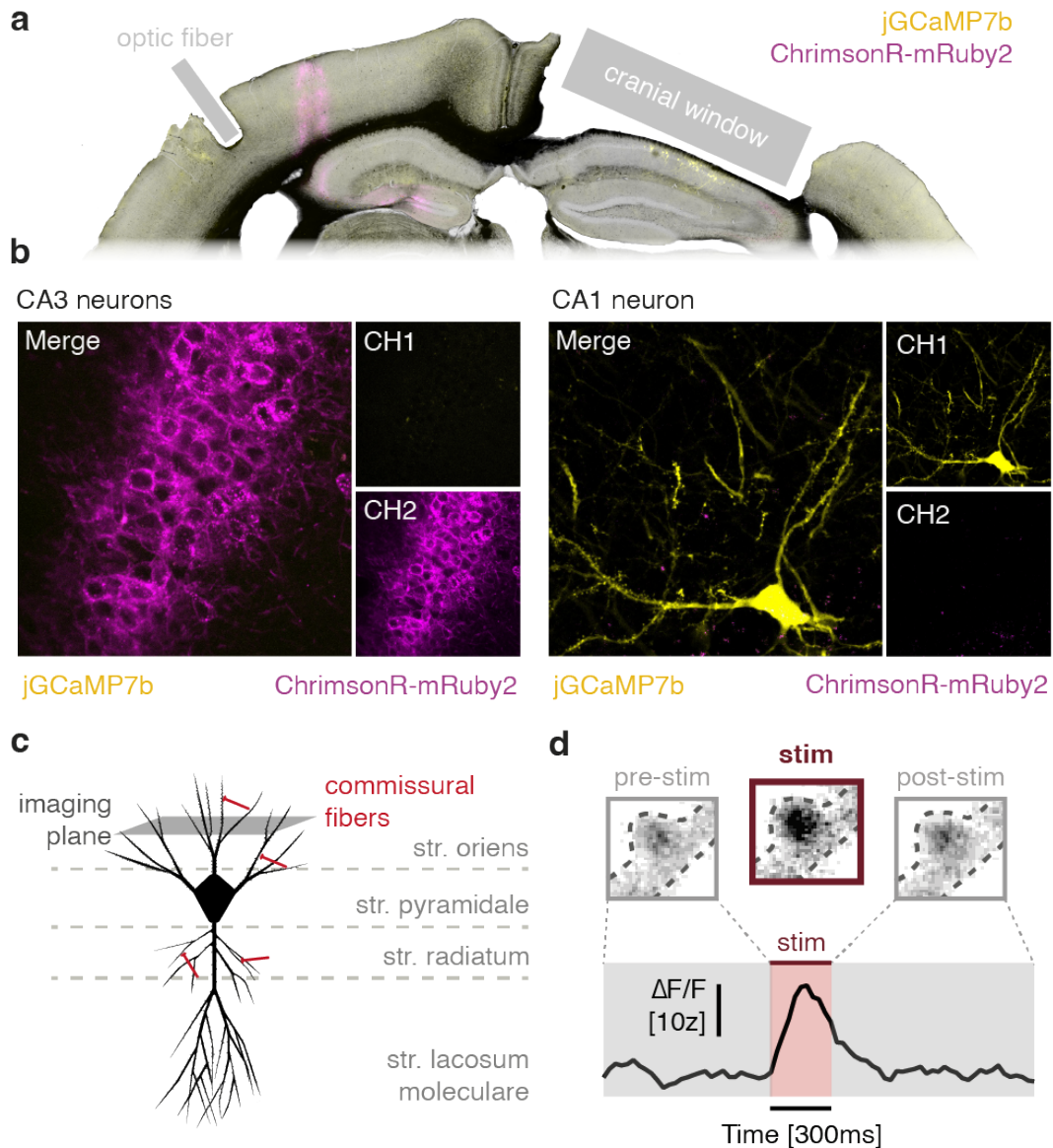
Figure 20. Imaging of spines in CA1. a Histology. clCA3 neurons express ChrimsonR-mRuby2 (magenta) and ilCA1 are sparsely expressing jGCaMP7b (yellow). An optic fiber is placed above clCA3 and a chronic window above ilCA1. **b** Confocal images of clCA3 and ilCA1 expressing neurons. ChrimsonR-mRuby2 and jGCaMP7b are respectively color-coded in magenta and yellow. **c** Schematic depicting ilCA1 neurons showing the imaging planes of dendrites in stratum *oriens*. **d** Example calcium trace of a single EPSCaT with corresponding t-projection before, during and after optogenetic stimulation.

To ensure that synaptic drive in ilCA1 was maintained constant across imaging sessions, we aimed to confirm that our optogenetic stimulation of clCA3 neurons was consistent over days. To do so, we injected five adult mice with ChrimsonR in clCA3 and non-conditional jGCaMP8m in ilCA1 for dense labeling (Figure 21a-b). In this way,

we could detect the population response in ilCA1 without being biased toward a small number of sparsely labeled neurons. We stimulated clCA3 neurons using the same protocol and recorded calcium responses from the same population of ilCA1 neurons every four days for over two weeks. We identified responding neurons in ilCA1 and analyzed their synaptically evoked calcium transients for all sessions. No difference in the mean amplitude was found over days, suggesting that overall optogenetically evoked synaptic transmission remained stable (Figure 21c-d). Thus, our experimental protocol enabled us to maintain stable synaptic transmission at Shaffer collateral synapses in awake mice for more than 2 weeks.
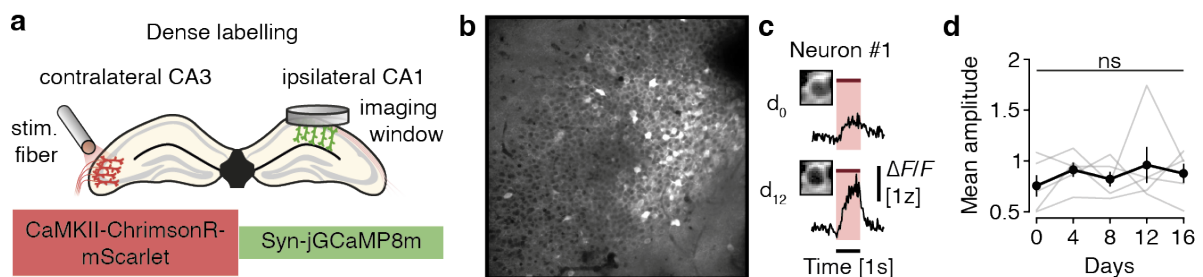
Figure 21. Stable optogenetic stimulation of ilCA1 over 2 weeks. a Schematic depicting the injections and chronic implants for dense labeling of ilCA1. **b** Example of a field of view of densely labelled neurons. **c** Averaged EPSCaTs from an example neuron on two timepoints. **d** Averaged mean amplitude of EPSCaTs over days of all responding neurons (n=5 mice, 387 neurons). Repeated measure ANOVA. ns: non-significant. Mean ± s.e.m.

b. Local spine calcium responses are evoked by subthreshold optogenetic stimulation of presynaptic neurons.

Since we aimed to investigate structural plasticity in functionally connected spines, we adjusted our optogenetic stimulation protocol such that optogenetically evoked excitatory postsynaptic calcium transients (EPSCaTs) could be identified while minimizing strong global calcium transients in the entire ilCA1 neuron, which could arise from suprathreshold depolarization and action potential backpropagation. With this protocol, most trials remained subthreshold, triggering dendritic events only in a small number of trials (5.90 ± 0.90 %) (Figure 19f-h). Keeping the stimulation protocol constant, we chronically recorded EPSCaTs in the same spines every four days over two weeks (Figure 19c, 20c). To verify the reliability of our adjusted optogenetic stimulation paradigm, we measured the average calcium transients over all trials across the entire dendrite, including suprathreshold events. Average calcium transients were similar across days (Figure 19i-j), validating the consistent stimulation of ilCA1 using this stimulation protocol.

To evaluate the calcium events fraction derived from specific synaptic inputs, for each spine calcium trace, the contribution of dendritic events was subtracted (Chen et al., 2013; Iacaruso et al., 2017). This method was effective in eliminating occasional weak induced dendritic calcium events that would lead to false-positive ESPCaTs in spines that did not receive synaptic input (Figure 19g). We thus could identify ilCA1 spines that received inputs from optogenetically stimulated clCA3 neurons (Figure 19k, l, 20d). As expected, spines were not showing EPSCaTs at every trial, given the low release probability of Schaffer collateral synapses. By averaging the postsynaptic responses of the entire session, we could successfully identify ilCA1 spines receiving inputs from clCA3 (Figure 19m-n) and distinguish them from spines not responding in that session.

When systematically following the same spines over sessions, we observed that most spines were responding only in one session and remained non-responding in the preceding or following sessions. (Figure 22a). A small fraction of spines showed responses in two (12.0%), three (4.6%) or four (1.1%) sessions (Figure 22b). Spines showing EPSCaTs for the first time were distributed among all sessions, with a slightly higher proportion exhibiting a first response on the first day of the experiment (Figure 22c). This suggests that functional connectivity gets reconfigured between sessions and therefore, individual synaptic inputs drift over time.

Given the drift at the single synapse level, we asked whether the total fraction of responding spines over days was stable, so that average synaptic input is preserved, as suggested from the overall stable dendritic responses. We measured the total number of daily-assessed responding spines (Figure 19o) and the fraction of responding spines per dendrite for every session (Figure 19p). We found that the fraction of daily-assessed responding spines remained stable across sessions, indicating that average dendritic input was preserved. This notion is further supported by a constant spine density across all sessions (Figure 22d). Taken together, we identified individual spines receiving synaptic input from clCA3 neurons. Synaptic inputs were highly variable over time at the level of a single synapse, but average dendritic input was maintained stable throughout our experiment.
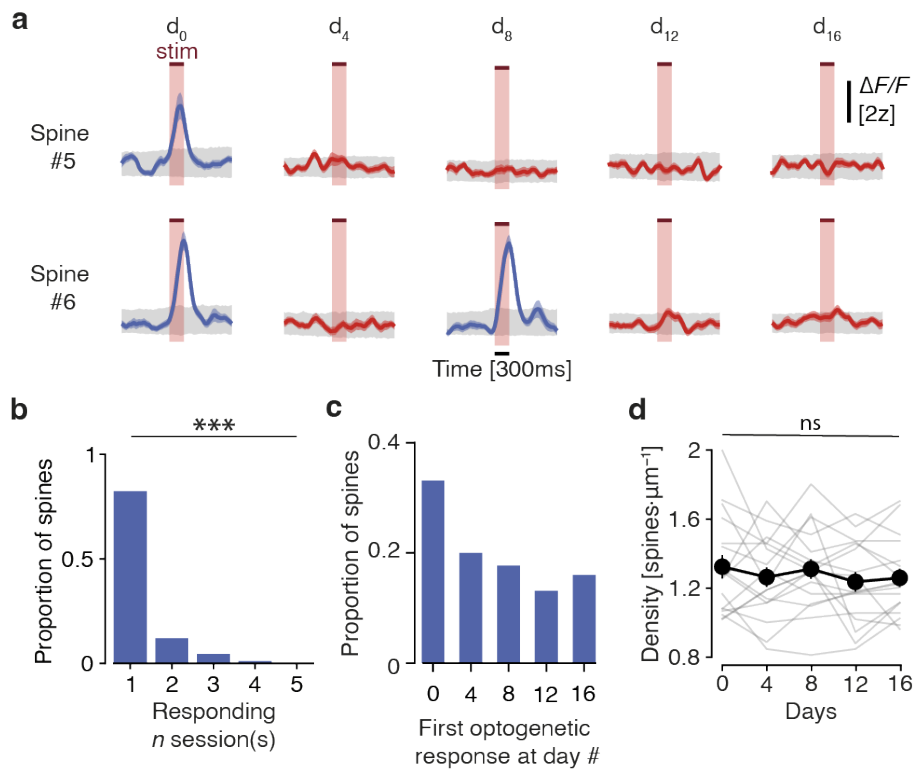
Figure 22. Responding spines mainly exhibit EPSCaTs within a single session. a Examples of responding status changing over time. Spine #5 is responding once while spine #6 is responding twice to optogenetic stimulation. Mean ± s.e.m. **b** Proportion of spines depending on responses frequency. Chi-square test. **c** Proportion of spines depending on their first day of EPSCaTs. **d** Spine density of recorded dendrites. Repeated measures ANOVA.Ns: non-significant Mean ± s.e.m.

c. Globally responding spines are strongly connected to presynaptic partners and tend to form clusters.

As we are able to identify a subset of spines that showed optogenetic postsynaptic calcium responses at least once (globally responding spines; 18.8% of all spines), we asked if this pool of ilCA1 spines is more strongly connected to their presynaptic partners compared to spines that never show any EPSCaTs (globally non-responding spines; 81.2% of all spines) (Figure 23a). It is generally thought that the volume of the spines is correlated to their synaptic strength (El-Boustani et al., 2018; Hedrick et al., 2022; Holtmaat et al., 2005). Therefore, we estimated head volumes of globally responding and non-responding spines from time series without optogenetic stimulation (Figure 23b) and found that the volume of globally responding spines was significantly larger than that of globally non-responding spines (Figure 23c), suggesting that globally responding spines are more strongly connected to their presynaptic partner. Indeed, the volume of globally responding spines was positively correlated to

46

the amplitude of EPSCaTs, further suggesting that large spines belong to stronger synapses than small spines, as previously shown (Figure 23d) (Huganir and Nicoll, 2013; Lee and Kirkwood, 2011; Matsuzaki et al., 2001; Noguchi et al., 2011; Takumi et al., 1999).
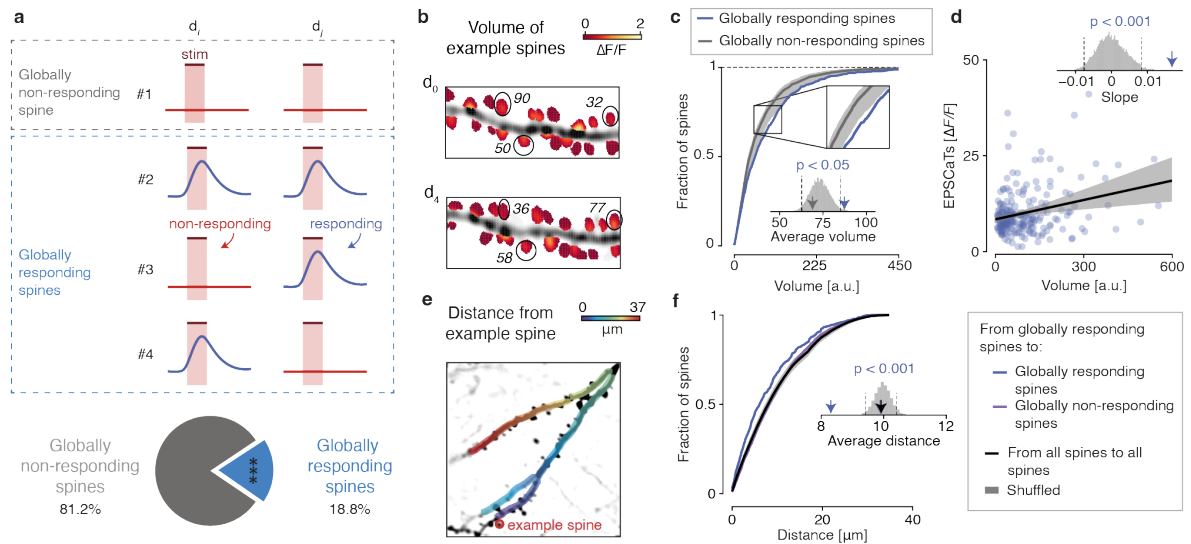
Figure 23. Globally responding spines have stronger connections and form clusters. a Fraction and definitions of globally responding and non-responding spines. Top: a globally non-responding spine never shows EPSCaTs and globally responding spines show at least once EPSCaTs. Bottom: total fraction of responsive spines. N=175 globally responding spines and 754 globally non-responding spines, 17 dendrites, 5 mice. Binomial test. ns: non-significant, ***: p < 0.001. **b** Example of spine volumes from a dendrite at two timepoints. The volume is derived from spine fluorescence relative to dendrite fluorescence. **c** Cumulative distributions of spine head volumes of globally responding (blue) and non-responding (dark grey) spines. Shuffled volumes indicated in shaded grey. **d** Correlation of EPSCaTs amplitude and volume of globally responding spines. Shuffled volumes indicated in shaded grey. **e** Distances separating the example spine to the other spines in dendritic length on example field of view of a dendrite. **f** Cumulative distributions of distances from globally responding spines. Shuffled volumes indicated in shaded grey.

To ensure that our spine volume estimate was not influenced by intracellular calcium levels, we acquired z-stacks at an isosbestic (calcium-independent) excitation wavelength (Figure 24a). We found a strong correlation between the two measures (Figure 24b-c), indicating that both strategies yielded comparable results. Additionally, we also controlled for the relationship between the volume obtained from the time series for all spines and calcium fluctuations during stimulation (Figure 24d). We did not find a significant correlation, suggesting that the estimated volume was not convolved by dynamic changes in brightness due to calcium fluctuations.

Next, we investigated the dendritic distribution of globally responding spines. Synaptic inputs have been shown to be clustered (Adoff et al., 2021; Hedrick et al., 2022) leading to efficient dendritic activation (Fu et al., 2012; Hedrick et al., 2022). Hence, we estimated the extent of spine clustering for globally responding spines, measuring the distance between spines (Figure 23e). Our comparison of the spatial spine distribution revealed closer spatial proximity among globally responding spines versus non-responding spines (Figure 23f). Therefore, functional inputs from a defined population of presynaptic neurons may form small functional clusters of spines on ilCA1 neurons.
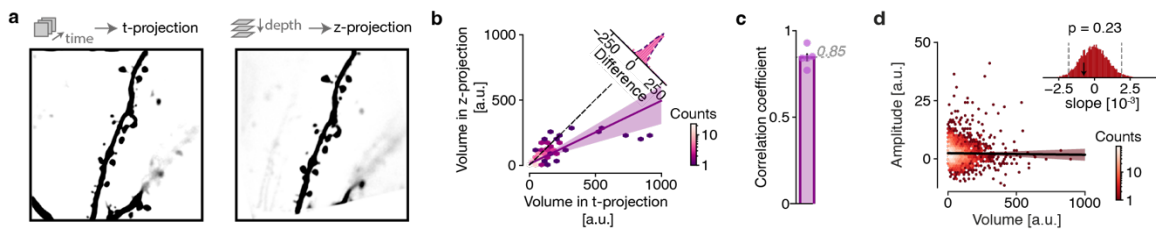
Figure 24. Spine volume estimated from the timeseries is independent from calcium activity. a Example projections from the same dendrite from the time series (t-projection) and from the stack (z-projection). **b** Correlation between the volume evaluated from z-projections and the volume from t-projections for all spines (n=164 spines, 4 dendrite, 5 sessions). **d** Correlation between head volume of spines and the amplitude of EPSCaTs. Null distribution of slopes. ***: p < 0.001.

d. Higher stability of globally responding spines

Since globally responding spines were larger and more clustered than randomly selected globally non-responding spines, we asked if they were more stable over time. We followed the same dendrite over 16 days and classified spines as persistent, transient, formed and eliminated according to the following criteria: Persistent spines were present during the entire time series, and transient spines appeared only temporarily and disappeared again during the time series. Formed spines appeared in one of the sessions and stayed until the end of the time series. Eliminated spines were present at the beginning of the time series and disappeared until the end of the time series. (Figure 25a). We first sorted spines into globally responding and non-responding spines and calculated their fractions in each of the four categories. We found that globally responding spines showed a higher persistent fraction and a lower fraction of formed spines compared to globally non-responding spines (Figure 25b). Moreover, both populations contained a large fraction of transient spines. In contrast to globally non-responding spines, the globally responding population of transient spines was often recurrent, that is, they disappeared and re-appeared at the same location of the dendrite on different days of the experiment (Fig. 25c). Recurrence was

lower in the population of transient globally non-responding spines. In contrast, the number of flips (transient elimination and reappearance) was similar between transient globally responding and globally non-responding spines.
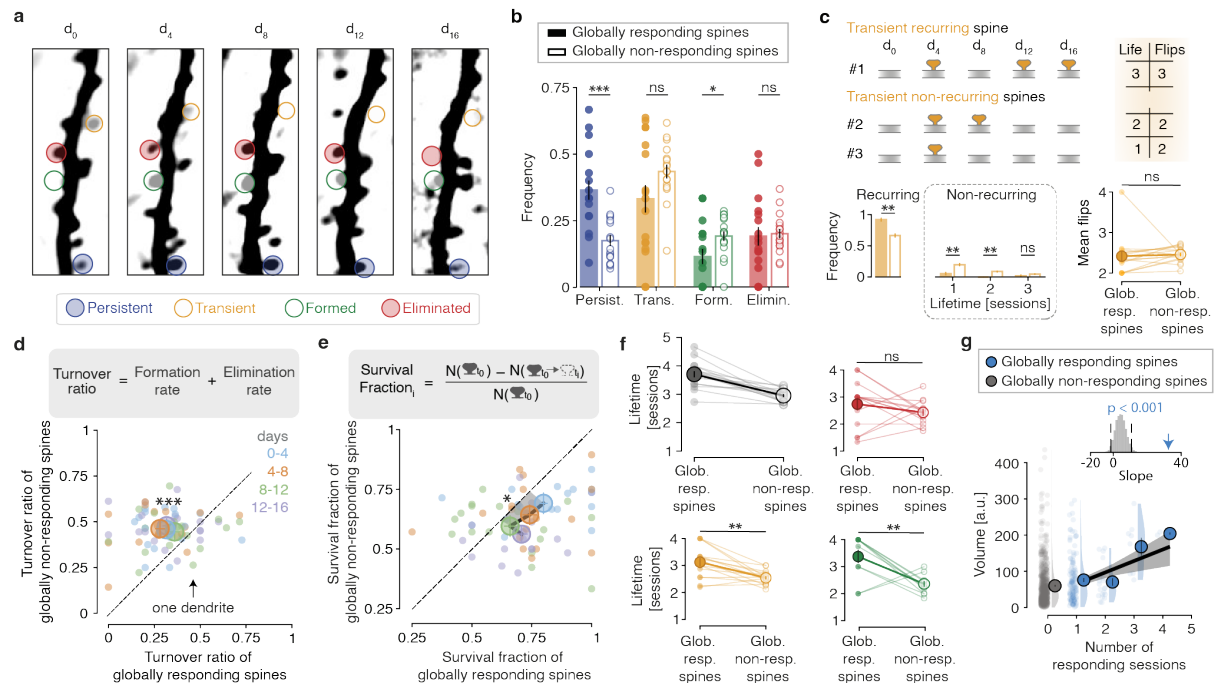
Figure 25. Enhanced stability of globally responding spines. a Example t-projections of dendrite over time with examples of persistent (blue), formed (green), eliminated (red), transient (yellow) spines. **b** Frequency of different types of spines for globally responding (filled) and non-responding (empty) spines. Paired t-test. Each dot represents a dendrite. **c** Characteristics of transient spines. Paired t-test with Bonferroni correction. Mean ± s.e.m. **d** Turnover ratio of globally responding versus non-responding spines over days. Repeated measures ANOVA. Mean ± s.e.m. **e** Survival fraction of globally responding versus non-responding spines across days. Repeated measures ANOVA. Mean ± s.e.m. Each dot represents a dendrite. **f** Lifetime of different types of spines for globally responding (filled) and non-responding (empty) spines. Paired t-test with Bonferroni correction. **g** Correlation between spine head volume and number of responding sessions. Shuffled data indicated in shaded grey. ns: non-significant, * $p < 0.05$, ** $p < 0.01$, *** $p < 0.001$.

To further characterize the dynamics of globally responding and globally non-responding spines, we analyzed different properties related to life expectancy in more detail. First, we assessed the turnover ratio, which is the sum of the formation and elimination rates between two imaging sessions. As predicted from the larger fraction of persistent spines in the globally responding population, we found the overall turnover

ratio to be lower for each imaging period (Fig. 25d). Moreover, an invariant turnover ratio in both populations shows that optogenetic stimulation does not influence spine stability per se – as previously demonstrated (Fig. 22d).
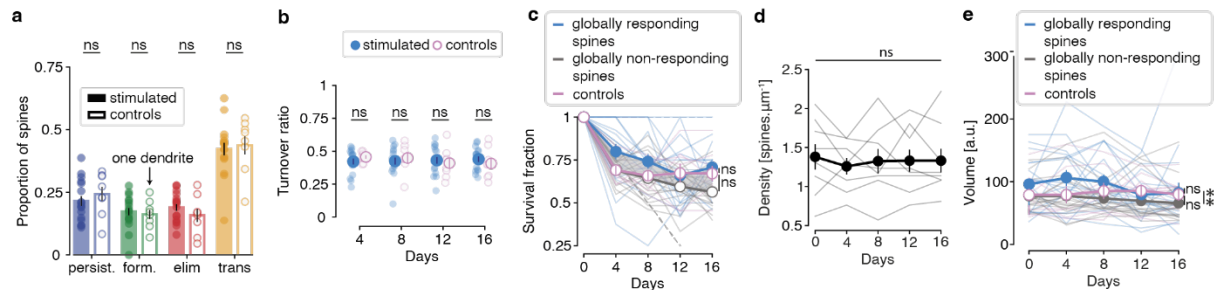
Figure 26. No difference in the overall stability of spines of controls and chronically optogenetically-stimulated dendrites. a Proportion of different types of spines for controls and optogenetically-stimulated dendrites. Unpaired t-test. N = 8 dendrites. Mean ± s.e.m. Each dot represents a dendrite. **b** Turnover ratio of stimulated dendrites and controls over days. Welch unpaired t-test **c** Survival fractions of control, globally responding and non-responding spines. Repeated measures ANOVA. **d** Density of spines for control dendrites. Repeated measure ANOVA. **e** Volume of spines for control, globally responding and non-responding spines. Repeated measure ANOVA. ns: non-significant.

We further confirmed that our chronic subthreshold optogenetic stimulation protocol does not influence spine stability. For this purpose, we compared the overall stability of spines from the optogenetically-stimulated dendrites to dendrites that were never stimulated in control animals (n = 8 control dendrites, 2 mice). We found identical distributions of the four different spine categories (Figure 26a), indicating that optogenetic stimulation has no global effect on spine dynamics. Furthermore, we found no difference in the turnover ratio or survival fraction between spines on optogenetically stimulated and control dendrites (Figure 26b-c). Thus, similar to optogenetically stimulated dendrites (Fig. 26d), the spine density on control dendrites remained stable over days (Figure 26d). Finally, there was no difference in spine volume of globally responding and non-responding spines versus control (Figure 26e). In addition to the stable amplitude of EPSCaTs in dendrites (Figure 19i), those results indicate that the optogenetic stimulation did not evoke any overall significant changes over time, but rather served to identify strong existing synaptic connections.
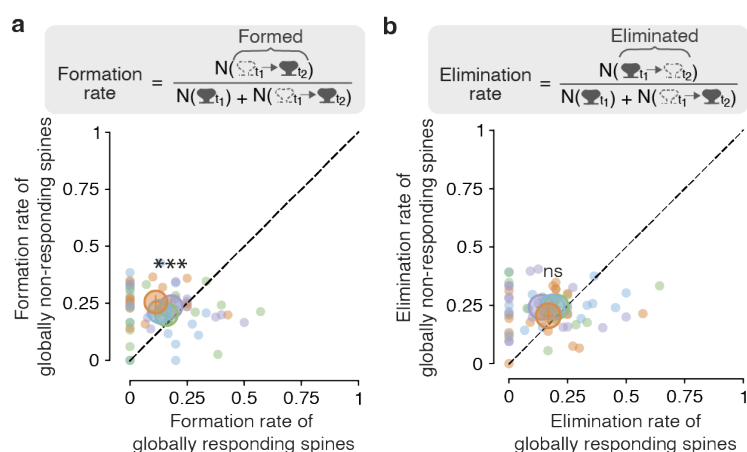
Figure 27. Spine turnover of globally responding spines is exclusively influenced by the formation rate. a Formation rate and **b** elimination rate of globally responding versus non-responding spines over days. Repeated measures ANOVA. Mean ± s.e.m.

In agreement with the lower number of formed spines, the formation rate of globally responding spines was decreased compared to globally non-responding spines (Figure 27a). In contrast, the elimination rates for globally responding and non-responding spines were similar over days (Figure 27b). Both the formation and elimination rates remained stable in both populations over days, in agreement with the constant turnover ratios over time. A high turnover ratio could also be explained by a high formation rate of new spines without altered stability of existing spines. To address this question, we measured the survival fraction of all initially identified spines for each imaging time point. We found that the survival fraction of globally responding spines was consistently higher than that of globally non-responding spines, further confirming the higher stability of globally responding spines (Figure 25e). The increased stability of globally responding spines, and thus extended lifetime (Figure 25f) could be solely explained by the larger fraction of persistent spines in that population. Therefore, we asked whether lifetime is generally higher in spines when they were globally responding by measuring the lifetime of all non-persistent spines. Indeed, those spines that formed during the experiment (transient & formed) showed a longer average lifetime when they were globally responding to the presynaptic optogenetic stimulation. Thus, globally responding spines, which tend to be stronger than globally non-responding ones, display an overall longer lifetime.

As indicated above, globally responding spines did not display evoked activity in all imaging sessions. Thus, we asked whether spine volume was correlated with the frequency of responses (i.e., the number of imaging sessions in which there was a response). We found a significant positive correlation (Figure 25g) between the frequency of responses and the average volume of globally responding spines, confirming the relationship between spine volume, functional connectivity and stability. To test this relationship further, we categorized all spines, irrespective of their activity, as persistent, transient, formed and eliminated and tested the spine volume distribution in each category, hypothesizing that persistent spines should have a larger volume –

suggesting indirectly that they are stronger than non-persistent ones. In total, approx. 20 % of all spines were persistent (19.7%) during the 16-day imaging period, while almost half were transient (45.6%). The remaining spines were almost equally constituting formed (16.9%) and eliminated fractions (17.8%, Figure 28a).
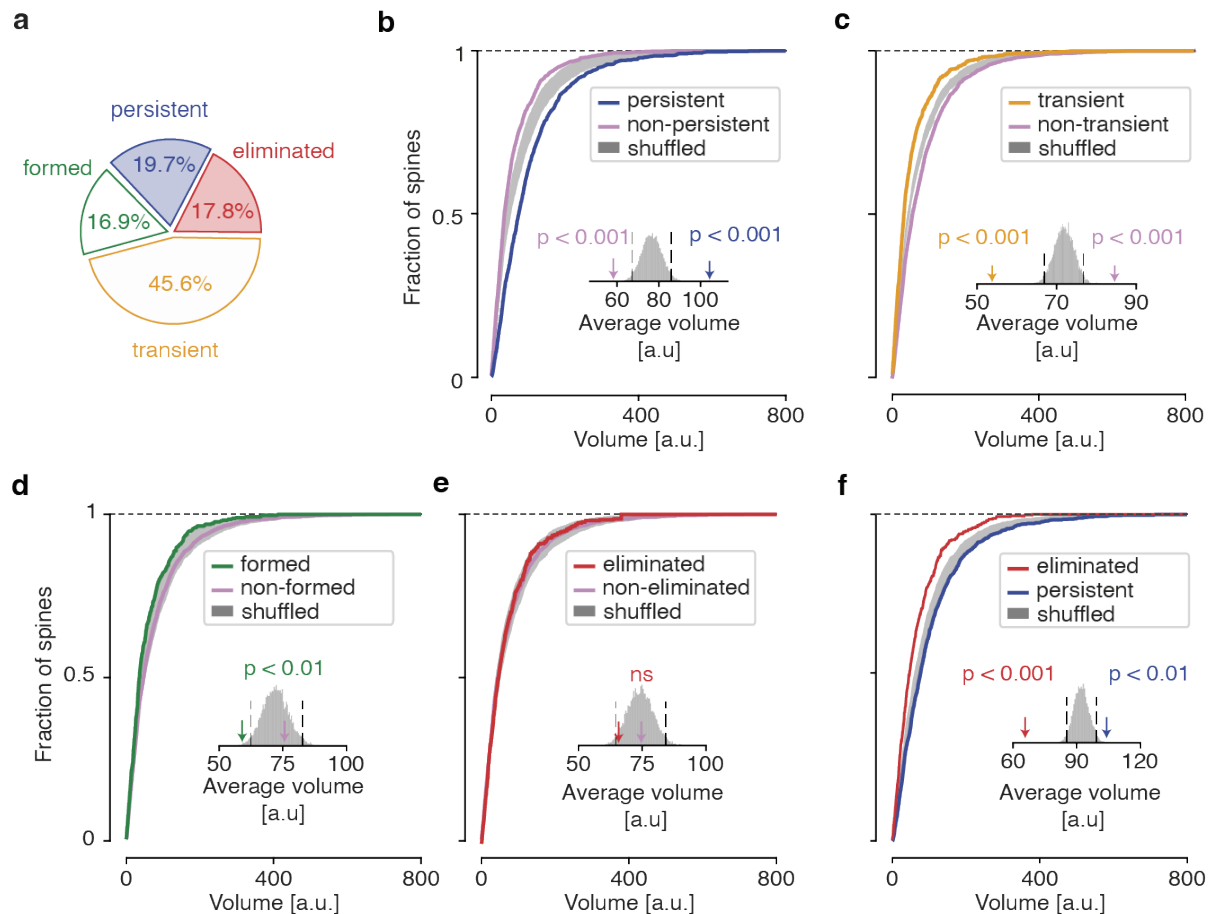
Figure 28. Large spines have extended stability. a Percentages of the different types of spines (persistent, formed, transient and eliminated). **b-e** Cumulative distributions of the head volumes of persistent (**b**), transient (**c**), formed (**d**) and eliminated (**e**) versus other (pink) spines. **f** Cumulative distributions of the head volumes of persistent versus eliminated spines. Shuffled volumes are indicated in shaded grey.

When comparing the head volumes of persistent spines to all other non-persistent spines, we found that persistent spines were significantly larger (Figure 28b), in agreement with previous work (Holtmaat et al., 2005). In contrast, the head volume of transient and formed spines was smaller than the remaining spines, in line with a lower strength and weaker integration of newly formed synapses (Figure 28c, d). In particular, the formed spines appeared as the weakest, given their small size

compared to the large remaining population of spines, containing a large portion of transient spines. Eliminated spines showed no significant difference from all other spines (Figure 28e). However, since the remaining population is dominated by small formed and transient spines, this indicates that also eliminated spines tend to be smaller than persistent ones. Indeed, a direct comparison between the eliminated and persistent categories confirmed that eliminated spines are associated with a smaller volume (Figure 28f). In conclusion, persistent spines have larger head volumes than non-persistent spines of all categories – suggesting a stronger connection to their presynaptic partners, while non-persistent spines were likely less strongly connected.

We also analyzed the spatial distribution of the four spine categories and found a shorter distance between persistent spines compared to their distance to other spines (Figure 29a), suggesting that persistent spines tend to cluster together. In comparison, no difference was found in the distance between transient spines (Figure 29b) or eliminated spines (Figure 29d). Notably, newly formed spines appeared closer to other spines than to each other (Figure 29c), suggesting that they preferably form near existing synapses.
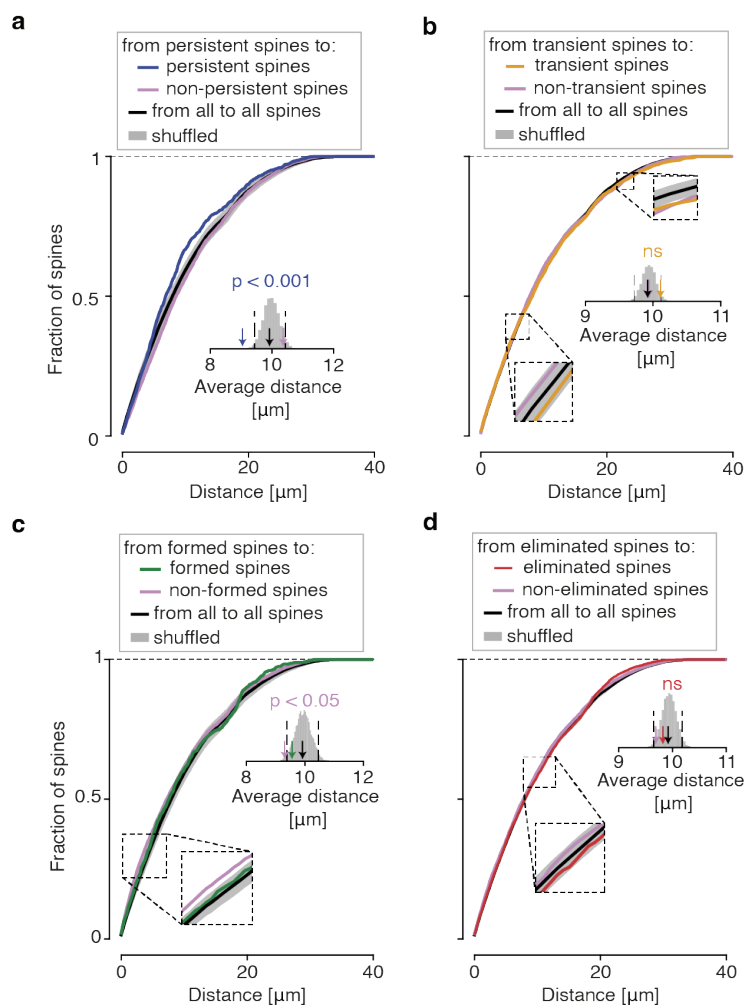
Figure 29. Persistent spines form clusters. a-d Cumulative distributions of distances between persistent spines, transient spines, formed spines and eliminated spines compared to the distances to the other spines. Shuffled distances are indicated in shaded grey.

Taken together, we demonstrate a close relationship between spine size, functional connectivity and spine stability at Schaffer collateral synapses in vivo. Globally responding synapses are stable and show a clustered organization, thereby maintaining connectivity between pre- and postsynaptic neurons.

2. Project #2: Place cell remapping in the hippocampus

  a. Combined two-photon imaging and optogenetic stimulation in mice performing a spatial navigation task.

To monitor ilCA1 activity, we densely labeled ilCA1 pyramidal neurons in adult mice with non-conditionally expressed jGCaMP8m and implanted a chronic hippocampal window. In the same animals, we optically manipulated clCA3 inputs to ilCA1 by expressing the red light-activated soma-targeted opsin, ChrimsonR, and delivered light through an implanted optic fiber (Figure 30a). Post-mortem histology validated efficient targeting of the desired hippocampal subregions (Figure 30b). Head-fixed, water-deprived mice were trained to collect a water drop by licking at a given location along a 2m linear treadmill divided into five distinct tactile cue sections (Figure 30c). Each session was divided into three consecutive blocks: 20 laps before light delivery (sham or optogenetic stimulation; pre), 10 laps with light delivery (sham or optogenetic stimulation; stim), and 20+ laps post light delivery (sham or optogenetic stimulation; post). To reduce the off-target effects of light delivery on behavior and place representation in sessions with optogenetic stimulation, mice were habituated to light delivery during the training sessions (5-10 days) and on the experimental days before and after the optogenetic stimulation (d_1 and d_3), by applying extracranial light delivery (hereafter referred to as sham stimulation) randomly in one of four possible locations on the treadmill. Once mice reached an expert level (continuous running for at least 50 laps and average lick selectivity greater than 0.8) in the task, CA1 activity was first recorded without CA3 optogenetic activation (day before). To compare the effect of CA3 optogenetic stimulation to baseline and to inspect the long-term effects of the stimulation protocol, we recorded CA1 activity on the days before and after CA3 activation.

After training, mice slowed down upon approaching the reward zone, a pattern that was unaffected by light delivery (sham or optogenetic stimulation, Figure 31a). Moreover, mice also exhibited anticipatory and zone-specific licking (Figure 31b). Taken together, the running and licking behaviors demonstrate that the mice have learned the task and the location of the water reward.
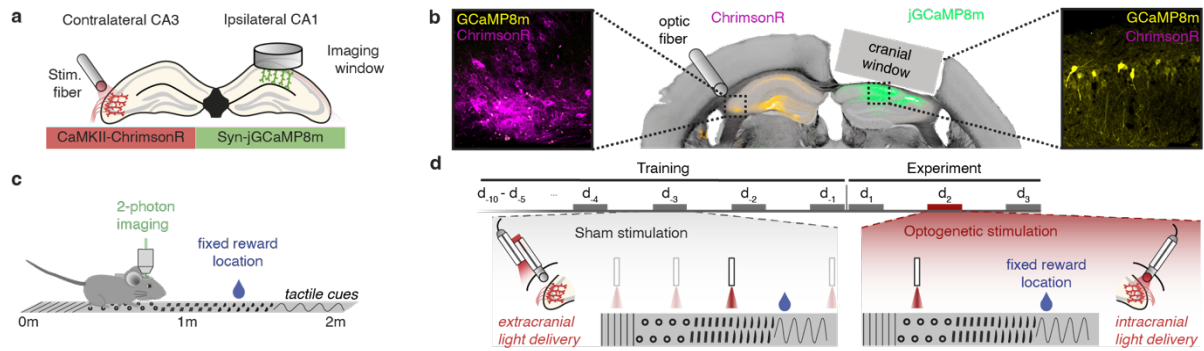
Figure 30. Combined two-photon imaging and optogenetic stimulation in mice performing a spatial navigation task. a Schematic depicting virus injection in clCA3 and ilCA1 and chronic implants. **b** Expression of injected virus construct GCaMP8m (yellow) in CA1 and ChrimsonR (magenta) in CA3. **c** Schematic depicting the spatial navigation task performed by head-fixed, water-deprived mice under the two-photon microscope. **d** Experimental timeline with light delivery conditions across days. Except on optogenetic stimulation day (red, d_2), extracranial light was delivered at one of the four random locations on the treadmill (grey). On the optogenetic stimulation day, intracranial light was delivered at a fixed location.

To confirm the absence of non-specific effects of optogenetic stimulation on behavior, we compared the speed and lick selectivity in conditions with and without optogenetic stimulation. First, speed in laps during and post-optogenetic stimulation was compared to the speed in laps pre-stimulation. A small, but insignificant, deceleration was found when stimulating CA3 neurons (opto sessions, Figure 31c-d). Moreover, specific licking behavior was mostly preserved across trials, with licking mostly occurring within a region of less than 40cm of the belt. Licking behavior was unaffected by light delivery, whether in sham or opto sessions (Figure 31e-f). Thus, optogenetic stimulation of clCA3 did not generally alter running and licking behavior.
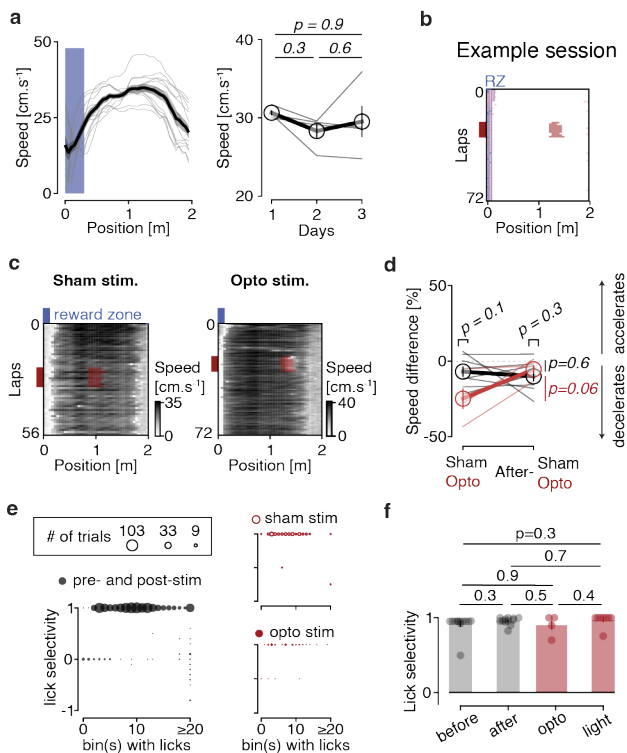
Figure 31. Behavioral performance of mice in a spatial navigation task. a Average speed across sessions. Mean ± s.e.m. Paired t-test with Bonferonni correction **b** Example session with licking behavior. Mice licking shows a high selectivity for the reward zone. **c** Example of speed in control (left, sham light) and optogenetic stimulation days (right, opto light). Optogenetic stimulation is indicated in shaded red. **d** Speed difference relative to speed pre-stimulation in sham (grey) or optogenetic stimulation condition (opto, red). Unpaired t-test with Bonferroni correction. **e** Lick selectivity in different conditions (bins = 2cm). **f** Comparison of lick selectivity across conditions (before and after stimulation, during optogenetic stimulation and sham light delivery) on 2cm bins. Mean ± s.e.m. Unpaired t-test.

b. Longitudinal recording of CA1 place cells

We next examined the calcium activity of ilCA1 cells to confirm the existence of place cells while mice performed the spatial navigation task (Figure 32a). Place cells were independently identified (Figure 32b, see Methods) on the distinct parts of each day (pre- and post-stimulation). As the CA1 place code has been shown to drift across days (Hainmueller and Bartos, 2018; Ziv et al., 2013), we then asked to which extent place coding was modified in our recordings. Ranking place cells according to their preferred location on a different day showed a large place code remapping over time (Figure 32c), as previously demonstrated (Ziv et al., 2013). Individually, only 5.6% of place cells were preserved over the three consecutive days, while 21% were present at least for 2 days and the main fraction, 73.4% of place cells did not qualify as place cells on more than one day. This phenomenon indicates extensive synaptic fluctuations across days. Comparing the correlation of the cross-validated cell × position activity maps shows that particularly the place code obtained on the days before and after optogenetic clCA3 stimulation was significantly different from the place code obtained on the stimulation day (Figure 32d). As the place code on the stimulation day was particularly different, we next investigated if place cells were newly induced following optogenetic stimulation of clCA3 inputs.
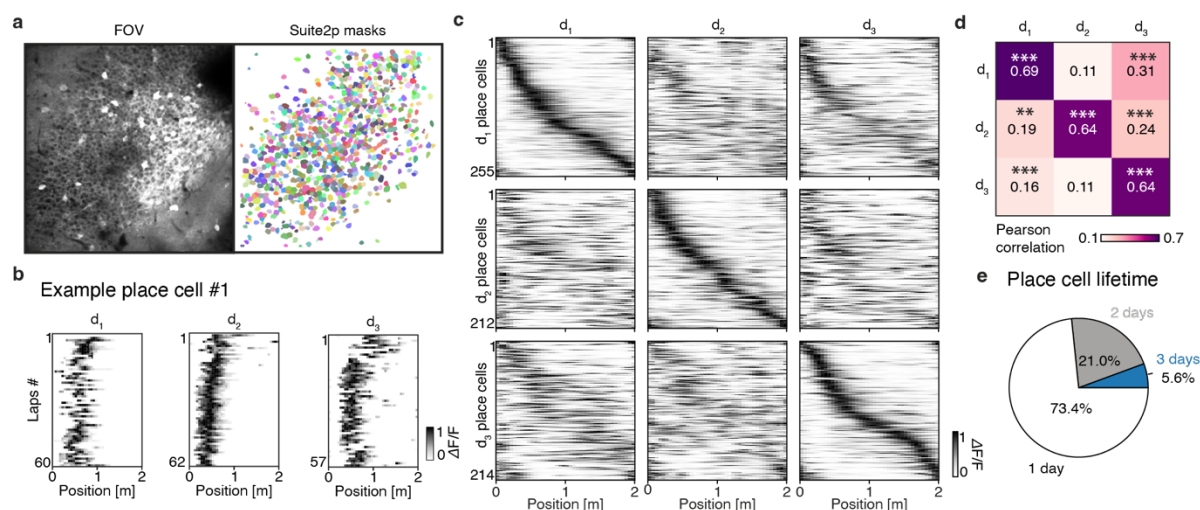
Figure 32. Longitudinal ilCA1 place cells recording. a Example field of view expressing jGCaMP8m in CA1 (left) and corresponding suite2p ROIs masks (right). **b** Place fields of an example place cell with similar place tuning across days. **c** Place fields of place cells identified separately in each individual day. The vertical ordering of place cells is cross-validated (defined on odd/even laps and applied on even/odd laps respectively) on the day they are identified; the order is then applied on the other days. **d** Pearson correlation between position × cell maps in (c). **e** Place cell lifetime.

c. Induction of CA1 place cells upon CA3 optogenetic stimulation.

To manipulate inputs to ilCA1, we elicited presynaptic firing of clCA3 neurons and recorded postsynaptic responses in ilCA1. ~20% of all recorded ilCA1 cells demonstrated a specific increase in calcium activity during optogenetic stimulation compared to sham light only (~10%; Figure 33a-c; see Methods), indicating that a significant fraction of cells responded to optogenetic stimulation only. We then looked specifically for place cells appearing in the post-stimulation laps (absent in pre laps). Out of these 94 new place cells, only 10 specifically responded to the optogenetic stimulation (Figure 33d), indicating that place cells can emerge either in during or post-stimulation at the optogenetic stimulation or on another location on the treadmill. Several induced place cells appeared on the different days post-stimulation (10 cells on sham days, 13 cells on the stimulation day and one of the sham days and 1 cell on all days). As those place cells are not present in the pre laps, they are specifically re-induced following light stimulation. Thus, neurons could be classified in a 2 × 3 taxonomy depending on their response to optogenetic stimulation (yes or no) and place coding (early, induced, or non-place cells) (Figure 33e). As already described previously (Bittner et al., 2015; Geiller et al., 2022; McKenzie et al., 2021), we hypothesized that induced place cells could exhibit place fields in different positions on the treadmill. We thus compared the overall place representation or early vs. induced

place cells across days (Figure 33f). No significant difference in the overall place representation was found, although a small, but not significant, increase in place representation in the first part of the treadmill, close to the reward zone, could be observed (Figure 33g, h).
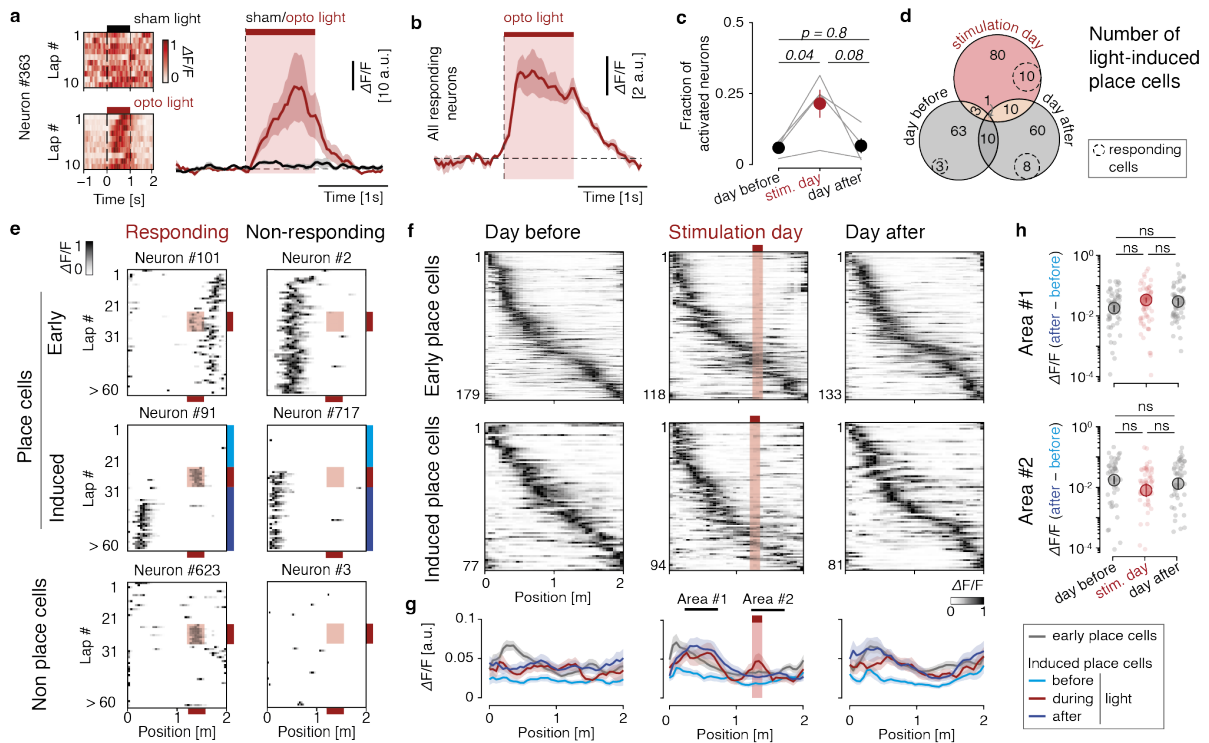
Figure 33. Induction of CA1 place cells after CA3 optogenetic stimulation. a Responses to sham (black)/optogenetic (red) stimulation of an example CA1 responding cell for each individual lap (left) and averaged over laps (right). Optogenetic stimulation is indicated in shaded red. Mean ± s.e.m. **b** Average responses of all responding cells (n=4 mice). Optogenetic stimulation is indicated in shaded red. Mean ± s.e.m. **c** Fraction of light-activated (sham or opto) cells across days. Paired t-test with Bonferroni correction. Mean ± s.e.m. **d** Number of light-induced place cells across days. Numbers of responding place cells among light-induced are indicated by dotted circles. **e** Examples of different types of cells depending on their response to optogenetic stimulation (responding vs. non-responding) and trial induction (early vs. induced vs. non place cell). Position and laps of optogenetic stimulation is indicated in shaded red. **f** Cross-validated maps of early (top) and induced (bottom) place cells across days. Position of optogenetic stimulation is indicated in shaded red. **g** Place tuning following induction of place cells in (**f**). Mean ± s.e.m. **h** Mean ΔF/F in Area #1 (top) and #2 (bottom) as defined in (**g**) across days. Unpaired t-test. Mean ± s.e.m.

d. Perturbation of early CA1 population place code by CA3 optogenetic activation

Given that induced place cells did not specifically and reproducibly map onto precise regions along the treadmill, we thus asked whether alteration of CA1 inputs by optogenetic activation of CA3 induced a more diffuse change at the population level. We addressed this question using two separate approaches.

First, we probed the stability of population place coding, by correlating population vector codes in pre vs. post light delivery (excluding laps with sham or optogenetic stimulation; see Methods) (Figure 34a, b). The resulting close-to-diagonal matrices indicate that population vector codes are stable within a session and are more likely to generalize to nearby positions. However, this stability property seemed disrupted on the optogenetic stimulation day, whereby correlation coefficients along the diagonal were smaller on days with stimulation compared to days without optogenetic stimulation (both before and after). As the potential loss of place tuning of some early place cells could explain a loss of stability in population vector codes, we computed correlation maps using only sustained early place cells, defined as cells exhibiting place tuning both pre- and post-stimulation. Again, the place code was less stable on the stimulation day compared to days without stimulation (Figure 34c). Altogether, our results demonstrate that, while place coding is perturbed by the optogenetically-induced alteration of clCA3 inputs, this perturbation has no long-term consequences on the following day (Figure 34d).

To further confirm this result, we aimed to assess whether the information carried at the population level before stimulation could still accurately determine the position of the animal once the optogenetic stimulation had occurred. To this end, we trained a Bayesian decoder to estimate the animal's position using population activity pre-stimulation (see Methods) and quantified its prediction error post-stimulation (Figure 34e). First, training the decoder using early place cells, we found a larger decoding error on the day of optogenetic stimulation compared to days without simulation, both before and after (Figure 34f, g). Training the decoder exclusively on early place cells yielded the same results. For both decoders, no significant difference was found on the next day when compared to the day before or after stimulation, confirming the observation that the perturbation of population place code induced by the alteration of CA1 presynaptic inputs was mostly transient.
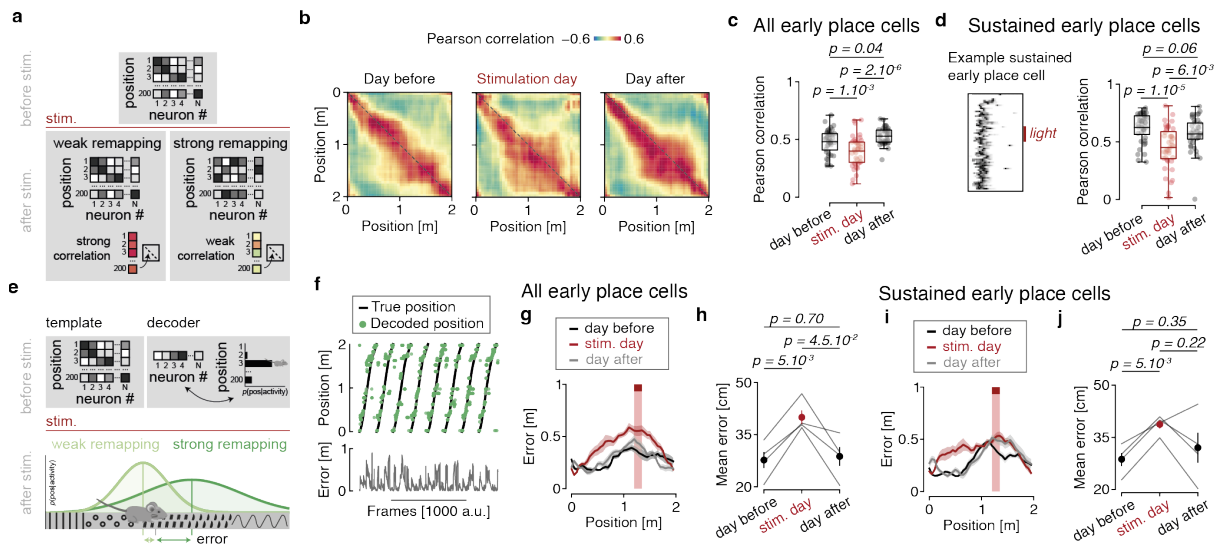
Figure 34. Perturbation of early CA1 population place code by CA3 optogenetic activation. a Schematic of population code vectors analysis. *Illustration from Maxime Maheu.* **b** Correlation of population vector codes defined pre- vs. post-stimulation for early place cells, separately across days. **c** Pearson correlation coefficients from the diagonals of maps in (a) across days. Paired *t*-test with Bonferonni correction. Mean ± s.e.m. **d** Same as (c) for sustained place cells only (of which an example is shown on the left). Paired *t*-test with Bonferonni correction. Mean ± s.e.m. **e** Schematic of Bayesian decoding analysis. *Illustration from Maxime Maheu*. **f** Decoding of position based on fluorescence of early place cells using a Bayesian decoder trained on pre-stimulation laps and applied on post-stimulation laps. Top: overlap of decoded position and true position. Bottom: decoder error per frame. **g** Decoding error as a function of position after training the decoder on all early place cells. Position of optogenetic stimulation is indicated in shaded red. Mean ± s.e.m. **h** Average decoder error across days based on (e). Paired t-test with Bonferonni correction. Mean ± s.e.m. **i** Same as (e) but after training the decoder on sustained early place cells only. Mean ± s.e.m. **j** Same as (f). Paired t-test with Bonferonni correction. Mean ± s.e.m.

Discussion

In the first part of this dissertation, I chronically investigated the relationship between synaptic strength and spine lifetime in the CA1 region of the hippocampus. While *in vitro* studies have suggested a possible link between activity and morphological adjustments, *in vivo* studies in the hippocampus are still lacking. Combining chronic calcium imaging of ipsilateral CA1 (ilCA1) spines and optogenetic stimulation of contralateral CA3 (clCA3) presynaptic inputs, I systematically identified responding and non-responding spines, detecting optogenetically evoked postsynaptic calcium transients at single spines. I found that globally responding spines (those responding to optogenetic stimulation on at least one day) were more stable than globally non-responding neighboring spines. The globally responding spines had larger head volumes, suggestive of a stronger synaptic connection than globally non-responding spines. In addition, globally responding spines showed a higher tendency to form clusters on dendrites. The existence of clusters could be a manifestation of local plasticity signals that selectively stabilize neighboring spines and could correspond to the local storage of closely related information.

In the second part of this dissertation, I investigated the contribution of presynaptic clCA3 inputs to representational drift and remapping of the environment in ilCA1. I combined calcium imaging of ilCA1 cells and optogenetic stimulation of clCA3 presynaptic inputs. By stimulating clCA3 presynaptic inputs, I was able to induce a limited number of new place cells. The place fields of the newly induced cells were not significantly located at any particular position in the environment, although there was a tendency for new place cells to form near the reward zone instead of near the stimulated location as expected. In addition, a transient remapping was observed for early place cells in ilCA1, indicating altered functional connectivity of the complete circuit following the optogenetic stimulation. This remapping in ilCA1 was not stable and, on the next day, no sign of the perturbation was observed anymore, suggesting that the spatial code in ilCA1 is in a stable state and requires constant input to drive the system to a new state.

3. Project #1: Enhanced lifetime of Schaffer collaterals

a. Modulation of connectivity strength influences spine lifetime

In vitro studies have shown that synaptic plasticity is important for determining the survival probability of a spine (Figure 35). Inducing long-term depression leads to a decreased survival probability, while long-term potentiation can concomitantly lead to an increased survival probability of the stimulated spine and a decreased survival probability of distant neighboring spines (Wiegert et al., 2018; Wiegert and Oertner, 2013). However, those effects are not rigid in time and additional synaptic plasticity events can erase the previously modified strength.
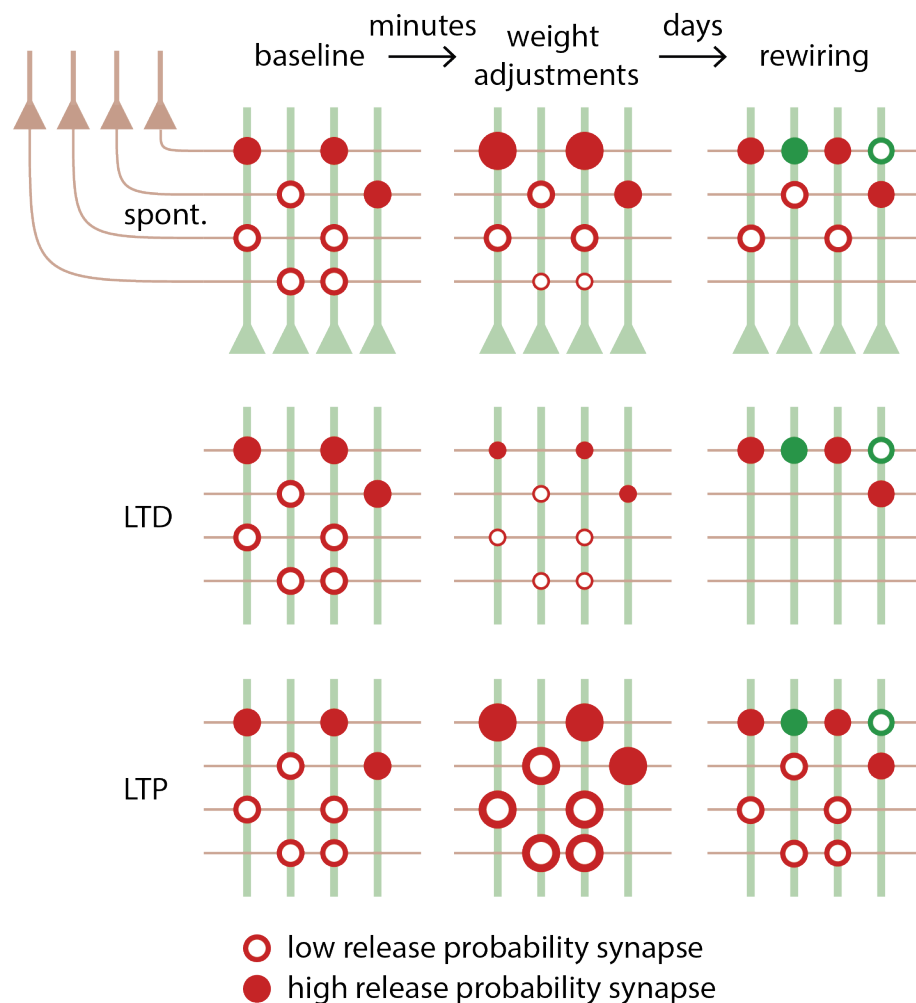
Figure 35. Synaptic rewiring. Following synaptic plasticity events, weights are adjusted in minutes timescales. These weights are further modified upon rewiring. LTD: long-term depression; LTP: long-term potentiation. *Illustration from Simon Wiegert.*

Structural modifications have been related to synaptic strength: an increase in spine head volume is associated with potentiation while a decrease in volume is associated with depression (Matsuzaki et al., 2004; Noguchi et al., 2019). In my work, I followed CA1 spines for more than two weeks and repeatedly optogenetically stimulated presynaptic clCA3 neurons to identify spines connected to presynaptic partners. I found that globally responding spines (those responding to optogenetic stimulation on at least one day) had larger head volumes. However, no manifestation of induced synaptic plasticity could be identified, as shown by the similarity in survival fraction, turnover ratio and average volumes between stimulated and non-stimulated dendrites. Yet, we cannot exclude that compensatory mechanisms permit the equalization of the total synaptic strength on the dendrite, thus masking the existence of synaptic potentiation events. Although we cannot relate spine stability directly to synaptic plasticity, our work indicates that the globally responding spines exhibit a stronger connection compared to globally non-responding neighboring spines. As globally responding spines have a longer lifetime, stronger connections appear to be more stable compared to globally non-responding neighboring spines. Thus, this result is in line with the previous *in vitro* studies. As no synaptic plasticity events have been demonstrated here, an alternative hypothesis is that repetitive activation of synaptic transmission could have been sufficient to maintain an already existing strong synaptic connection.

It is important to point out that two-photon microscopy is diffraction-limited and therefore does not yield an accurate measurement of spine volume. Nevertheless, previous work demonstrate that two-photon microscopy-estimated volumes were correlated to volumes determined by electron microscopy (Adoff et al., 2021; El-Boustani et al., 2018). In our work, a strong correlation was found between volumes estimated from multiple time series and the volume assessed from corresponding stacks. Thus, while absolute volume measurements are limited, the estimation of relative spine head volumes in this thesis was reliable.

Further work is necessary to investigate the effect of long-term synaptic plasticity events on spine lifetime *in vivo*. Using the approach I described in this thesis, long-term potentiation and long-term depression may be induced at ilCA1 spines through optogenetic stimulation of clCA3 neurons in future studies. Multiple protocols have already been established *in vitro* for this purpose, such as high-frequency stimulation (100Hz) for LTP and low-frequency stimulation (1Hz) of presynaptic inputs (Dudek and Bear, 1992; Wiegert et al., 2018; Wiegert and Oertner, 2013). Complementing the approach for long-term spine imaging presented here with the induction of long-term plasticity events occurring in a behavioral paradigm, such as a spatial navigation task, could even further confirm the enhanced stability of potentiated spines.

b. In vivo assessment of spine connectivity

In this dissertation, I combined optogenetic stimulation in presynaptic neurons with calcium imaging (i.e., jGCaMP7b) in postsynaptic cells to identify functionality-connected spines. Using this approach, I could longitudinally monitor local calcium transients at individual spines. Calcium sensors are the state-of-the-art tool for monitoring large-scale cellular activity in chronic preparation. Such sensors allow for direct identification of activated cells in the living brain, as calcium influx, which correlates with postsynaptic activation of synapses, can be optically recorded (Chen et al., 2013; Dana et al., 2019). Moreover, following synaptic plasticity events, the amplitude and frequency of evoked calcium transients are modified by changes in the strength of the synaptic connection, supporting the use of calcium indicators for the study of synaptic strength. Still, multiple drawbacks of this approach should be mentioned.

First, optogenetic stimulation of presynaptic partners might evoke responses of multiple synapses, which in turn can trigger a back-propagating action potential. The resulting calcium influx may mask initial sources of synaptic inputs, especially at a standard 30Hz imaging frame rate. Post-processing methods can partially recover initially responding spines; however, weak synaptic responses might be lost in this process, thus preferentially biasing the results towards strong synaptic inputs.

Another challenge associated with using a calcium sensor comes from the buffering effect of such proteins. The calcium buffering effect could theoretically induce modifications at the synapse. The importance of calcium in synaptic plasticity has been demonstrated, notably through its interaction with the calmodulin and, subsequently CaMKII protein, which is essential for synaptic potentiation (Coultrap et al., 2014; Yasuda et al., 2022). We cannot preclude a direct effect of the sensor on the results promoting synaptic plasticity (Rose et al., 2014).

Finally, some synapses lack NMDA receptors, or have only a few, through which calcium enters the spine, making the use of calcium sensors for this case not optimal.

To anticipate such flaws, the use of newly generated glutamate sensors could be considered (Adoff et al., 2021; Aggarwal et al., 2023). Although optimization for its use *in vivo* is required, an additional advantage is the possibility to measure the probability of response of spines. An enhanced probability of release is expected from strong synapses. Although an increase in calcium transient is to be expected in the couple of hours following a potentiation, an increase in the release probably is also a good marker for successful potentiation in the case of experiments of long-term potentiation induction.

c. Rewiring of CA1 synaptic inputs on short timescales

Monitoring spine responses from optogenetic stimulation across days, a low number of spines were responding to the optogenetic stimulation, representing approximatively 19% of all recorded spines. Several factors can explain this result. First, CA1 spines on basal dendrites receive inputs from different regions, including ipsilateral CA3, amygdala and entorhinal cortex (Klausberger and Somogyi, 2008; Pfeiffer et al., 2018). Thus, non-responding spines may receive inputs from any of these other regions. Secondly, we cannot ensure that all contralaterally connected CA3 neurons were expressing a sufficient amount of Chrimson to be reliably activated. Related to this, light propagation is limited and therefore clCA3 neurons that are located relatively far from the fiber tip may have received insufficient light to be activated. Finally, calcium sensors, such as jGCaMP7b used in my work, have a sensitivity below the minimum calcium ranges in spines with a slow kinetic (Zhang et al., 2023). In combination with the noise present in the recordings of spine activity, the detected spine transients are probably biased toward strong calcium inputs. We thus cannot exclude that spines detected as responding on a given day are spines exhibiting strong synaptic inputs, and that part of non-responding spines were undetected, weakly responding spines. Along these lines only 40 trials were recorded per dendritic branch, implying that low-release probability synapses may also be undetected, although the use of train of light pulses makes this possibility unlikely.

The hypothesis that low-release probability synapses are probably undetected could also explain the low fraction of spines exhibiting responses in multiple sessions, as found in this study. This result might reveal that synaptic weights are rapidly modified. Although it is an hypothesis, this could account for the transfer of newly formed memory to a new storage site (Bontempi et al., 1999; Frankland and Bontempi, 2005; Marr and Brindley, 1997; McClelland et al., 1995; Squire, 1986; Teng and Squire, 1999), such as the cortex, and the homogenization of the total synaptic weight of individual dendrites. In doing so, neurons might increase their capacity for encoding new memories by allowing synaptic weights to be further increased upon new potentiation. Thus, the hippocampus may display fast rewiring of its synaptic inputs to grant the flexibility required for the formation of new memories.

In this study, spines were monitored every four days, similar to previously published work (Attardo et al., 2015b; Gu et al., 2014). This approach has been adopted for different reasons: minimizing the animal stress and phototoxicity, as well as to reduce sensor bleaching while frequently monitoring the spines. Especially, as spines are small units, a small amount of sensor proteins is present. Prolonged exposure of proteins to light over an extended period accelerates signal bleaching, despite diffusive replenishment. Former computational models of spine survival are compatible with a spine lifetime beyond four days, suggesting that complete synaptic rewiring is unlikely in such a short-term timescale. In addition, controls also showed that postsynaptic

calcium responses upon iterative optogenetic stimulation were consistent across days, withholding the variability in stimulated presynaptic clCA3 cells. Yet, synaptic modifications in between experimental days cannot be excluded, and further experiments are required to demonstrate daily rewiring of synaptic inputs related to memory formation and storage.

d. Spines as temporary storage for memories in the hippocampus

Memory storage is a primary research focus, yet the long-standing question of memory location remains unanswered. Two non-excluding hypotheses have been proposed. On one hand, spines could serve as a precise location for memory storage. On the other hand, the sequence of activity with critically timed inputs could be sufficient for memory formation and retrieval (Abraham and Robins, 2005).

From decades of research, studies have attempted to demonstrate the possibility of memory storage in spines. In the cortex, following the observation of low turnover rate and extended spine lifetime (Grutzendler et al., 2002; Holtmaat et al., 2005; Trachtenberg et al., 2002), the discovery of lifelong spines has notably been a major finding in the field (Yang et al., 2009). This observation implies that the disappearance of a single spine could have a dramatic impact on memory retrieval but also put major constraints on the flexibility required by the network to store new memories. So far, computational models failed at reproducing observed memory retrieval when adding such constraints to the system (Fusi, 2002; Fusi et al., 2005; Fusi and Abbott, 2007). Furthermore, in the hippocampus, a main region implicated in episodic memory, research tends to show that spines do not have a lifelong but a rather short lifetime (Attardo et al., 2015; Gu et al., 2014; Pfeiffer et al., 2018; Yang et al., 2021). However, different factors probably influence the lifetime of spines. Indeed, anesthesia has already been found to influence spine lifetime, notably a mix of ketamine and xylazine has been shown to increase the survival fraction of CA1 spines and thus spine lifetime (Yang et al., 2021). Aside from external elements, the activity history of a spine might be a good predictor of spine survival.

As I followed a group of functionally connected spines, my work suggests that not all CA1 spines have a short lifetime but rather that different pools of spines can exhibit different survival probabilities. Identifying ilCA1 spines functionally connected to clCA3 across 16 days, I could demonstrate that specifically those spines were stable when compared to non-responding neighboring spines, as shown by a decrease in turnover rate and an increase in survival probability thanks to an increase in the lifetime of persistent, formed and transient spines. However, I monitored those spines over two weeks and thus cannot elaborate on longer timescales. As the survival fraction of responding spines remains high at the end of the experiment, I cannot exclude that all spines will eventually disappear.

① **eGRASP labelling of connected synapses**
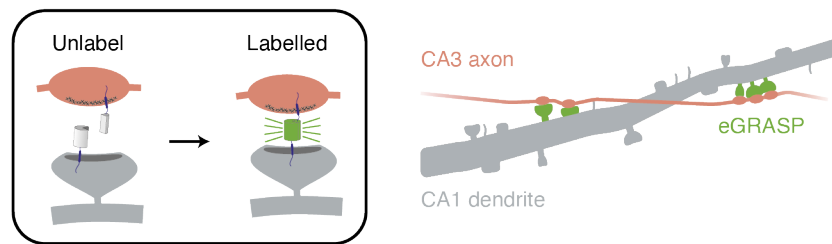
② **SynTagMA labelling of active synapses**

> **Figure 36. Labeling of CA1 spines using eGRASP or SynTagMA technologies.** eGRASP permits to label connected synapses by the expression of proteins splits in pre- and postsynaptic compartment. SynTagMA permits to label active synapses upon UV light delivery.

Labeling of specific spines formed during a task could be a key experiment to confirm the existence of lifelong spines in the hippocampus. So far, available experimental tools are limited in their use for this purpose. A recombinant tool, such as eGRASP, can be used to label spines connected to a specific presynaptic partner. One part being expressed at the axonal bouton and the other part being expressed at the spines of the postsynaptic partner, the labeling protein is reconstituted at the synaptic cleft (Choi et al., 2018). However, this bond between the two parts of the labeling protein is covalent. Therefore, a potential concern could be the increased stability of spines, artificially maintaining the two compartments in proximity. Alternatively, SynTagMa is a tool that can label active spines upon violet light delivery (Perez-Alvarez et al., 2020a). Yet, this tool is limited to a few hours of labeling, hence further improvements are needed for this specific purpose (Figure 36).

Another possibility to investigate the importance of spines for memory storage is to specifically erase spines implicated in the encoding of memory. Memories are formed and consolidated following synaptic plasticity events. Selectively interfering with hippocampal long-term potentiation, in the next 24h, impairs memory encoding. Hence, spines appear to be important for information storage. However, this effect did not last more than 24 hours. Instead, the erasure of memories was only possible by interfering with long-term potentiation in the cortex 48 hours after hippocampal encoding (Goto et al., 2021). Thus, in the hippocampus, spines could be temporary storage units undergoing significant rewiring on a short-time scale.

4. Project #2: Place cell remapping in the hippocampus

a. Fast rewiring of synaptic inputs accounting for place cell remapping

A main function of the hippocampus is to encode the environment in the context of spatial navigation. Many scientists have focused their research on the formation and maintenance of spatial memories in the hippocampus. The presence of place cells — cells whose activity is tuned to specific positions in the environment — was demonstrated more than 50 years ago (O'Keefe and Dostrovsky, 1971). A particularity of the hippocampal CA1 region is the rapid remapping of the code over days, despite a stable environment and invariant behavior in rodents (Ziv et al., 2013). The origin of this remapping is still largely unknown. Two main hypotheses can be proposed, relying on the sensory variability of the environment or the intrinsic cellular connectivity variability in the hippocampus.

The CA1 region of the hippocampus integrates both the sensory elements and the internal representation of the environment. Variability in the sensory elements in the environment, such as light or olfactory differences, possibly due to previous mice in the setup, might be sufficient for sensory input modifications, hence substantially modifying the hippocampal place code (Liberti et al., 2022). A recent paper investigating place cell remapping in bats has shown little remapping in CA1 over days (Liberti et al., 2022). Comparing equivalent flight trajectories shows that the place code is stable. On the contrary, changes of the light in a familiar environment or when compared to variations of flight trajectories both show a discrepancy in place cell tuning. Thus, sensory variability could indeed explain the dynamic remapping of the hippocampal spatial code.

Previous work shows little changes in place cell selectivity during a session of a spatial navigation task (Ziv et al., 2013), and a decreased number of newly formed place cells after 20 laps of the same linear circuit (Sheffield et al., 2017). In this dissertation, we attempted to induce place code remapping by partially modifying the inputs received by CA1 cells using optogenetic stimulation. Already, in control experiments assessing the general effect of the light delivered during optogenetic activation, we found substantial changes in the daily sessions before and after extracranial light delivery (sham stimulation). As a change in the environment occurred, plausible explanations could be a modification of the place code relative to the new transient sensory input and an undetected change in the running behavior of mice, despite maintained performance in the task. The structure of the session being similar between training and experimental control days, a surprise effect of light delivery is unlikely. This is notably shown by a similar running speed and licking behavior during sham laps. Thus, multiple lines of evidence indicate that differences in sensory inputs are a factor for place cell remapping.

The hypothesis of intrinsic properties of CA1 pyramidal cells is however not excluded to explain the loss of spatial tuning across days. A recent study on CA1 spine place tuning has shown that all recorded place cells receive inputs from different locations of the treadmill. Most place spines with different tuning are uniformly distributed across dendrites. Yet, dendritic clusters of place spines have been found to be correlated to the spatial tuning of the cell (Adoff et al., 2021). Thus, these clusters could dictate the spatial tuning of the cell through coordinated activity, providing an increased drive to the cell. As synaptic plasticity was shown to influence neighboring spines (Nishiyama and Yasuda, 2015; Oh et al., 2015; Wiegert and Oertner, 2013), the generated activity across days could thus influence the existence of spine clusters. By eliminating spines present in specific clusters, cellular spatial tuning might be modified and be responsible for the observed drifting, particularly if the elimination is proven to be rather unspecific, consequently shortening spine lifetime. This mechanism could explain the short lifetime found in a computational model of CA1 spine lifespan (Attardo et al., 2015b).

Experiments exploring spatial tuning of synaptic inputs across time could unravel the rewiring of clustered spines. Indeed, the change in place tuning might be explained either by the elimination of spines in specific activity-correlated clusters or by a tuning drift of presynaptic cells. Recent research demonstrated that CA3 presynaptic cell tuning is also drifting, although at a slower rate than in CA1 (Dong et al., 2021). Since CA3 cells constitute one of the major inputs to CA1, a change in CA3 cellular-specific firing could drive the drift in CA1. To explore this possibility, independent modification of CA3 presynaptic timed inputs could help in understanding how changes in CA3 mapping could drive CA1 remapping.

b. CA1 place cell remapping by presynaptic inputs shift

In this dissertation, I followed CA1 place cells across days and combined two-photon imaging with optogenetic stimulation of presynaptic clCA3 cells to induce perturbation of CA1 inputs. Optogenetic stimulation of presynaptic clCA3 neurons led to the induction of a low number of place cells, despite a large number of CA1 cells responding to stimulation. Previous work has shown that when stimulating a large number of CA1 cells for place cell induction, only a small fraction of these neurons would acquire spatial tuning (McKenzie et al., 2021; Rolotti et al., 2022). The low yield of synaptically induced place cells might be due to local inhibition controlling the formation of new place cells. In this way, the formation of an abundant number of place cells is suppressed. So far, induction of single place cells through behavioral timescale plasticity remains the best approach to induce place cells (Bittner et al., 2017, 2015; Magee and Grienberger, 2020).

Still, comparing the place fields of early place cells and those of induced place cells, these new fields tend to form preferentially near the reward zone, whereas the stimulated zone was located farther away from it. Nevertheless, increasing the number of recorded neurons is necessary to confirm this qualitative result, as previous work rather found a uniform distribution of new place fields on the treadmill (McKenzie et al., 2021).

Apart from the formation of new place cells, optogenetic stimulation of presynaptic clCA3 cells also modified the activity of early place cells, place cells present before the stimulation. Population analysis of the code shaped by early place cells reveals a decreased correlation of the code when comparing the maps before and after optogenetic stimulation. While this decreased correlation could be due to the loss of early place cells, considering only sustained early place cells (place cells that are present pre- and post-stimulation), this decreased correlation was still present. Using a population decoder confirmed this finding. For each session, a decoder was trained on the cellular activity of place cells present pre-stimulation. Testing on the second part of the session (post-stimulation) showed that the decoder produced larger errors on the day of the stimulation, suggesting a lasting CA1 remapping. This drift, however, was not accompanied by a change in the behavior of the mouse and the light alone was not sufficient to explain the observed shift. This outcome suggests that a temporary change in clCA3 inputs is sufficient for a drift in the representation of the environment in CA1 on a one-day timescale.

c. Flexibility versus stability of memory systems

Learning is a process by which new memories are formed to acquire new knowledge. The mechanism by which new memories are formed and stored has been long studied but yet remains elusive. While stored memories require stability, flexibility is necessary to form new memories. How the two processes can coexist is unclear. Spatial memories are formed and stored, at least temporarily, in the hippocampus (Abraham and Robins, 2005; Burgess et al., 2002; Squire, 1986). Drifts in the representation have however been observed both in the rodents CA3 and CA1 (Dong et al., 2021; Hainmueller and Bartos, 2018; Ziv et al., 2013).

In this work, recording CA1 place cells on the day after optogenetic stimulation of presynaptic inputs revealed that the optogenetic perturbation did not produce a permanent change in the code. The perturbation of the code modified the code only on the day of the stimulation, suggesting that the representation of the environment in CA1 is in a stable state and that temporary change in presynaptic clCA3 inputs is not sufficient to permanently remap the environment. Instead, a gradual off-line drift of the inputs is likely necessary to push the system into a new state. This system probably

allows for a stability of formed memories to be transferred to the cortex while allowing flexibility for new inputs.

Materials and methods

1. Mice

Adult (2 to 9 months of age) C57BL/6J mice of both sexes were used in this study. The mice originated from the Charles River company and housed in pathogen-free conditions at the University Medical Center Hamburg-Eppendorf. A light/dark cycle of 12/12 hours is used. The humidity and temperature in the room were kept constant (40% relative humidity; 20°C). Food and water were available ad libitum except during training and experimental days for the place cell project (Project #2). All procedures were performed in compliance with German law according and the guidelines of Directive 2010/63/EU. Protocols were approved by the Behörde für Gesundheit und Verbraucherschutz of the City of Hamburg under the license numbers 32/17 and 33/19.

2. Surgeries

a. Virus injections.

C57BL/6J wild-type mice were anesthetized with 2% isoflurane/1L of O_2. After 5 minutes, mice were transferred to the stereotaxic frame, and anesthesia was maintained with 1.5% isoflurane/1L of O_2. To evaluate the depth of anesthesia and analgesia, the paw withdrawal reflex test was performed with a toe-pinch. Then, Buprenorphine (0.1 mg/kg) and Carprofen (4 mg/kg) were both injected subcutaneously. A heating blanket was present under the mouse throughout surgery to maintain the body temperature and eye ointment (*Vidisic*, Bausch + Lomb) was used to prevent eye drying. The fur on the head was trimmed and carefully removed to avoid later contamination in the surgical field. The skin was then disinfected using Betaisodona. The mouse was then fixed on the stereotaxic frame and a 3-4cm midline scalp incision was made close to the injection sites. The skin was pushed to the side and a bone scarper was used for cleaning (Fine Science Tools, Heidelberg, Germany). Above the injection sites, two holes were made using a dental drill (*Foredom*, Bethel, Connecticut, USA). 0.3µL of AAV9-CaMKII-ChrimsonR-mScarlet-KV2.1 (*AddGene* # 124651-AAV9) viral suspension was first injected in left CA3 (-2.0mm AP, -2.3mm ML, -2.5mm DV relative to Bregma) using a custom-made air-pressure driven injection system. For the spine experiments (Project #1), 0.5µL of the mix AAV9-CaMKII-Cre and AAV1-Syn-flex-jGCaMP7b-WPRE (*AddGene* #104493-AAV1) or AAV9-loxp-hsyn-GCaMP7b-mRuby3 was injected in right CA1 (-2.0mm AP, +1.5mm ML, -1.5mm DV relative to Bregma). In a set of experiments for Project #1 and in Project #2, mice were instead injected with 0.5µL of AAV9-Syn-jGCaMP8m (*AddGene* #162375-AAV9) in CA1. The scalp was then sutured. Mice were removed from anesthesia and let

recover in a clean cage on a heating blanket. For three days after surgery, mice were provided with Meloxicam mixed into soft food.

b. Hippocampal window surgery for *in vivo* calcium imaging.

At least two weeks after virus injections, a second surgery for hippocampal window surgery took place. Mice were anesthetized as described above. After the removal of fur, the skin covering the implantation sites was removed. The skull was cleaned and roughened with a bone scraper. A first hole using the dental drill was made upon CA3 (-2.0mm AP, -3.5mm ML, titled 35° towards the left) and an optic fiber (*Doric Lenses*, 1.25mm ferrule diameter, 0.22 NA, 1.3 ± 0.1mm length) was inserted and glued to the skull. Once the glue dried, a circular 3mm bone piece, centered around the CA1 injection site, was carefully removed using a trephine (*MW Dental*, ISO 020). The dura and somatosensory cortex above the hippocampus were carefully aspirated until the apparition of the white matter tracts of the corpus callosum. Sterile PBS was used to wash the craniotomy all along, and a custom-made hippocampal imaging window was inserted. For Project #2, previous to inserting the hippocampal window, a drop of transparent Kwik-Sil was applied in the craniotomy for reduced motion in recordings of behaving mice (Dombeck et al., 2010). To build the window, a hollow glass cylinder was glued to a No. 1 coverslip on the bottom with UV-curable glass glue (*Norland* NOA61, Cranbury, New Jersey, USA). The imaging window and a head plate (*Luigs & Neumann*, Ratingen, Germany) were attached to the skull with cyanoacrylate gel (*UHU* SuperGel). Dental cement (Super Bond C&B, *Sun Medical*) was then applied until the complete closure of the cranial surgery. As before, animals were provided with care after the end of the surgery and could recover for at least two weeks before the beginning of experiments.

3. *In vivo* two-photon imaging

a. Two-photon imaging cellular calcium imaging of anesthetized mice.

To verify the expression of the injected virus in CA1, at least one short session of two-photon imaging is set about two weeks after recovery from hippocampal window implantation, thus a month after virus injection. For that, mice are anesthetized with 2% isoflurane in 1L of O_2 in an induction box. After 5 minutes, mice are rapidly transferred to the microscope and head-fixed. A custom-made mask, with isoflurane flowing, is placed around their nose. For maintenance under anesthesia, the isoflurane rate is set between 1.5 and 2% in 1-1.2L of O_2, and consciousness stages are monitored by the experimenter, thanks to pupil size (small under anesthesia), breathing amplitude, and rate through a camera in the imaging box. Under the mouse,

a heating mat is present for body temperature maintenance. The window was centered under the two-photon microscope (MOM scope, Sutter Instrument, Novato, California, USA modified by Rapp Optoelectronics, Wedel, Germany), and virus expression was verified in the hippocampus using epifluorescence and then two-photon imaging. Mice are eventually removed from anesthesia and put back in their cage when awake until recovery.

b. Two-photon imaging spine calcium imaging of awake mice.

Mice are progressively handled and habituated to the imaging setup and head fixation for at least a week before starting experiments. Additional habituation sessions were occasionally added until the mice showed no more signs of stress, usually expressed as uninterrupted and disorganized runs. Mice were placed on a linear treadmill (*Luigs & Neumann*, Ratingen, Germany) for close-loop experiments described below. A 633nm laser (*Omicron*) is connected to the implanted fiber optic on the mouse through two patch cords. From the laser combiner (*Omicron*, LightHUB®), a main patch cord (*Doric Lenses,* optic fiber 200μm, NA 0.22, 2m long, SMA-SMA) is connected to a patch cord (*Doric Lenses*, optic fiber 200μm, NA 0.22, 1m long, SMA-MF1.25), itself connected to the implanted optic fiber through a dark mating sleeve (*Doric Lenses*). To avoid light contamination from the optogenetic stimulation, a filter (*Semrock,* #SP01-633RU-32) is inserted before the photomultipliers, and the path between the objective and the photomultipliers is further covered with black tissue. As previously, the window is centered under the microscope using epifluorescence, and expression is checked with two-photon microscopy. Images were acquired with a Ti: Sa laser (Chameleon Vision-S, Coherent) tuned to 930 nm to excite jGCaMP7b and a 40× water immersion objective (Nikon CFI 40×, 0.80 NA, 3.5 mm WD, Nikon, Amsterdam, the Netherlands). Single planes (512 × 512 pixels) are acquired at 30 Hz with a resonant scanner using 10 to 40mW (930 nm) with ScanImage 2017b. In the first session, multiple fields of view (FOV) per mouse are acquired. For each FOV, optogenetic stimulation using a strong protocol (20 trials, 10Hz, 10 pulses of 50ms each, spaced by 5s) is used to evoke neuronal postsynaptic calcium transients. A custom Python script is used to control the laser, trigger the beginning of the session, and trigger the onset of each trial. The treadmill is continuously monitored so that if the mouse is quiet for the last second, an optogenetic trial is initiated. After post-hoc identification of responding neurons as described below, imaging of dendrites of responding neurons is performed on a subsequent session. For each session and each dendrite, subthreshold optogenetic stimulation is performed (40 trials, 10Hz, 3 pulses of 10ms each, spaced by 5s) every four days for over two weeks. The order of imaged dendrites is shuffled at the beginning of each session.

c. Two-photon imaging cellular calcium imaging of behaving mice.

When mice are placed on the treadmill, as previously, the window is centered under the two-photon microscope using epifluorescence, and the laser fiber is connected to the custom sleeve (extracranial light delivery) or the implanted fiber for the experimental day with optogenetic stimulation (intracranial light delivery). The behavioral task is initiated once the field of view is ready to be imaged. For each mouse, a field of view is chosen before training. In this session, mice are quiet and awake and 50 trials of optogenetic stimulation are used for offline identification of responding neurons in the field of view. Following the end of the behavioral experiments, the same field of view is acquired and cellular responses to optogenetic stimulation are recorded. Images were then acquired with a Ti: Sa laser (Chameleon Vision-S, Coherent) tuned to 930 nm to excite jGCaMP8m and a 16× water immersion objective (Nikon CFI 16×, 0.80 NA, 3 mm WD, Nikon, Amsterdam, the Netherlands). Single planes (512 × 512 pixels) are acquired at 30 Hz with a resonant scanner using 30 to 100mW with ScanImage 2017b.

4. Behavioral experiments

a. Behavior setup.

For the spatial navigation task, a custom-made treadmill (*Luigs and Neumann*), with five tactile cues distributed uniformly along a 2m belt, is controlled by a Python script (*Luigs and Neumann*) sampling the treadmill at 20Hz. A white band is placed under the belt so that when the white band passes above the infrared light (IR light), light is reflected and a signal is sent to the software to record the end of the lap. This signal is then sent as an input to the Bpod (*Sanworks*, USA). For a higher precision of the animal position, an additional rotary encoder (1024 positions, E6B2-CWZ6GH, *Yumo*, China) is placed on a 3D custom-built wheel under the belt. This secondary encoder signal is read out online by a rotary encoder module (1034; *Sanworks*, USA), which sends angular position through an analog channel to the master NI board co-registering behavioral events with 2p frame acquisition (sampling rate of 1500Hz). In parallel, the position of the animal is streamed to send a trigger to the optogenetic laser during the stimulated laps at a chosen location.

For lick detection, a high-speed camera (*The Imaging Source*, Germany) is placed on the side of the mouse and controlled by a custom-made script on the open-source Bonsai RX visual reactive program (Available at https://bonsai-rx.org/) (Lopes et al., 2015). A region of interest (ROI) is drawn on the live stream of the camera to detect the tongue of the animal. When pixel values in the ROI are greater than manually defined baseline values, a signal is communicated to Bpod (through a local TCP protocol), which triggers a digital output connected to the master NI board

(*National Instruments*, USA) following each lick. When a lick occurred in the reward zone, Bpod triggered water delivery by opening a solenoid valve (LHDA1231115H; Lee Company®, USA) connected to a port interface board (1004; Sanworks®, USA) (Figure 37).
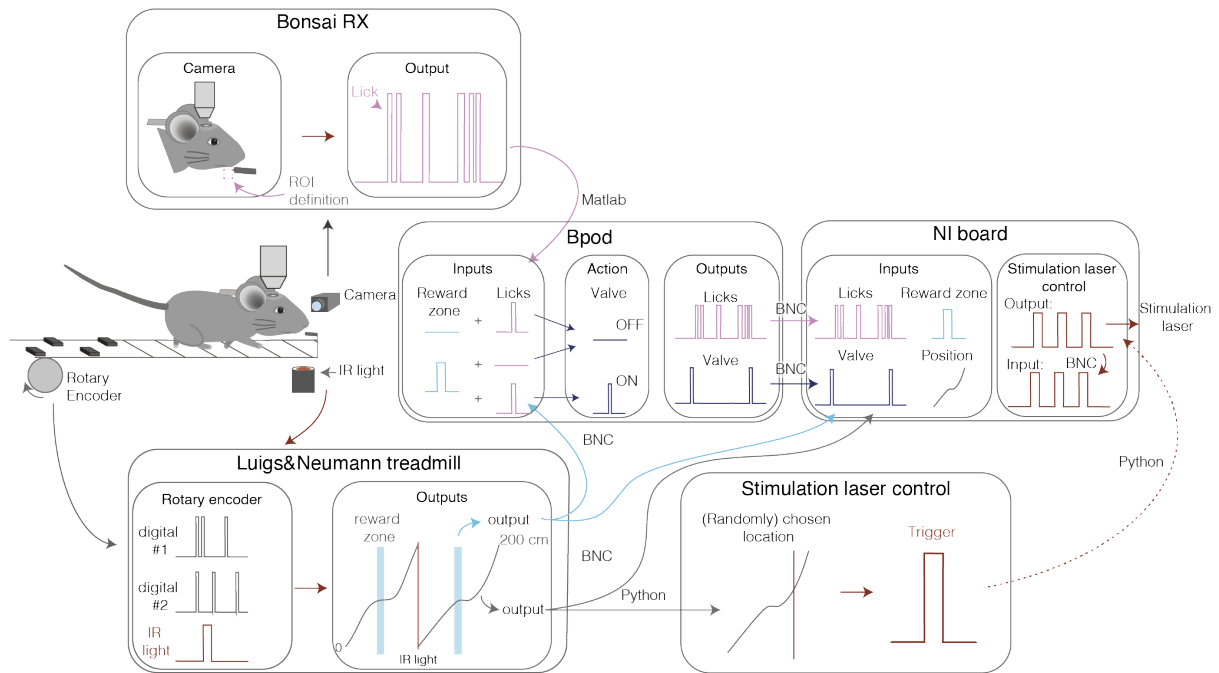
Figure 37. Behavioral setup of a spatial navigation task. The position and the licks of the animal are recorded and a water reward is delivered in the reward zone. Additionally, a light stimulation is triggered at a precise location on the treadmill.

b. Behavioral training.

As for Project #1, mice were gradually habituated to the setup and head fixation. Once signs of stress disappeared, mice were water-restricted and provided with 2mL of water per daily session. The weight of each mouse is daily monitored at the beginning of the session and care is taken so that weights do not fall under 85% of their original weight. On the first phase of training, the first day following water restriction, mice are habituated to the reward spout. First, a drop of water is delivered by the spout for the mice to lick, and then the mice get free water when licking the reward spout by itself. On the second phase of training, usually starting on the second day of training, mice are required to run on the treadmill and a reward is automatically provided at a precise location on the treadmill, the reward zone. This phase often lasts 2 to 3 days. In the last phase of training, mice would be required to lick at the reward zone to receive a

reward. Usually, mice already anticipate the reward zone and start licking before the reward zone at the end of the previous phase. Additionally, a 1s sham light is randomly shined at one out of four positions on the treadmill to habituate the mouse for light delivery during optogenetic stimulation. For this, two sleeves are glued together, and the laser fiber is held next to the implanted fiber. In total, training lasted between 5 and 10 days.

5. Tissue preparation and histology

Mice were injected with a lethal dose of a mix of ketamine and xylazine and transcardially perfused with 1x PBS followed by 4% paraformaldehyde (PFA). Brains were removed and stored in 4% PFA. Brains were sliced at 60µm using a vibratome (VT1000S, Leica). Slices were mounted on microscope slides using an aqueous mounting medium (FluoroMount®) and coverslips (1871, Carl Roth®, Germany). Stitched images were acquired with an epifluorescent microscope (AxioObserver, Zeiss®, Germany) using the 10x objective (Plan-Apochromat, Zeiss®, Germany) for slice overviews and a confocal microscope (LSM 900, Zeiss®, Germany) using a 20x objective (Plan-Apochromat, Zeiss®, Germany) for detailed close-ups.

6. Data analysis

a. Project #1: Enhanced lifetime of Schaffer collaterals

i. Spine calcium trace extraction

Time series were motion-corrected using Suite2p (version 0.10.2; Table 1) (Pachitariu et al., 2016). A t-projection from each motion-corrected recording for each day was made. T-projections were registered together using the rigid body or translation mode of the plugin *StackReg* (Thevenaz et al., 1998) of the open-source platform *Fiji* (Schindelin et al., 2012). Regions of interest (ROIs) were manually drawn around visually identified spines on motion-corrected frames in *Fiji*. ROIs were separately drawn for dendrites and the background. Calcium traces were extracted on the motion-corrected frames using a custom-made script by averaging the fluorescence of all pixels about each ROI (Macro Fiji).

Parameter	Variable name	Value
Registration		
Expected decay from the calcium sensor, in seconds (i.e., jGCaMP8m)	tau	0.7
Number of recorded channels	nchannels	1
Number of the functional channel	functional_chan	1
Sampling rate of the microscope, in frames per second	fs	30
Run the registration algorithm twice	two_step_registration	1
Number of frames used to generate the reference image used for registration	nimg_init	2000
Number of frames to register simultaneously in each batch	batch_size	200
Maximum shift allowed for registration, as fraction of the frame width or height	maxregshift	0.3
Precision of subpixel registration (1/ subpixel steps)	subpixel	10
Smoothing applied in time, in number of standard deviations in time frames	smooth_sigma_time	1.2
Smoothing, in number of standard deviations in pixels	smooth_sigma	1.15
Bad frames to be excluded for cropping the time-series. Set to 0 to exclude more frames.	th_badframes	0

Use non-rigid registration for correction in the depth axis	non_rigid	True
Size of blocks used for non-rigid registration, in pixels	block_size	[128,128]
Threshold to apply smoothing for registration	snr_thresh	1.2
Maximum block shift allowed for non-rigid registration, relative to the shift of rigid registration	maxregshiftNR	20
Region of interest detection with CellPose		
Run ROI detection algorithm	roidetect	False

Table 1. Parameters used in Suite2p for motion correction and signal extraction for spine imaging.

ii. Dendrite exclusions

A total of nine mice were recorded, among which two control mice (non-stimulated dendrites controls). Two mice were excluded due to the high-frequency motion of the dendrites. From the five experimental mice, 28 dendrites were recorded for two weeks. Among them, 5 dendrites were excluded due to excessive motion on at least one session and 6 dendrites were excluded due to insufficient number of responsive spines.

iii. Trial exclusions

All data were analyzed using custom-made scripts with Python (Python Software Foundation, NH, USA) installed on an open-source Anaconda environment (Anon, 2020. *Anaconda Software Distribution*, Anaconda Inc. Available at: https://docs.anaconda.com/) and the PyCharm integrated development environment (*JetBrains*, Prague, Czech Republic). First, residual motion present in motion-

corrected recordings was identified using cross-correlation on the motion-corrected frames and excluded from the analysis. To be considered, trials required to be constituted of at least 1 second of stable baseline (without excessive motion as determined ahead), and at least 70% of the data points during stimulation need to be stable.

iv. Identification of dendritic transients.

To identify dendritic transients, the distribution of the data points for each neuron was used. Using a bootstrap analysis, the null distribution was obtained by permutation of the onset of the optogenetic stimulation at random locations. Then, significant optogenetically-evoked dendritic transients were detected as $\Delta F/F$ greater than the $\Delta F/F$ obtained from the 95% of the values of the mean-shuffled $\Delta F/F$ (10,000 shuffles, $p < 0.05$). A transient was further confirmed if, during the optogenetic stimulation, more than 30% of the data points were significant as described above.

v. Identification of responding spines

Because suprathreshold calcium events mask the spine-specific calcium transients, robust regression is used to reduce the contamination of dendritic calcium activity on spine calcium traces, as previously reported (Chen et al., 2013; Iacaruso et al., 2017). To decrease the high-frequency noise in traces, spine calcium traces were convolved using a 5-bin boxcar. For each spine, an average trace using all trials is used to determine if a spine shows excitatory postsynaptic calcium transients (EPSCaTs). As for dendrites, a spine is classified as responding if more than 30% of the time points during the optogenetic stimulation are greater than 95% of the values of the mean-shuffled $\Delta F/F$ (10,000 shuffles, $p < 0.05$).

A spine is qualified as globally responding if optogenetically-evoked transients were detected in at least one out of the five sessions.

vi. Morphological analysis.

All spines were visually inspected and annotated for their existence on each day. Spines were then classified into four categories depending on the survival sequences, as follows:

- Formed if appearing on one of the sessions and staying until the end of experiments.

- Eliminated if present since the first session but disappearing from the experiments without reappearing in any of the following sessions
- Persistent if present on all recording days
- Transient if appearing and disappearing during the experimental days.

The turnover ratio was calculated as the sum of formed and eliminated spines divided by the number of spines present between the days. The survival fraction is calculated as the fraction of spines present on the given that were already existing on the first day of the experiment.

Spine densities were obtained by dividing the number of spines present on dendrites by the length of the dendritic segment.

vii. Spine volume estimation.

The volume of each spine was estimated as previously reported (El-Boustani et al., 2018; Hedrick et al., 2022). Briefly, each t-projection was deconvolved using the plugins Diffraction PSF 3D and Iterative Deconvolve 3D (Dougherty, 2012) (Fiji). All pixels in the ROI drawn around the spine above the mean fluorescence of the background were summed and divided by the average fluorescence of the same number of pixels taken from the closest dendrite ROI.

For estimation of spine volume on the stacks obtained with the isosbestic, a z-projection is computed from the registered frames (StackReg, Fiji) excluding frames with excessive motion. The same formula is used as above for the comparison.

vii. Distance estimation.

The interspine distances were calculated as previously reported (Hedrick et al., 2022). Briefly, the distance between two spines is calculated as the dendritic length between the base of a pair of spines. The mass centers of the spines are projected on the dendrite. A path is then obtained using the Dijkstra's algorithm and the resulting distance is converted to micrometers based on a previous field of view measurement on the microscope.

viii. Linear regression

For linear regressions, the function *linregress* from the Python library *Scipy* (Virtanen et al., 2020) is used. Random permutations of the data are then used to determine the confidence interval of the regression (10,000 shuffles, $p < 0.05$). The *p*-value is

thereafter computed with the *percentileofscore* function from the *Scipy* library (p < 0.05).

b. Project #2: Place cell remapping in the hippocampus

i. Behavior analysis

For each session, a file was generated for the recorded behavior parameters from the master NI board. For licks, reward zone, and optogenetic triggers, the analog values, ranging from 0 to 5V, were binarized when an event occurred and then down-sampled to match the sampling rate of the microscope (30Hz).

For the treadmill processing, each position across a lap ranges between -4.5V and 4.5V. After conversion from the voltage to a position in meters (0 - 2m), the recorded data is down-sampled to match the sampling rate of the microscope (30Hz). The speed is then derived from the position of the animal.

ii. Recordings registration.

All recordings for each mouse were provided to the *Suite2p* toolbox (version 0.13.0) to correct for motion and register all frames together (Table 2). The integrated module *CellPose* was used for the detection of neurons in the field of view (Stringer et al., 2021). Neurons were manually sorted and manually labeled when non-identified by the script. Fluorescence from the regions of interest (ROIs) and the surrounding neuropil was then extracted and used for analysis.

Parameter	Variable name	Value
Registration		
Expected decay from the calcium sensor, in seconds (i.e., jGCaMP8m)	tau	0.1
Number of recorded channels	nchannels	1
Number of the functional channel	functional_chan	1
Sampling rate of the microscope, in frames per second	fs	30

Run the registration algorithm twice	two_step_registration	1
Number of frames used to generate the reference image used for registration	nimg_init	2000
Number of frames to register simultaneously in each batch	batch_size	200
Maximum shift allowed for registration, as fraction of the frame width or height	maxregshift	0.1
Precision of subpixel registration (1/ subpixel steps)	subpixel	10
Smoothing applied in time, in number of standard deviations in time frames	smooth_sigma_time	0.1
Smoothing, in number of standard deviations in pixels	smooth_sigma	1.15
Bad frames to be excluded for cropping the time-series. Set to 0 to exclude more frames.	th_badframes	0
Use non-rigid registration for correction in the depth axis	non_rigid	True
Size of blocks used for non-rigid registration, in pixels	block_size	[128,128]
Threshold to apply smoothing for registration	snr_thresh	1.2
Maximum block shift allowed for non-rigid registration, relative to the shift of rigid registration	maxregshiftNR	20

Region of interest detection with CellPose		
Run ROI detection algorithm	roidetect	True
Image to use for *CellPose* ROI detection. 3: use of the enhanced mean image	anatomical_only	3
Diameter used for detection of ROIs	diameter	12
Threshold for cell detection used in *CellPose*	cellprob_threshold	0
Maximum error flow for each detected mask	flow_threshold	1.5
Window for spatial high-pass filtering	spatial_hp_cp	0
Model used for training the *CellPose* network. "cyto" for cytosolic dataset.	pretrained_model	cyto
Signal extraction		
Extract the signal from the neuropil	neuropil_extract	True
Number of pixels kept between the ROI and the donut for neuropil extraction	inner_neuropil_radius	2
Miminum size of the neuropil donuts, in pixels	min_neuropil_pixels	150
Use of pixels that belong to two different ROIs	allow_overlap	True

Table 2. Parameters used in Suite2p for motion correction and signal extraction of place cell recordings.

iii. Exclusion criteria.

Different criteria were used for the exclusion of mice from the analysis. Were excluded mice that: (1) exhibit insufficient behavior performance: running less than 50 laps per day, low licking selectivity (inferior to 0.8 for multiple days), no continuous running; (2) exhibit excessive motion for time series to be sufficiently corrected; (3) Exhibit excessive shift in the field of view between days, especially in the depth axis.

iv. Pre-processing steps for fluorescent signal

To correct for fluorescence bleaching and increase the signal-to-noise ratio in the data, a baseline correction has been applied. For each neuron, the neuropil was subtracted from the raw fluorescence: $F_{neuron} = F_{raw} - 0.7 \times F_{neuropil}$ (Chen et al., 2013; Pachitariu et al., 2016; Peron et al., 2015). The fluorescent data was then separately pre-processed for each session. Slow changes in the traces were corrected, normalizing the fluorescence with the 30th-percentile value determined on a 3-second interval window around each data point. This baseline-corrected signal was then smoothed using a 5-bin boxcar.

v. Detection of transients

The baseline-corrected fluorescence traces were then analyzed with the ratio of positive-to-negative-going transients analysis, with varying amplitudes and durations, as described previously (Dombeck et al., 2007), with minor modifications. The baseline was determined by taking the median calcium activity for each cell and the median absolute deviation (MAD) is used for the calculation of positive and negative transients. This analysis is used to identify the significant $\Delta F/F$ transients with less than a 5% chance of being generated by noise. These transients are then used for the following analysis and all baseline timepoints are set to zero.

vi. Place cells maps

Timepoints with speed below 10 cm.s^{-1} were excluded from further analysis. For each neuron, averages of transients-only $\Delta F/F$ for each bin (5 cm bins) position were computed for each lap. For each session, a map is obtained for pre- and post-stimulations. For both blocks, place cells are independently determined. Significant activity in each bin is determined as the average transients-only $\Delta F/F$ of corresponding laps (pre: first 20 complete laps; post: last 20 complete laps) greater than 95% of the values of the mean-shuffled $\Delta F/F$ (10 000 shuffles, p < 0.05). A cell is qualified as a

place cell if all the following criteria are met: (1) at least one place field (streaks of significant activity) ranges between 10 and 75cm; (2) significant activity is found in at least 30% of the laps following place field apparition.

Place maps are cross-validated by averaging the rank obtained from the peak activity of average transients-only *Δ*F/F of place cells in odd and even trials respectively applied to even and odd trials. For comparison across days, the mean rank from one day is applied to the other days. The same steps were applied when computing the maps for early place cells and induced place cells. Pearson correlations are finally determined by correlating the bin with the peak activity of ordered place cells in pre- and post-stimulation in each session.

vii. Population code vectors correlation

For each binned position, the population vector activity of early place cells for pre-stimulation was correlated with the same vector for post-stimulation on different experimental days (before, stimulation, and after). The diagonals of the maps are then correlated between days using Pearson correlation (See figure 34a).

viii. Bayesian decoder

Animal's position x_i was decoded at each time-point (frame) using the multi-unit activity a_{cells} (transients-only $\Delta F/F_0$) of all N place cells, as follows (Adoff et al., 2021; Pettit et al., 2022; Wilson and McNaughton, 1993; Zhang et al., 1998; Ziv et al., 2013):

$$p(x_i | a_{\text{cells}}) = C \left(\prod_{j=1}^{N} f_j(x_i)^{a_i} \right) . e^{-\sum_{j=1}^{N} f_j(x_i)}$$

where $f_j(x_i)$ is the template activity of place cell j at position x_i, a_i is the recorded activity in the current time-point, and C is a normalization constant (ensuring the distribution integrates to 1) chosen so as to implement a flat, uniform prior over positions. The decoded position corresponds to the maximum a posteriori.

To assess the stability of the place code before vs. after optogenetic stimulation, we trained the Bayesian decoder (i.e., estimated $f(x)$) using activity and positions from the first part of the recording (pre) and evaluated its performance at predicting the (unseen) positions based on neuronal activity in the second part of the recording (post) (see figure 34e).

ix. Responding neurons

To identify neurons responding to optogenetic stimulation, for each neuron, an average trace from a baseline-corrected evoked calcium responses is used. A neuron is classified as responding if more than 50% of the time points during the optogenetic stimulation are greater than 95% of the values of the mean-shuffled ΔF/F (10,000 shuffles, p < 0.05).

7. Statistics.

Statistical analyses were performed using custom scripts on Python or R Studio (*Foundation for Statistical Computing*, Vienna, Austria). Bootstrap analysis was performed with custom-made Python script when indicated, using 10,000 random permutations of the data to generate a null distribution, and significance was determined when the data points were greater than 95% of the values obtained from shuffled data (p < 0.05).

Repeated measures ANOVA analyses (function *aov*, *stats* library), Student's *t*-tests (function *t.test*, *stats* library), Pearson's chi-square tests (function *chisq.test*, *stats* library) and exact binomial tests (function *binom.test*, *stats* library) were performed using R Studio when indicated. Dendrites and mice were qualified as random effects when appropriate. *Bonferonni* correction was used for the paired *t*-test.

8. Data and code availability

The code and datasets generated during this thesis are available upon request.

References

Abraham, W.C., Robins, A., 2005. Memory retention – the synaptic stability versus plasticity dilemma. Trends Neurosci. 28, 73–78. https://doi.org/10.1016/j.tins.2004.12.003

Adeniyi, P.A., Shrestha, A., Ogundele, O.M., 2020. Distribution of VTA Glutamate and Dopamine Terminals, and their Significance in CA1 Neural Network Activity. Neuroscience 446, 171–198. https://doi.org/10.1016/j.neuroscience.2020.06.045

Adoff, M.D., Climer, J.R., Davoudi, H., Marvin, J.S., Looger, L.L., Dombeck, D.A., 2021. The functional organization of excitatory synaptic input to place cells. Nat. Commun. 12, 1–15. https://doi.org/10.1038/s41467-021-23829-y

Aggarwal, A., Liu, R., Chen, Y., Ralowicz, A.J., Bergerson, S.J., Tomaska, F., Mohar, B., Hanson, T.L., Hasseman, J.P., Reep, D., Tsegaye, G., Yao, P., Ji, X., Kloos, M., Walpita, D., Patel, R., Mohr, M.A., Tillberg, P.W., Looger, L.L., Marvin, J.S., Hoppa, M.B., Konnerth, A., Kleinfeld, D., Schreiter, E.R., Podgorski, K., 2023. Glutamate indicators with improved activation kinetics and localization for imaging synaptic transmission. Nat. Methods 20, 925–934. https://doi.org/10.1038/s41592-023-01863-6

Aitken, K., Garrett, M., Olsen, S., Mihalas, S., 2022. The geometry of representational drift in natural and artificial neural networks. PLOS Comput. Biol. 18, e1010716. https://doi.org/10.1371/journal.pcbi.1010716

Alme, C.B., Miao, C., Jezek, K., Treves, A., Moser, E.I., Moser, M.-B., 2014. Place cells in the hippocampus: Eleven maps for eleven rooms. Proc. Natl. Acad. Sci. 111, 18428–18435. https://doi.org/10.1073/pnas.1421056111

Andersen, P., 1960. Interhippocampal Impulses. Acta Physiol. Scand. 48, 178–208. https://doi.org/10.1111/j.1748-1716.1960.tb01856.x

Andersen, P., Morris, R., Amaral, D., Bliss, T., O'Keefe, J., 2007. The Hippocampus book. Oxford University Press, Oxford.

Andersen, P., Sundberg, S.H., Sveen, O., Wigström, H., 1977. Specific long-lasting potentiation of synaptic transmission in hippocampal slices. Nature 266, 736–737. https://doi.org/10.1038/266736a0

Araya, R., Jiang, J., Eisenthal, K.B., Yuste, R., 2006. The spine neck filters membrane potentials. Proc. Natl. Acad. Sci. 103, 17961–17966. https://doi.org/10.1073/pnas.0608755103

Arellano, J.I., Benavides-Piccione, R., DeFelipe, J., Yuste, R., 2007. Ultrastructure of Dendritic Spines: Correlation Between Synaptic and Spine Morphologies. Front. Neurosci. 1, 131–143. https://doi.org/10.3389/neuro.01.1.1.010.2007

Aschauer, D.F., Eppler, J.-B., Ewig, L., Chambers, A.R., Pokorny, C., Kaschube, M., Rumpel, S., 2022. Learning-induced biases in the ongoing dynamics of sensory representations predict stimulus generalization. Cell Rep. 38.

https://doi.org/10.1016/j.celrep.2022.110340

Attardo, A., Fitzgerald, J.E., Schnitzer, M.J., 2015a. Impermanence of dendritic spines in live adult CA1 hippocampus. Nature 523, 592–596. https://doi.org/10.1038/nature14467

Attardo, A., Fitzgerald, J.E., Schnitzer, M.J., 2015b. Impermanence of dendritic spines in live adult CA1 hippocampus. Nature 523, 592–596. https://doi.org/10.1038/nature14467

Bang, J.W., Hamilton-Fletcher, G., Chan, K.C., 2023. Visual Plasticity in Adulthood: Perspectives from Hebbian and Homeostatic Plasticity. The Neuroscientist 29, 117–138. https://doi.org/10.1177/10738584211037619

Bastrikova, N., Gardner, G.A., Reece, J.M., Jeromin, A., Dudek, S.M., 2008. Synapse elimination accompanies functional plasticity in hippocampal neurons. Proc. Natl. Acad. Sci. U. S. A. 105, 3123–3127. https://doi.org/10.1073/pnas.0800027105

Bauer, J., Lewin, U., Herbert, E., Gjorgjieva, J., Schoonover, C., Fink, A., Rose, T., Bonhoeffer, T., Hübener, M., 2024. Sensory experience steers representational drift in mouse visual cortex. https://doi.org/10.1101/2023.09.22.558966

Bear, M.F., Malenka, R.C., 1994. Synaptic plasticity: LTP and LTD. Curr. Opin. Neurobiol. 4, 389–399. https://doi.org/10.1016/0959-4388(94)90101-5

Bell, M., Bartol, T., Sejnowski, T., Rangamani, P., 2019. Dendritic spine geometry and spine apparatus organization govern the spatiotemporal dynamics of calcium. J. Gen. Physiol. 151, 1017–1034. https://doi.org/10.1085/jgp.201812261

Beniaguev, D., Shapira, S., Segev, I., London, M., 2022. Multiple Synaptic Contacts combined with Dendritic Filtering enhance Spatio-Temporal Pattern Recognition capabilities of Single Neurons. https://doi.org/10.1101/2022.01.28.478132

Bir, S.C., Ambekar, S., Kukreja, S., Nanda, A., 2015. Julius Caesar Arantius (Giulio Cesare Aranzi, 1530–1589) and the hippocampus of the human brain: history behind the discovery. J. Neurosurg. 122, 971–975. https://doi.org/10.3171/2014.11.JNS132402

Bittner, K.C., Grienberger, C., Vaidya, S.P., Milstein, A.D., Macklin, J.J., Suh, J., Tonegawa, S., Magee, J.C., 2015. Conjunctive input processing drives feature selectivity in hippocampal CA1 neurons. Nat. Neurosci. 18, 1133–1142. https://doi.org/10.1038/nn.4062

Bittner, K.C., Milstein, A.D., Grienberger, C., Romani, S., Magee, J.C., 2017. Behavioral time scale synaptic plasticity underlies CA1 place fields. Science 357, 1033–1036. https://doi.org/10.1126/science.aan3846

Bliss, T.V., Lancaster, B., Wheal, H.V., 1983. Long-term potentiation in commissural and Schaffer projections to hippocampal CA1 cells: an in vivo study in the rat. J. Physiol. 341, 617–626. https://doi.org/10.1113/jphysiol.1983.sp014828

Bliss, T.V., Lomo, T., 1973. Long-lasting potentiation of synaptic transmission in the dentate area of the anaesthetized rabbit following stimulation of the perforant path. J. Physiol. 232, 331–356. https://doi.org/10.1113/jphysiol.1973.sp010273

Bliss, T.V.P., 1979. Synaptic plasticity in the hippocampus. Trends Neurosci. 2, 42–45. https://doi.org/10.1016/0166-2236(79)90019-5

Bliss, T.V.P., Collingridge, G.L., 1993. A synaptic model of memory: long-term potentiation in the hippocampus. Nature 361, 31–39. https://doi.org/10.1038/361031a0

Bloodgood, B.L., Giessel, A.J., Sabatini, B.L., 2009. Biphasic Synaptic Ca Influx Arising from Compartmentalized Electrical Signals in Dendritic Spines. PLOS Biol. 7, e1000190. https://doi.org/10.1371/journal.pbio.1000190

Bontempi, B., Laurent-Demir, C., Destrade, C., Jaffard, R., 1999. Time-dependent reorganization of brain circuitry underlying long-term memory storage. Nature 400, 671–675. https://doi.org/10.1038/23270

Bosch, M., Castro, J., Saneyoshi, T., Matsuno, H., Sur, M., Hayashi, Y., 2014. Structural and molecular remodeling of dendritic spine substructures during long-term potentiation. Neuron 82, 444–459. https://doi.org/10.1016/j.neuron.2014.03.021

Bourne, J.N., Harris, K.M., 2008. Balancing Structure and Function at Hippocampal Dendritic Spines. Annu. Rev. Neurosci. 31, 47–67. https://doi.org/10.1146/annurev.neuro.31.060407.125646

Bragin, A.G., Zhadina, S.D., Vinogradova, O.S., Kozhechkin, S.N., 1977. Topography and some characteristics of the dentate fascia-field CA3 relations investigated in hippocampal slices in vitro. Brain Res. 135, 55–66. https://doi.org/10.1016/0006-8993(77)91051-4

Brzosko, Z., Zannone, S., Schultz, W., Clopath, C., Paulsen, O., 2017. Sequential neuromodulation of Hebbian plasticity offers mechanism for effective reward-based navigation. eLife 6, e27756. https://doi.org/10.7554/eLife.27756

Buhl, E.H., Halasy, K., Somogyi, P., 1994. Diverse sources of hippocampal unitary inhibitory postsynaptic potentials and the number of synaptic release sites. Nature 368, 823–828. https://doi.org/10.1038/368823a0

Burgess, N., Maguire, E.A., O'Keefe, J., 2002. The human hippocampus and spatial and episodic memory. Neuron 35, 625–641. https://doi.org/10.1016/s0896-6273(02)00830-9

Buzsáki, G., 1980. Long-term potentiation of the commissural path-CA1 pyramidal cell synapse in the hippocampus of the freely moving rat. Neurosci. Lett. 19, 293–296. https://doi.org/10.1016/0304-3940(80)90276-1

Carroll, R.C., Lissin, D.V., Zastrow, M. von, Nicoll, R.A., Malenka, R.C., 1999. Rapid redistribution of glutamate receptors contributes to long-term depression in hippocampal cultures. Nat. Neurosci. 2, 454–460. https://doi.org/10.1038/8123

Chaudhuri, R., Fiete, I., 2016. Computational principles of memory. Nat. Neurosci. 19, 394–403. https://doi.org/10.1038/nn.4237

Chen, T.-W., Wardill, T.J., Sun, Y., Pulver, S.R., Renninger, S.L., Baohan, A., Schreiter, E.R., Kerr, R.A., Orger, M.B., Jayaraman, V., Looger, L.L., Svoboda, K., Kim, D.S., 2013.

Ultrasensitive fluorescent proteins for imaging neuronal activity. Nature 499, 295–300. https://doi.org/10.1038/nature12354

Cho, H., Shin, W., Lee, H., Suh, B., Kim, E., Han, Jin-hee, Cho, H., Shin, W., Lee, H., Lee, Y., Kim, M., Oh, J., Han, Junho, Jeong, Y., 2021. Article Turnover of fear engram cells by repeated experience Article Turnover of fear engram cells by repeated experience. Curr. Biol. 1–12. https://doi.org/10.1016/j.cub.2021.10.004

Choi, D.I., Kim, Jooyoung, Lee, H., Kim, Ji-il, Sung, Y., Choi, J.E., Venkat, S.J., Park, P., Jung, H., Kaang, B.-K., 2021. Synaptic correlates of associative fear memory in the lateral amygdala. Neuron 109, 2717-2726.e3. https://doi.org/10.1016/j.neuron.2021.07.003

Choi, J.H., Sim, S.E., Kim, J. il, Choi, D.I.I., Oh, J., Ye, S., Lee, J., Kim, T.H., Ko, H.G., Lim, C.S., Kaang, B.K., 2018. Interregional synaptic maps among engram cells underlie memory formation. Science 360, 430–435. https://doi.org/10.1126/science.aas9204

Cholvin, T., Hainmueller, T., Bartos, M., 2021. The hippocampus converts dynamic entorhinal inputs into stable spatial maps. Neuron 109, 3135-3148.e7. https://doi.org/10.1016/j.neuron.2021.09.019

Choquet, D., 2018. Linking Nanoscale Dynamics of AMPA Receptor Organization to Plasticity of Excitatory Synapses and Learning. J. Neurosci. 38, 9318–9329. https://doi.org/10.1523/JNEUROSCI.2119-18.2018

Citri, A., Malenka, R.C., 2008. Synaptic plasticity: Multiple forms, functions, and mechanisms. Neuropsychopharmacology 33, 18–41. https://doi.org/10.1038/sj.npp.1301559

Comrie, A.E., Frank, L.M., Kay, K., 2022. Imagination as a fundamental function of the hippocampus. Philos. Trans. R. Soc. B Biol. Sci. 377, 20210336. https://doi.org/10.1098/rstb.2021.0336

Cornejo, V.H., Ofer, N., Yuste, R., 2022. Voltage compartmentalization in dendritic spines in vivo. Science 375, 82–86. https://doi.org/10.1126/science.abg0501

Coultrap, S.J., Freund, R.K., O'Leary, H., Sanderson, J.L., Roche, K.W., Dell'Acqua, M.L., Bayer, K.U., 2014. Autonomous CaMKII Mediates Both LTP and LTD Using a Mechanism for Differential Substrate Site Selection. Cell Rep. 6, 431–437. https://doi.org/10.1016/j.celrep.2014.01.005

Dana, H., Sun, Y., Mohar, B., Hulse, B.K., Kerlin, A.M., Hasseman, J.P., Tsegaye, G., Tsang, A., Wong, A., Patel, R., Macklin, J.J., Chen, Y., Konnerth, A., Jayaraman, V., Looger, L.L., Schreiter, E.R., Svoboda, K., Kim, D.S., 2019. High-performance calcium sensors for imaging activity in neuronal populations and microcompartments. Nat. Methods 16, 649–657. https://doi.org/10.1038/s41592-019-0435-6

Davis, H.P., Squire, L.R., 1984. Protein synthesis and memory: A review. Psychol. Bull. 96, 518–559. https://doi.org/10.1037/0033-2909.96.3.518

Debanne, D., Boudkkazi, S., Campanac, E., Cudmore, R.H., Giraud, P., Fronzaroli-

Molinieres, L., Carlier, E., Caillard, O., 2008. Paired-recordings from synaptically coupled cortical and hippocampal neurons in acute and cultured brain slices. Nat. Protoc. 3, 1559–1568. https://doi.org/10.1038/nprot.2008.147

DeFelipe, J., Fariñas, I., 1992. The pyramidal neuron of the cerebral cortex: Morphological and chemical characteristics of the synaptic inputs. Prog. Neurobiol. 39, 563–607. https://doi.org/10.1016/0301-0082(92)90015-7

Deitch, D., Rubin, A., Ziv, Y., 2021. Representational drift in the mouse visual cortex. Curr. Biol. 31, 4327-4339.e6. https://doi.org/10.1016/j.cub.2021.07.062

Denk, W., Strickler, J.H., Webb, W.W., 1990. Two-Photon Laser Scanning Fluorescence Microscopy. Science 248, 73–76. https://doi.org/10.1126/science.2321027

Deuchars, J., West, D.C., Thomson, A.M., 1994. Relationships between morphology and physiology of pyramid-pyramid single axon connections in rat neocortex in vitro. J. Physiol. 478, 423–435. https://doi.org/10.1113/jphysiol.1994.sp020262

Diamantaki, M., Coletta, S., Nasr, K., Zeraati, R., Laturnus, S., Berens, P., Preston-Ferrer, P., Burgalossi, A., 2018. Manipulating Hippocampal Place Cell Activity by Single-Cell Stimulation in Freely Moving Mice. Cell Rep. 23, 32–38. https://doi.org/10.1016/J.CELREP.2018.03.031/ATTACHMENT/0648A91E-BEFF-4A7C-86D9-48A51DC09EC7/MMC1.PDF

Dombeck, D.A., Harvey, C.D., Tian, L., Looger, L.L., Tank, D.W., 2010. Functional imaging of hippocampal place cells at cellular resolution during virtual navigation. Nat. Neurosci. 13, 1433–1440. https://doi.org/10.1038/nn.2648

Dombeck, D.A., Khabbaz, A.N., Collman, F., Adelman, T.L., Tank, D.W., 2007. Imaging Large-Scale Neural Activity with Cellular Resolution in Awake, Mobile Mice. Neuron 56, 43–57. https://doi.org/10.1016/j.neuron.2007.08.003

Dong, C., Madar, A.D., Sheffield, M.E.J., 2021. Distinct place cell dynamics in CA1 and CA3 encode experience in new environments. Nat. Commun. 12, 1–13. https://doi.org/10.1038/s41467-021-23260-3

Dougherty, R., 2012. Extensions of DAMAS and Benefits and Limitations of Deconvolution in Beamforming | Aeroacoustics Conferences. Adv. Test. Tech. Phased Arrays. https://doi.org/10.2514/6.2005-2961

Douglas, R.M., Goddard, G.V., 1975. Long-term potentiation of the perforant path-granule cell synapse in the rat hippocampus. Brain Res. 86, 205–215. https://doi.org/10.1016/0006-8993(75)90697-6

Driscoll, L.N., Pettit, N.L., Minderer, M., Chettih, S.N., Harvey, C.D., 2017. Dynamic Reorganization of Neuronal Activity Patterns in Parietal Cortex. Cell 170, 986-999.e16. https://doi.org/10.1016/j.cell.2017.07.021

Dudai, Y., 2002. Molecular bases of long-term memories: a question of persistence. Curr.

Opin. Neurobiol. 12, 211–216. https://doi.org/10.1016/S0959-4388(02)00305-7

Dudek, S.M., Alexander, G.M., Farris, S., 2016. Rediscovering area CA2: unique properties and functions. Nat. Rev. Neurosci. 17, 89–102. https://doi.org/10.1038/nrn.2015.22

Dudek, S.M., Bear, M.F., 1992. Homosynaptic long-term depression in area CA1 of hippocampus and effects of N-methyl-D-aspartate receptor blockade. Proc. Natl. Acad. Sci. U. S. A. 89, 4363–4367. https://doi.org/10.1073/pnas.89.10.4363

Dudok, B., Szoboszlay, M., 2021. Recruitment and inhibitory action of hippocampal axo-axonic cells during behavior. Neuron. https://doi.org/10.1016/j.neuron.2021.09.033

Dupret, D., O'Neill, J., Pleydell-Bouverie, B., Csicsvari, J., 2010. The reorganization and reactivation of hippocampal maps predict spatial memory performance. Nat. Neurosci. 13, 995–1002. https://doi.org/10.1038/nn.2599

Dürst, C.D., Wiegert, J.S., Schulze, C., Helassa, N., Török, K., Oertner, T.G., 2022. Vesicular release probability sets the strength of individual Schaffer collateral synapses. Nat. Commun. 13, 6126. https://doi.org/10.1038/s41467-022-33565-6

Eichenbaum, H., Dudchenko, P., Wood, E., Shapiro, M., Tanila, H., 1999. The Hippocampus, Memory, and Place Cells: Is It Spatial Memory or a Memory Space? Neuron 23, 209–226. https://doi.org/10.1016/S0896-6273(00)80773-4

El-Boustani, S., Ip, J.P.K., Breton-Provencher, V., Knott, G.W., Okuno, H., Bito, H., Sur, M., 2018. Locally coordinated synaptic plasticity of visual cortex neurons in vivo. Science 360, 1349–1354. https://doi.org/10.1126/science.aao0862

Ellis-Davies, G.C.R., 2019. Two-Photon Uncaging of Glutamate. Front. Synaptic Neurosci. 10.

Engelhardt, E., 2016. Hippocampus discovery First steps. Dement. Neuropsychol. 10, 58–62. https://doi.org/10.1590/S1980-57642016DN10100011

Evans, M.H., Petersen, R.S., Humphries, M.D., 2020. On the use of calcium deconvolution algorithms in practical contexts. https://doi.org/10.1101/871137

Fan, L.Z., Kim, D.K., Jennings, J.H., Tian, H., Wang, P.Y., Ramakrishnan, C., Randles, S., Sun, Y., Thadhani, E., Kim, Y.S., Quirin, S., Giocomo, L., Cohen, A.E., Deisseroth, K., 2023. All-optical physiology resolves a synaptic basis for behavioral timescale plasticity. Cell S0092867422015781. https://doi.org/10.1016/j.cell.2022.12.035

Fedorov, N.B., Sergeeva, O.A., Skrebitsky, V.G., 1993. Priming stimulation facilitates Hebb-type plasticity in the Schaffer collateral-commissural pathways of the mouse hippocampus. Exp. Brain Res. 94, 270–272. https://doi.org/10.1007/BF00230295

Felipe, Y., Kossio, K., Goedeke, S., Klos, C., 2020. Drifting Assemblies for Persistent Memory neurons . For faithful storage these assemblies are assumed to consist of the same neurons 1–21.

Feng, G., Mellor, R.H., Bernstein, M., Keller-Peck, C., Nguyen, Q.T., Wallace, M.,

Nerbonne, J.M., Lichtman, J.W., Sanes, J.R., 2000. Imaging Neuronal Subsets in Transgenic Mice Expressing Multiple Spectral Variants of GFP. Neuron 28, 41–51. https://doi.org/10.1016/S0896-6273(00)00084-2

Fiala, J.C., Feinberg, M., Popov, V., Harris, K.M., 1998. Synaptogenesis via dendritic filopodia in developing hippocampal area CA1. J. Neurosci. Off. J. Soc. Neurosci. 18, 8900–8911. https://doi.org/10.1523/JNEUROSCI.18-21-08900.1998

Fifková, E., Van Harreveld, A., 1977. Long-lasting morphological changes in dendritic spines of dentate granular cells following stimulation of the entorhinal area. J. Neurocytol. 6, 211–230. https://doi.org/10.1007/BF01261506

Frank, A.C., Huang, S., Zhou, M., Gdalyahu, A., Kastellakis, G., Silva, T.K., Lu, E., Wen, X., Poirazi, P., Trachtenberg, J.T., Silva, A.J., 2018. Hotspots of dendritic spine turnover facilitate clustered spine addition and learning and memory. Nat. Commun. 9, 422. https://doi.org/10.1038/s41467-017-02751-2

Frankland, P.W., Bontempi, B., 2005. The organization of recent and remote memories. Nat. Rev. Neurosci. 6, 119–130. https://doi.org/10.1038/nrn1607

French, R.M., 1999. Catastrophic forgetting in connectionist networks. Trends Cogn. Sci. 3, 128–135. https://doi.org/10.1016/S1364-6613(99)01294-2

Frey, U., Huang, Y.-Y., Kandel, E.R., 1993. Effects of cAMP Simulate a Late Stage of LTP in Hippocampal CA1 Neurons. Science 260, 1661–1664. https://doi.org/10.1126/science.8389057

Fröhlich, F., 2016. Chapter 4 - Synaptic Plasticity, in: Fröhlich, F. (Ed.), Network Neuroscience. Academic Press, San Diego, pp. 47–58. https://doi.org/10.1016/B978-0-12-801560-5.00004-5

Fu, M., Yu, X., Lu, J., Zuo, Y., 2012. Repetitive motor learning induces coordinated formation of clustered dendritic spines in vivo. Nature 483, 92–96. https://doi.org/10.1038/nature10844

Fusi, S., 2002. Hebbian spike-driven synaptic plasticity for learning patterns of mean firing rates. Biol. Cybern. 87, 459–470. https://doi.org/10.1007/s00422-002-0356-8

Fusi, S., Abbott, L.F., 2007. Limits on the memory storage capacity of bounded synapses. Nat. Neurosci. 10, 485–493. https://doi.org/10.1038/nn1859

Fusi, S., Drew, P.J., Abbott, L.F., 2005. Cascade Models of Synaptically Stored Memories. Neuron 45, 599–611. https://doi.org/10.1016/j.neuron.2005.02.001

Gauthier, J.L., Tank, D.W., 2018. A Dedicated Population for Reward Coding in the Hippocampus. Neuron 99, 179-193.e7. https://doi.org/10.1016/j.neuron.2018.06.008

Geiller, T., Fattahi, M., Choi, J., 2017. Place cells are more strongly tied to landmarks in deep than in superficial CA1. https://doi.org/10.1038/ncomms14531

Geiller, T., Sadeh, S., Rolotti, S.V., Blockus, H., Vancura, B., Negrean, A., Murray, A.J.,

Rózsa, B., Polleux, F., Clopath, C., Losonczy, A., 2022. Local circuit amplification of spatial selectivity in the hippocampus. Nature 601, 105–109. https://doi.org/10.1038/s41586-021-04169-9

Go, M.A., Rogers, J., Gava, G.P., Davey, C.E., Prado, S., Liu, Y., Schultz, S.R., 2021. Place Cells in Head-Fixed Mice Navigating a Floating Real-World Environment. Front. Cell. Neurosci. 15.

Goelet, P., Castellucci, V.F., Schacher, S., Kandel, E.R., 1986. The long and the short of long–term memory—a molecular framework. Nature 322, 419–422. https://doi.org/10.1038/322419a0

Goto, A., Bota, A., Miya, K., Wang, J., Tsukamoto, S., Jiang, X., Hirai, D., Murayama, M., Matsuda, T., McHugh, T.J., Nagai, T., Hayashi, Y., 2021. Stepwise synaptic plasticity events drive the early phase of memory consolidation. Science 374, 857–863. https://doi.org/10.1126/science.abj9195

Gray, E.G., 1959. Electron Microscopy of Synaptic Contacts on Dendrite Spines of the Cerebral Cortex. Nature 183, 1592–1593. https://doi.org/10.1038/1831592a0

Greenough, W.T., Bailey, C.H., 1988. The anatomy of a memory: convergence of results across a diversity of tests. Trends Neurosci. 11, 142–147. https://doi.org/10.1016/0166-2236(88)90139-7

Grienberger, C., Milstein, A.D., Bittner, K.C., Romani, S., Magee, J.C., 2017. Inhibitory suppression of heterogeneously tuned excitation enhances spatial coding in CA1 place cells. Nat. Neurosci. 20, 417–426. https://doi.org/10.1038/nn.4486

Grieves, R.M., Wood, E.R., Dudchenko, P.A., 2016. Place cells on a maze encode routes rather than destinations. eLife 5, e15986. https://doi.org/10.7554/eLife.15986

Grutzendler, J., Kasthuri, N., Gan, W.B., 2002. Long-term dendritic spine stability in the adult cortex. Nature 420, 812–816. https://doi.org/10.1038/nature01276

Gu, L., Kleiber, S., Schmid, L., Nebeling, F., Chamoun, M., Steffen, J., Wagner, J., Fuhrmann, M., 2014. Long-Term In Vivo Imaging of Dendritic Spines in the Hippocampus Reveals Structural Plasticity. https://doi.org/10.1523/JNEUROSCI.1464-14.2014

Gu, Q., 2002. Neuromodulatory transmitter systems in the cortex and their role in cortical plasticity. Neuroscience 111, 815–835. https://doi.org/10.1016/S0306-4522(02)00026-X

Guan, H., Middleton, S.J., Inoue, T., McHugh, T.J., 2021. Lateralization of CA1 assemblies in the absence of CA3 input. Nat. Commun. 12, 6114. https://doi.org/10.1038/s41467-021-26389-3

Gulledge, A.T., Kampa, B.M., Stuart, G.J., 2005. Synaptic integration in dendritic trees. J. Neurobiol. 64, 75–90. https://doi.org/10.1002/neu.20144

Hainmueller, T., Bartos, M., 2018. Parallel emergence of stable and dynamic memory engrams in the hippocampus. Nature 558, 292–296. https://doi.org/10.1038/s41586-018-0191-

2

Harris, K.M., Kater, S.B., 1994. Dendritic Spines: Cellular Specializations Imparting Both Stability and Flexibility to Synaptic Function. Annu. Rev. Neurosci. 17:341-71.

Harris, K.M., Stevens, J.K., 1989. Dendritic spines of CA 1 pyramidal cells in the rat hippocampus: serial electron microscopy with reference to their biophysical characteristics. J. Neurosci. 9, 2982–2997. https://doi.org/10.1523/JNEUROSCI.09-08-02982.1989

Harvey, C.D., Svoboda, K., 2007. Locally dynamic synaptic learning rules in pyramidal neuron dendrites. Nature 450, 1195–1200. https://doi.org/10.1038/nature06416

Harvey, C.D., Yasuda, R., Zhong, H., Svoboda, K., 2008. The Spread of Ras Activity Triggered by Activation of a Single Dendritic Spine. Science 321, 136–140. https://doi.org/10.1126/science.1159675

Hayama, T., Noguchi, J., Watanabe, S., Takahashi, N., Hayashi-Takagi, A., Ellis-Davies, G.C.R., Matsuzaki, M., Kasai, H., 2013. GABA promotes the competitive selection of dendritic spines by controlling local Ca2+ signaling. Nat. Neurosci. 16, 1409–1416. https://doi.org/10.1038/nn.3496

Hayashi, Y., Kobayakawa, K., Kobayakawa, R., 2023. The temporal and contextual stability of activity levels in hippocampal CA1 cells. Proc. Natl. Acad. Sci. 120, e2221141120. https://doi.org/10.1073/pnas.2221141120

Hayashi-Takagi, A., Yagishita, S., Nakamura, M., Shirai, F., Wu, Y.I., Loshbaugh, A.L., Kuhlman, B., Hahn, K.M., Kasai, H., 2015. Labelling and optical erasure of synaptic memory traces in the motor cortex. Nature 525, 333–338. https://doi.org/10.1038/nature15257

Hebb, D.O., 1949. The Organization of Behavior, in: John Wiley and Sons.

Hedrick, N.G., Lu, Z., Bushong, E., Singhi, S., Nguyen, P., Magaña, Y., Jilani, S., Kook Lim, B., Ellisman, M., Komiyama, T., 2022. Learning binds new inputs into functional synaptic clusters via spinogenesis. https://doi.org/10.1038/s41593-022-01086-6

Higley, M.J., Sabatini, B.L., 2012. Calcium Signaling in Dendritic Spines. Cold Spring Harb. Perspect. Biol. 4, a005686–a005686. https://doi.org/10.1101/cshperspect.a005686

Holtmaat, A., Caroni, P., 2016. Functional and structural underpinnings of neuronal assembly formation in learning. Nat. Neurosci. 19, 1553–1562. https://doi.org/10.1038/nn.4418

Holtmaat, A., Svoboda, K., 2009. Experience-dependent structural synaptic plasticity in the mammalian brain. Nat. Rev. Neurosci. 10, 647–658. https://doi.org/10.1038/nrn2699

Holtmaat, A.J.G.D., Trachtenberg, J.T., Wilbrecht, L., Shepherd, G.M., Zhang, X., Knott, G.W., Svoboda, K., 2005. Transient and persistent dendritic spines in the neocortex in vivo. Neuron 45, 279–291. https://doi.org/10.1016/j.neuron.2005.01.003

Huganir, R.L., Nicoll, R.A., 2013. AMPARs and Synaptic Plasticity: The Last 25 Years. Neuron 80, 704–717. https://doi.org/10.1016/j.neuron.2013.10.025

Hull, C.L., 1943. Principles of behavior: an introduction to behavior theory, Principles of behavior: an introduction to behavior theory. Appleton-Century, Oxford, England.

Iacaruso, M.F., Gasler, I.T., Hofer, S.B., 2017. Synaptic organization of visual space in primary visual cortex. Nature 547, 449–452. https://doi.org/10.1038/nature23019

Jane, D., 2007. AMPA Glutamate Receptor, in: Enna, S.J., Bylund, D.B. (Eds.), xPharm: The Comprehensive Pharmacology Reference. Elsevier, New York, pp. 1–19. https://doi.org/10.1016/B978-008055232-3.60374-5

Jang, A.I., Nassar, M.R., Dillon, D.G., Frank, M.J., 2019. Positive reward prediction errors during decision-making strengthen memory encoding. Nat. Hum. Behav. 3, 719–732. https://doi.org/10.1038/s41562-019-0597-3

Jensen, K.T., Kadmon Harpaz, N., Dhawale, A.K., Wolff, S.B.E., Ölveczky, B.P., 2022. Long-term stability of single neuron activity in the motor system. Nat. Neurosci. 25, 1664–1674. https://doi.org/10.1038/s41593-022-01194-3

Jensen, T.P., Zheng, K., Cole, N., Marvin, J.S., Looger, L.L., Rusakov, D.A., 2019. Multiplex imaging relates quantal glutamate release to presynaptic Ca2+ homeostasis at multiple synapses in situ. Nat. Commun. 10, 1414. https://doi.org/10.1038/s41467-019-09216-8

Jeong, N., Singer, A.C., 2022. Learning from inhibition: Functional roles of hippocampal CA1 inhibition in spatial learning and memory. Curr. Opin. Neurobiol. 76, 102604. https://doi.org/10.1016/j.conb.2022.102604

Ji, J., Maren, S., 2008. Differential roles for hippocampal areas CA1 and CA3 in the contextual encoding and retrieval of extinguished fear. Learn. Mem. 15, 244–251. https://doi.org/10.1101/lm.794808

Johansen, J.P., Hamanaka, H., Monfils, M.H., Behnia, R., Deisseroth, K., Blair, H.T., LeDoux, J.E., 2010. Optical activation of lateral amygdala pyramidal cells instructs associative fear learning. Proc. Natl. Acad. Sci. U. S. A. 107, 12692–12697. https://doi.org/10.1073/pnas.1002418107

Kandel, E.R., 2001. The Molecular Biology of Memory Storage: A Dialogue Between Genes and Synapses. Science 294, 1030–1038. https://doi.org/10.1126/science.1067020

Kandel, E.R., Dudai, Y., Mayford, M.R., 2014. The Molecular and Systems Biology of Memory. Cell 157, 163–186. https://doi.org/10.1016/j.cell.2014.03.001

Kasai, H., Ucar, H., Morimoto, Y., Eto, F., Okazaki, H., 2023. Mechanical transmission at spine synapses: Short-term potentiation and working memory. Curr. Opin. Neurobiol. 80, 102706. https://doi.org/10.1016/j.conb.2023.102706

Kim, S., Jung, D., Royer, S., 2020. Place cell maps slowly develop via competitive learning and conjunctive coding in the dentate gyrus. Nat. Commun. 11, 4550. https://doi.org/10.1038/s41467-020-18351-6

Kinsky, N.R., Sullivan, D.W., Mau, W., Hasselmo, M.E., Eichenbaum, H.B., 2018.

Hippocampal Place Fields Maintain a Coherent and Flexible Map across Long Timescales. Curr. Biol. 28, 3578-3588.e6. https://doi.org/10.1016/j.cub.2018.09.037

Kitamura, T., Ogawa, S.K., Roy, D.S., Okuyama, T., Morrissey, M.D., Smith, L.M., Redondo, R.L., Tonegawa, S., 2017. Engrams and circuits crucial for systems consolidation of a memory. Science 356, 73–78. https://doi.org/10.1126/science.aam6808

Klausberger, T., Somogyi, P., 2008. Neuronal Diversity and Temporal Dynamics: The Unity of Hippocampal Circuit Operations. Science. https://doi.org/10.1126/science.1149381

Knott, G.W., Holtmaat, A., Wilbrecht, L., Welker, E., Svoboda, K., 2006. Spine growth precedes synapse formation in the adult neocortex in vivo. Nat. Neurosci. 9, 1117–1124. https://doi.org/10.1038/nn1747

Kohl, M.M., Shipton, O.A., Deacon, R.M., Rawlins, J.N.P., Deisseroth, K., Paulsen, O., 2011. Hemisphere-specific optogenetic stimulation reveals left-right asymmetry of hippocampal plasticity. Nat. Neurosci. 14, 1413–1415. https://doi.org/10.1038/nn.2915

Konorski, J., 1948. Conditioned reflexes and neuron organization, Conditioned reflexes and neuron organization. Cambridge University Press, New York, NY, US.

Korobova, F., Svitkina, T., 2010. Molecular Architecture of Synaptic Actin Cytoskeleton in Hippocampal Neurons Reveals a Mechanism of Dendritic Spine Morphogenesis. Mol. Biol. Cell 21, 165–176. https://doi.org/10.1091/mbc.e09-07-0596

Kovalchuk, Y., Eilers, J., Lisman, J., Konnerth, A., 2000. NMDA Receptor-Mediated Subthreshold Ca2+ Signals in Spines of Hippocampal Neurons. J. Neurosci. 20, 1791–1799. https://doi.org/10.1523/JNEUROSCI.20-05-01791.2000

Kwon, H.-B., Sabatini, B.L., 2011. Glutamate induces de novo growth of functional spines in developing cortex. Nature 474, 100–104. https://doi.org/10.1038/nature09986

Lai, C.S.W., Adler, A., Gan, W.B., 2018. Fear extinction reverses dendritic spine formation induced by fear conditioning in the mouse auditory cortex. Proc. Natl. Acad. Sci. U. S. A. https://doi.org/10.1073/pnas.1801504115

Lai, C.S.W., Franke, T.F., Gan, W.-B., 2012. Opposite effects of fear conditioning and extinction on dendritic spine remodelling. Nature 483, 87–91. https://doi.org/10.1038/nature10792

Lamanna, J., Isotti, F., Ferro, M., Racchetti, G., Anchora, L., Rucco, D., Malgaroli, A., 2021. Facilitation of dopamine-dependent long-term potentiation in the medial prefrontal cortex of male rats follows the behavioral effects of stress. J. Neurosci. Res. 99, 662–678. https://doi.org/10.1002/jnr.24732

Lamothe-Molina, P.J., Franzelin, A., Beck, L., Li, D., Auksutat, L., Fieblinger, T., Laprell, L., Alhbeck, J., Gee, C.E., Kneussel, M., Engel, A.K., Hilgetag, C.C., Morellini, F., Oertner, T.G., 2022. ΔFosB accumulation in hippocampal granule cells drives cFos pattern separation during spatial learning. Nat. Commun. 13, 6376. https://doi.org/10.1038/s41467-022-33947-w

Lamprecht, R., LeDoux, J., 2004. Structural plasticity and memory. Nat. Rev. Neurosci. 5, 45–54. https://doi.org/10.1038/nrn1301

Lee, D., Lin, B.-J., Lee, A.K., 2012. Hippocampal Place Fields Emerge upon Single-Cell Manipulation of Excitability During Behavior. Science 337, 849–853. https://doi.org/10.1126/science.1221489

Lee, H.-K., Kirkwood, A., 2011. AMPA receptor regulation during synaptic plasticity in hippocampus and neocortex. Semin. Cell Dev. Biol., Prions and Amyloids & Synapse and Brain 22, 514–520. https://doi.org/10.1016/j.semcdb.2011.06.007

Lee, S.J.R., Escobedo-Lozoya, Y., Szatmari, E.M., Yasuda, R., 2009. Activation of CaMKII in single dendritic spines during long-term potentiation. Nature 458, 299–304. https://doi.org/10.1038/nature07842

Leutgeb, J.K., Leutgeb, S., Moser, M.-B., Moser, E.I., 2007. Pattern Separation in the Dentate Gyrus and CA3 of the Hippocampus. Science 315, 961–966. https://doi.org/10.1126/science.1135801

Lewis, R.G., Florio, E., Punzo, D., Borrelli, E., 2021. The Brain's Reward System in Health and Disease. Adv. Exp. Med. Biol. 1344, 57–69. https://doi.org/10.1007/978-3-030-81147-1_4

Liberti, W.A., Schmid, T.A., Forli, A., Snyder, M., Yartsev, M.M., 2022. A stable hippocampal code in freely flying bats. Nature 604, 98–103. https://doi.org/10.1038/s41586-022-04560-0

Lin, M.Z., Schnitzer, M.J., 2016. Genetically encoded indicators of neuronal activity. Nat. Neurosci. 19, 1142–1153. https://doi.org/10.1038/nn.4359

Lisman, J., Yasuda, R., Raghavachari, S., 2012. Mechanisms of CaMKII action in long-term potentiation. Nat. Rev. Neurosci. 13, 169–182. https://doi.org/10.1038/nrn3192

Lisman, J.E., Raghavachari, S., Tsien, R.W., 2007. The sequence of events that underlie quantal transmission at central glutamatergic synapses. Nat. Rev. Neurosci. 8, 597–609. https://doi.org/10.1038/nrn2191

Liu, X., Ramirez, S., Pang, P.T., Puryear, C.B., Govindarajan, A., Deisseroth, K., Tonegawa, S., 2012. Optogenetic stimulation of a hippocampal engram activates fear memory recall. Nature 484, 381–385. https://doi.org/10.1038/nature11028

Lømo, T., 2003. The discovery of long-term potentiation. Philos. Trans. R. Soc. Lond. B. Biol. Sci. 358, 617–620. https://doi.org/10.1098/rstb.2002.1226

Lopes, G., Bonacchi, N., Frazão, J., Neto, J.P., Atallah, B.V., Soares, S., Moreira, L., Matias, S., Itskov, P.M., Correia, P.A., Medina, R.E., Calcaterra, L., Dreosti, E., Paton, J.J., Kampff, A.R., 2015. Bonsai: an event-based framework for processing and controlling data streams. Front. Neuroinformatics 9. https://doi.org/10.3389/fninf.2015.00007

Lorente de Nó, R., 1934. Studies on the structure of the cerebral cortex. II. Continuation of

the study of the ammonic system. J Psychol Neurol 46:113-177.

Lovett-Barron, M., Kaifosh, P., Kheirbek, M.A., Danielson, N., Zaremba, J.D., Reardon, T.R., Turi, G.F., Hen, R., Zemelman, B.V., Losonczy, A., 2014. Dendritic inhibition in the hippocampus supports fear learning. Science 343, 857–863. https://doi.org/10.1126/science.1247485

Lüscher, C., Malenka, R.C., 2012. NMDA Receptor-Dependent Long-Term Potentiation and Long-Term Depression (LTP/LTD). Cold Spring Harb. Perspect. Biol. 4, a005710. https://doi.org/10.1101/cshperspect.a005710

Lynch, G.S., Dunwiddie, T., Gribkoff, V., 1977. Heterosynaptic depression: A postsynaptic correlate of long-term potentiation [31]. Nature 266, 737–739. https://doi.org/10.1038/266737a0

Madar, A.D., Ewell, L.A., Jones, M.V., 2019. Pattern separation of spiketrains in hippocampal neurons. Sci. Rep. 9, 5282. https://doi.org/10.1038/s41598-019-41503-8

Magee, J.C., Grienberger, C., 2020. Synaptic Plasticity Forms and Functions. Annu. Rev. Neurosci. 43, 95–117. https://doi.org/10.1146/annurev-neuro-090919-022842

Maity, S., Jarome, T.J., Blair, J., Lubin, F.D., Nguyen, P.V., 2016. Noradrenaline goes nuclear: epigenetic modifications during long-lasting synaptic potentiation triggered by activation of β-adrenergic receptors. J. Physiol. 594, 863–881. https://doi.org/10.1113/JP271432

Malinow, R., 1994. LTP: Desperately Seeking Resolution. Science 266, 1195–1196. https://doi.org/10.1126/science.7973700

Malinow, R., 1991. Transmission between pairs of hippocampal slice neurons: quantal levels, oscillations, and LTP. Science 252, 722–724. https://doi.org/10.1126/science.1850871

Manabe, T., Nicoll, R.A., 1994. Long-Term Potentiation: Evidence Against an Increase in Transmitter Release Probability in the CA1 Region of the Hippocampus. Science 265, 1888–1892. https://doi.org/10.1126/science.7916483

Manuel Valero, A., Valero, M., Navas-Olive, A., de la Prida, L.M., rgy Buzsá ki, G., 2022. Inhibitory conductance controls place field dynamics in the hippocampus. Cell Rep. 40, 111232. https://doi.org/10.1016/J.CELREP.2022.111232

Marblestone, A.H., Wayne, G., Kording, K.P., 2016. Toward an Integration of Deep Learning and Neuroscience. Front. Comput. Neurosci. 10.

Margolis, D.J., Lütcke, H., Schulz, K., Haiss, F., Weber, B., Kügler, S., Hasan, M.T., Helmchen, F., 2012. Reorganization of cortical population activity imaged throughout long-term sensory deprivation. Nat. Neurosci. 15, 1539–1546. https://doi.org/10.1038/nn.3240

Markram, H., Lübke, J., Frotscher, M., Sakmann, B., 1997. Regulation of synaptic efficacy by coincidence of postsynaptic APs and EPSPs. Science 275, 213–215. https://doi.org/10.1126/science.275.5297.213

Marks, T.D., Goard, M.J., 2021. Stimulus-dependent representational drift in primary visual cortex. Nat. Commun. 12, 5169. https://doi.org/10.1038/s41467-021-25436-3

Marr, D., Brindley, G.S., 1997. Simple memory: a theory for archicortex. Philos. Trans. R. Soc. Lond. B Biol. Sci. 262, 23–81. https://doi.org/10.1098/rstb.1971.0078

Martig, A.K., Mizumori, S.J.Y., 2010. Place Cells, in: Koob, G.F., Moal, M.L., Thompson, R.F. (Eds.), Encyclopedia of Behavioral Neuroscience. Academic Press, Oxford, pp. 70–78. https://doi.org/10.1016/B978-0-08-045396-5.00154-8

Martin, S.J., Grimwood, P.D., Morris, R.G., 2000. Synaptic plasticity and memory: an evaluation of the hypothesis. Annu. Rev. Neurosci. 23, 649–711. https://doi.org/10.1146/annurev.neuro.23.1.649

Martin, S.J., Shires, K.L., da Silva, B.M., 2019. Hippocampal Lateralization and Synaptic Plasticity in the Intact Rat: No Left–Right Asymmetry in Electrically Induced CA3-CA1 Long-Term Potentiation. Neuroscience 397, 147–158. https://doi.org/10.1016/j.neuroscience.2018.11.044

Marvin, J.S., Borghuis, B.G., Tian, L., Cichon, J., Harnett, M.T., Akerboom, J., Gordus, A., Renninger, S.L., Chen, T.W., Bargmann, C.I., Orger, M.B., Schreiter, E.R., Demb, J.B., Gan, W.B., Hires, S.A., Looger, L.L., 2013. An optimized fluorescent probe for visualizing glutamate neurotransmission. Nat. Methods 10, 162–170. https://doi.org/10.1038/nmeth.2333

Marvin, J.S., Scholl, B., Wilson, D.E., Podgorski, K., Kazemipour, A., Müller, J.A., Schoch, S., Quiroz, F.J.U., Rebola, N., Bao, H., Little, J.P., Tkachuk, A.N., Cai, E., Hantman, A.W., Wang, S.S.H., DePiero, V.J., Borghuis, B.G., Chapman, E.R., Dietrich, D., DiGregorio, D.A., Fitzpatrick, D., Looger, L.L., 2018. Stability, affinity, and chromatic variants of the glutamate sensor iGluSnFR. Nat. Methods 15, 936–939. https://doi.org/10.1038/s41592-018-0171-3

Marvin, J.S., Shimoda, Y., Magloire, V., Leite, M., Kawashima, T., Jensen, T.P., Kolb, I., Knott, E.L., Novak, O., Podgorski, K., Leidenheimer, N.J., Rusakov, D.A., Ahrens, M.B., Kullmann, D.M., Looger, L.L., 2019. A genetically encoded fluorescent sensor for in vivo imaging of GABA. Nat. Methods 16, 763–770. https://doi.org/10.1038/s41592-019-0471-2

Matozaki, T., Nakanishi, H., Takai, Y., 2000. Small G-protein networks:: Their crosstalk and signal cascades. Cell. Signal. 12, 515–524. https://doi.org/10.1016/S0898-6568(00)00102-9

Matsuzaki, M., Ellis-Davies, G.C.R., Nemoto, T., Miyashita, Y., Iino, M., Kasai, H., 2001. Dendritic spine geometry is critical for AMPA receptor expression in hippocampal CA1 pyramidal neurons. Nat. Neurosci. 4, 1086–1092. https://doi.org/10.1038/nn736

Matsuzaki, M., Honkura, N., Ellis-Davies, G.C.R., Kasai, H., 2004. Structural basis of long-term potentiation in single dendritic spines. Nature 429, 761–766. https://doi.org/10.1038/nature02617

McClelland, J.L., McNaughton, B.L., O'Reilly, R.C., 1995. Why there are complementary learning systems in the hippocampus and neocortex: insights from the successes and failures of connectionist models of learning and memory. Psychol. Rev. 102, 419–457.

https://doi.org/10.1037/0033-295X.102.3.419

McKenzie, S., Huszár, R., English, D.F., Kim, K., Christensen, F., Yoon, E., Buzsáki, G., 2021. Preexisting hippocampal network dynamics constrain optogenetically induced place fields. Neuron 109, 1040-1054.e7. https://doi.org/10.1016/j.neuron.2021.01.011

McMahon, S.M., Jackson, M.B., 2018. An Inconvenient Truth: Calcium Sensors Are Calcium Buffers. Trends Neurosci. 41, 880–884. https://doi.org/10.1016/j.tins.2018.09.005

Meyer, D., Bonhoeffer, T., Scheuss, V., 2014. Balance and stability of synaptic structures during synaptic plasticity. Neuron 82, 430–443. https://doi.org/10.1016/j.neuron.2014.02.031

Micou, C., O'Leary, T., 2023. Representational drift as a window into neural and behavioural plasticity. Curr. Opin. Neurobiol. 81, 102746. https://doi.org/10.1016/j.conb.2023.102746

Miles, R., Le Duigou, C., Simonnet, J., Telenczuk, M., Fricker, D., 2014. Recurrent synapses and circuits in the CA3 region of the hippocampus: an associative network. Front. Cell. Neurosci. 7.

Mitchell, D.E., Martineau, É., Tazerart, S., Araya, R., 2019. Probing Single Synapses via the Photolytic Release of Neurotransmitters. Front. Synaptic Neurosci. 11.

Miyawaki, A., 2011. Development of probes for cellular functions using fluorescent proteins and fluorescence resonance energy transfer. Annu. Rev. Biochem. 80, 357–373. https://doi.org/10.1146/annurev-biochem-072909-094736

Mizrahi, A., Crowley, J.C., Shtoyerman, E., Katz, L.C., 2004. High-Resolution In Vivo Imaging of Hippocampal Dendrites and Spines. J. Neurosci. 24, 3147–3151. https://doi.org/10.1523/JNEUROSCI.5218-03.2004

Monk, T.G., Weldon, B.C., Garvan, C.W., Dede, D.E., van der Aa, M.T., Heilman, K.M., Gravenstein, J.S., 2008. Predictors of cognitive dysfunction after major noncardiac surgery. Anesthesiology 108, 18–30. https://doi.org/10.1097/01.anes.0000296071.19434.1e

Moser, E.I., Moser, M.-B., McNaughton, B.L., 2017. Spatial representation in the hippocampal formation: a history. Nat. Neurosci. 20, 1448–1464. https://doi.org/10.1038/nn.4653

Moser, M.-B., Rowland, D.C., Moser, E.I., 2015. Place Cells, Grid Cells, and Memory. Cold Spring Harb. Perspect. Biol. 7, a021808. https://doi.org/10.1101/cshperspect.a021808

Murakoshi, H., Wang, H., Yasuda, R., 2011. Local, persistent activation of Rho GTPases during plasticity of single dendritic spines. Nature 472, 100–104. https://doi.org/10.1038/nature09823

Nadim, F., Bucher, D., 2014. Neuromodulation of neurons and synapses. Curr. Opin. Neurobiol., SI: Neuromodulation 29, 48–56. https://doi.org/10.1016/j.conb.2014.05.003

Nagelhus, A., Andersson, S.O., Cogno, S.G., Moser, E.I., Moser, M.-B., 2023. Object-centered population coding in CA1 of the hippocampus. Neuron 111, 2091-2104.e14. https://doi.org/10.1016/j.neuron.2023.04.008

Nägerl, U.V., Eberhorn, N., Cambridge, S.B., Bonhoeffer, T., 2004. Bidirectional Activity-Dependent Morphological Plasticity in Hippocampal Neurons. Neuron 44, 759–767. https://doi.org/10.1016/j.neuron.2004.11.016

Nakai, J., Ohkura, M., Imoto, K., 2001. A high signal-to-noise Ca2+ probe composed of a single green fluorescent protein. Nat. Biotechnol. 19, 137–141. https://doi.org/10.1038/84397

Nishiyama, J., Yasuda, R., 2015. Biochemical Computation for Spine Structural Plasticity. Neuron 87, 63–75. https://doi.org/10.1016/j.neuron.2015.05.043

Noguchi, A., Ikegaya, Y., Matsumoto, N., 2021. In Vivo Whole-Cell Patch-Clamp Methods: Recent Technical Progress and Future Perspectives. Sensors 21, 1448. https://doi.org/10.3390/s21041448

Noguchi, J., Matsuzaki, M., Ellis-Davies, G.C.R., Kasai, H., 2005. Spine-neck geometry determines NMDA receptor-dependent Ca2+ signaling in dendrites. Neuron 46, 609–622. https://doi.org/10.1016/j.neuron.2005.03.015

Noguchi, J., Nagaoka, A., Hayama, T., Ucar, H., Yagishita, S., Takahashi, N., Kasai, H., 2019. Bidirectional in vivo structural dendritic spine plasticity revealed by two-photon glutamate uncaging in the mouse neocortex. Sci. Rep. 9, 13922. https://doi.org/10.1038/s41598-019-50445-0

Noguchi, J., Nagaoka, A., Watanabe, S., Ellis-Davies, G.C.R., Kitamura, K., Kano, M., Matsuzaki, M., Kasai, H., 2011. In vivo two-photon uncaging of glutamate revealing the structure–function relationships of dendritic spines in the neocortex of adult mice. J. Physiol. 589, 2447–2457. https://doi.org/10.1113/jphysiol.2011.207100

Oertner, T.G., Sabatini, B.L., Nimchinsky, E.A., Svoboda, K., 2002. Facilitation at single synapses probed with optical quantal analysis. Nat. Neurosci. 5, 657–664. https://doi.org/10.1038/nn867

Ogelman, R., Gomez Wulschner, L.E., Hoelscher, V.M., Hwang, I.-W., Chang, V.N., Oh, W.C., 2024. Serotonin modulates excitatory synapse maturation in the developing prefrontal cortex. Nat. Commun. 15, 1368. https://doi.org/10.1038/s41467-024-45734-w

Oh, W.C., Parajuli, L.K., Zito, K., 2015. Heterosynaptic structural plasticity on local dendritic segments of hippocampal CA1 neurons. Cell Rep. 10, 162–169. https://doi.org/10.1016/j.celrep.2014.12.016

Okada, S., Igata, H., Sasaki, T., Ikegaya, Y., 2017. Spatial Representation of Hippocampal Place Cells in a T-Maze with an Aversive Stimulation. Front. Neural Circuits 11.

Okamoto, K.-I., Nagai, T., Miyawaki, A., Hayashi, Y., 2004. Rapid and persistent modulation of actin dynamics regulates postsynaptic reorganization underlying bidirectional plasticity. Nat. Neurosci. 7, 1104–1112. https://doi.org/10.1038/nn1311

O'Keefe, J., Dostrovsky, J., 1971. The hippocampus as a spatial map. Preliminary evidence from unit activity in the freely-moving rat. Brain Res. 34, 171–175.

https://doi.org/10.1016/0006-8993(71)90358-1

O'Keefe, J.M., Nadel, L., O'Keefe, J., 1978. The hippocampus as a cognitive map. Clarendon Press, Oxford.

Olshausen, B.A., Field, D.J., 1996. Emergence of simple-cell receptive field properties by learning a sparse code for natural images. Nature 381, 607–609. https://doi.org/10.1038/381607a0

Ormond, J., O'Keefe, J., 2022. Hippocampal place cells have goal-oriented vector fields during navigation. Nature 607, 741–746. https://doi.org/10.1038/s41586-022-04913-9

Otmakhova, N.A., Lisman, J.E., 1999. Dopamine Selectively Inhibits the Direct Cortical Pathway to the CA1 Hippocampal Region. J. Neurosci. 19, 1437–1445. https://doi.org/10.1523/JNEUROSCI.19-04-01437.1999

Otmakhova, N.A., Lisman, J.E., 1996. D1/D5 Dopamine Receptor Activation Increases the Magnitude of Early Long-Term Potentiation at CA1 Hippocampal Synapses. J. Neurosci. 16, 7478–7486. https://doi.org/10.1523/JNEUROSCI.16-23-07478.1996

Pachitariu, M., Stringer, C., Dipoppa, M., Schröder, S., Rossi, L.F., Dalgleish, H., Carandini, M., Harris, K.D., 2016. Suite2p: beyond 10,000 neurons with standard two-photon microscopy. https://doi.org/10.1101/061507

Palay, S.L., 1956. Synapses in the central nervous system. J. Biophys. Cytol 193–202. https://doi.org/10.1083/jcb.2.4.193

Palmer, A.E., Tsien, R.Y., 2006. Measuring calcium signaling using genetically targetable fluorescent indicators. Nat. Protoc. 1, 1057–1065. https://doi.org/10.1038/nprot.2006.172

Pchitskaya, E., Bezprozvanny, I., 2020. Dendritic Spines Shape Analysis—Classification or Clusterization? Perspective. Front. Synaptic Neurosci. 12.

Perea, G., Navarrete, M., Araque, A., 2009. Tripartite synapses: astrocytes process and control synaptic information. Trends Neurosci. 32, 421–431. https://doi.org/10.1016/j.tins.2009.05.001

Perez-Alvarez, A., Fearey, B.C., O'Toole, R.J., Yang, W., Arganda-Carreras, I., Lamothe-Molina, P.J., Moeyaert, B., Mohr, M.A., Panzera, L.C., Schulze, C., Schreiter, E.R., Wiegert, J.S., Gee, C.E., Hoppa, M.B., Oertner, T.G., 2020a. Freeze-frame imaging of synaptic activity using SynTagMA. Nat. Commun. 11, 2464. https://doi.org/10.1038/s41467-020-16315-4

Perez-Alvarez, A., Yin, S., Schulze, C., Hammer, J.A., Wagner, W., Oertner, T.G., 2020b. Endoplasmic reticulum visits highly active spines and prevents runaway potentiation of synapses. Nat. Commun. 11, 5083. https://doi.org/10.1038/s41467-020-18889-5

Peron, S.P., Freeman, J., Iyer, V., Guo, C., Svoboda, K., 2015. A Cellular Resolution Map of Barrel Cortex Activity during Tactile Behavior. Neuron 86, 783–799. https://doi.org/10.1016/j.neuron.2015.03.027

Peters, A., Kaiserman-Abramof, I.R., 1969. The small pyramidal neuron of the rat cerebral

cortex. Z. Für Zellforsch. Mikrosk. Anat. 100, 487–506. https://doi.org/10.1007/BF00344370

Peters, A.J., Chen, S.X., Komiyama, T., 2014. Emergence of reproducible spatiotemporal activity during motor learning. Nature 510, 263–267. https://doi.org/10.1038/nature13235

Pettit, D.L., Wang, S.S.-H., Gee, K.R., Augustine, G.J., 1997. Chemical Two-Photon Uncaging: a Novel Approach to Mapping Glutamate Receptors. Neuron 19, 465–471. https://doi.org/10.1016/S0896-6273(00)80361-X

Pettit, N.L., Yuan, X.C., Harvey, C.D., 2022. Hippocampal place codes are gated by behavioral engagement. Nat. Neurosci. 25, 561–566. https://doi.org/10.1038/s41593-022-01050-4

Pfeiffer, T., Poll, S., Bancelin, S., Angibaud, J., Inavalli, V.V.G.K., Keppler, K., Mittag, M., Fuhrmann, M., Nägerl, U.V., 2018. Chronic 2P-STED imaging reveals high turnover of dendritic spines in the hippocampus in vivo. eLife 7. https://doi.org/10.7554/eLife.34700

Portera-Cailliau, C., Pan, D.T., Yuste, R., 2003. Activity-Regulated Dynamic Behavior of Early Dendritic Protrusions: Evidence for Different Types of Dendritic Filopodia. J. Neurosci. 23, 7129–7142. https://doi.org/10.1523/JNEUROSCI.23-18-07129.2003

Pronier, É., Morici, J.F., Girardeau, G., 2023. The role of the hippocampus in the consolidation of emotional memories during sleep. Trends Neurosci. 46, 912–925. https://doi.org/10.1016/j.tins.2023.08.003

Qi, G., Yang, D., Ding, C., Feldmeyer, D., 2020. Unveiling the Synaptic Function and Structure Using Paired Recordings From Synaptically Coupled Neurons. Front. Synaptic Neurosci. 12, 5. https://doi.org/10.3389/fnsyn.2020.00005

Ramirez, S., Liu, X., Lin, P.-A., Suh, J., Pignatelli, M., Redondo, R.L., Ryan, T.J., Tonegawa, S., 2013. Creating a False Memory in the Hippocampus. Science 341, 387–391. https://doi.org/10.1126/science.1239073

Robins, A., 2004. Sequential learning in neural networks: A review and a discussion of pseudorehearsal based methods. Intell. Data Anal. 8, 301–322. https://doi.org/10.3233/IDA-2004-8306

Robins, A., Frean, M., 1998. Local Learning Algorithms for Sequential Tasks in Neural Networks. J. Adv. Comput. Intell. Intell. Inform. 2, 221–227. https://doi.org/10.20965/jaciii.1998.p0221

Robinson, N.T.M., Descamps, L.A.L., Russell, L.E., Buchholz, M.O., Bicknell, B.A., Antonov, G.K., Lau, J.Y.N., Nutbrown, R., Schmidt-Hieber, C., Häusser, M., 2020. Targeted Activation of Hippocampal Place Cells Drives Memory-Guided Spatial Behavior. Cell 183. https://doi.org/10.1016/j.cell.2020.09.061

Robles, E., Smith, S.J., Meyer, M.P., 2009. Synaptic Precursors: Filopodia, in: Squire, L.R. (Ed.), Encyclopedia of Neuroscience. Academic Press, Oxford, pp. 779–786. https://doi.org/10.1016/B978-008045046-9.00361-2

Rochefort, N.L., Konnerth, A., 2012. Dendritic spines: from structure to in vivo function. EMBO Rep. 13, 699–708. https://doi.org/10.1038/embor.2012.102

Roelfsema, P.R., Holtmaat, A., 2018. Control of synaptic plasticity in deep cortical networks. Nat. Rev. Neurosci. 19, 166–180. https://doi.org/10.1038/nrn.2018.6

Rolotti, S.V., Ahmed, M.S., Szoboszlay, M., Geiller, T., Negrean, A., Blockus, H., Gonzalez, K.C., Sparks, F.T., Solis Canales, A.S., Tuttman, A.L., Peterka, D.S., Zemelman, B.V., Polleux, F., Losonczy, A., 2022. Local feedback inhibition tightly controls rapid formation of hippocampal place fields. Neuron 110, 783-794.e6. https://doi.org/10.1016/j.neuron.2021.12.003

Rose, T., Goltstein, P.M., Portugues, R., Griesbeck, O., 2014. Putting a finishing touch on GECIs. Front. Mol. Neurosci. 7. https://doi.org/10.3389/fnmol.2014.00088

Rouhani, N., Niv, Y., 2021. Signed and unsigned reward prediction errors dynamically enhance learning and memory. eLife 10, e61077. https://doi.org/10.7554/eLife.61077

Sabatini, B.L., Oertner, T.G., Svoboda, K., 2002. The Life Cycle of Ca2+ Ions in Dendritic Spines. Neuron 33, 439–452. https://doi.org/10.1016/S0896-6273(02)00573-1

Sadeh, S., Clopath, C., 2022. Contribution of behavioural variability to representational drift. eLife 11, e77907. https://doi.org/10.7554/eLife.77907

Scanziani, M., Malenka, R.C., Nicoll, R.A., 1996. Role of intercellular interactions in heterosynaptic long-term depression. Nature 380, 446–450. https://doi.org/10.1038/380446a0

Schikorski, T., Stevens, C.F., 1997. Quantitative Ultrastructural Analysis of Hippocampal Excitatory Synapses. J. Neurosci. 17, 5858–5867. https://doi.org/10.1523/JNEUROSCI.17-15-05858.1997

Schindelin, J., Arganda-Carreras, I., Frise, E., Kaynig, V., Longair, M., Pietzsch, T., Preibisch, S., Rueden, C., Saalfeld, S., Schmid, B., Tinevez, J.-Y., White, D.J., Hartenstein, V., Eliceiri, K., Tomancak, P., Cardona, A., 2012. Fiji: an open-source platform for biological-image analysis. Nat. Methods 9, 676–682. https://doi.org/10.1038/nmeth.2019

Schultz, W., 2007. Behavioral dopamine signals. Trends Neurosci., Fifty years of dopamine research 30, 203–210. https://doi.org/10.1016/j.tins.2007.03.007

Schulz, P., Cook, E., Johnston, D., 1995. Using paired-pulse facilitation to probe the mechanisms for long-term potentiation (LTP). J. Physiol.-Paris 89, 3–9. https://doi.org/10.1016/0928-4257(96)80546-8

Schwartzkroin, P.A., Wester, K., 1975. Long-lasting facilitation of a synaptic potential following tetanization in the in vitro hippocampal slice. Brain Res. 89, 107–119. https://doi.org/10.1016/0006-8993(75)90138-9

Sharkey, N.E., Sharkey, A.J.C., 1995. An Analysis of Catastrophic Interference. Connect. Sci. 7, 301–330. https://doi.org/10.1080/09540099550039264

Shatz, C.J., 1992. The Developing Brain [WWW Document]. Sci. Am. URL

https://www.scientificamerican.com/article/the-developing-brain/ (accessed 2.16.24).

Sheffield, M.E.J., Adoff, M.D., Dombeck, D.A., 2017. Increased Prevalence of Calcium Transients across the Dendritic Arbor during Place Field Formation. Neuron 96, 490-504.e5. https://doi.org/10.1016/j.neuron.2017.09.029

Sheintuch, L., Geva, N., Deitch, D., Rubin, A., Ziv, Y., 2023. Organization of hippocampal CA3 into correlated cell assemblies supports a stable spatial code. Cell Rep. 42, 112119. https://doi.org/10.1016/j.celrep.2023.112119

Shinohara, Y., Hosoya, A., Yahagi, K., Ferecskó, A.S., Yaguchi, K., Sík, A., Itakura, M., Takahashi, M., Hirase, H., 2012. Hippocampal CA3 and CA2 have distinct bilateral innervation patterns to CA1 in rodents. Eur. J. Neurosci. 35, 702–710. https://doi.org/10.1111/j.1460-9568.2012.07993.x

Shipton, O.A., El-Gaby, M., Apergis-Schoute, J., Deisseroth, K., Bannerman, D.M., Paulsen, O., Kohl, M.M., 2014. Left-right dissociation of hippocampal memory processes in mice. Proc. Natl. Acad. Sci. U. S. A. 111, 15238–15243. https://doi.org/10.1073/pnas.1405648111

Simons, S.B., Caruana, D.A., Zhao, M., Dudek, S.M., 2011. Caffeine-induced synaptic potentiation in hippocampal CA2 neurons. Nat. Neurosci. 15, 23–25. https://doi.org/10.1038/nn.2962

Sotres-Bayon, F., Cain, C.K., LeDoux, J.E., 2006. Brain Mechanisms of Fear Extinction: Historical Perspectives on the Contribution of Prefrontal Cortex. Biol. Psychiatry 60, 329–336. https://doi.org/10.1016/j.biopsych.2005.10.012

Speranza, L., di Porzio, U., Viggiano, D., de Donato, A., Volpicelli, F., 2021. Dopamine: The Neuromodulator of Long-Term Synaptic Plasticity, Reward and Movement Control. Cells 10, 735. https://doi.org/10.3390/cells10040735

Squire, L.R., 1987. Memory and brain, Memory and brain. Oxford University Press, New York, NY, US.

Squire, L.R., 1986. Mechanisms of Memory. Science 232, 1612–1619. https://doi.org/10.1126/science.3086978

Stanek, J.K., Dickerson, K.C., Chiew, K.S., Clement, N.J., Adcock, R.A., 2019. Expected Reward Value and Reward Uncertainty Have Temporally Dissociable Effects on Memory Formation. J. Cogn. Neurosci. 31, 1443–1454. https://doi.org/10.1162/jocn_a_01411

Steffens, H., Mott, A.C., Li, S., Wegner, W., Švehla, P., Kan, V.W.Y., Wolf, F., Liebscher, S., Willig, K.I., 2021. Stable but not rigid: Chronic in vivo STED nanoscopy reveals extensive remodeling of spines, indicating multiple drivers of plasticity. Sci. Adv. 7, eabf2806. https://doi.org/10.1126/sciadv.abf2806

Steffens, H., Mott, A.C., Li, S., Wegner, W., Švehla, P., Kan, V.W.Y., Wolf, F., Liebscher, S., Willig, K.I., 2020. Stable but not rigid: Long-term in vivo STED nanoscopy uncovers extensive remodeling of stable spines and indicates multiple drivers of structural plasticity.

bioRxiv 2020.09.21.306902. https://doi.org/10.1101/2020.09.21.306902

Stein, I.S., Zito, K., 2019. Dendritic Spine Elimination: Molecular Mechanisms and Implications. The Neuroscientist 25, 27–47. https://doi.org/10.1177/1073858418769644

Stevens, C.F., Wang, Y., 1994. Changes in reliability of synaptic function as a mechanism for plasticity. Nature 371, 704–707. https://doi.org/10.1038/371704a0

Stringer, C., Wang, T., Michaelos, M., Pachitariu, M., 2021. Cellpose: a generalist algorithm for cellular segmentation. Nat. Methods 18, 100–106. https://doi.org/10.1038/s41592-020-01018-x

Sutton, R.S., Barto, A.G., 1981. Toward a modern theory of adaptive networks: Expectation and prediction. Psychol. Rev. 88, 135–170. https://doi.org/10.1037/0033-295X.88.2.135

Svoboda, K., Tank, D.W., Denk, W., 1996. Direct Measurement of Coupling Between Dendritic Spines and Shafts. Science 272, 716–719. https://doi.org/10.1126/science.272.5262.716

Swanson, L.W., Sawchenko, P.E., Cowan, W.M., 1980. Evidence that the commissural, associational and septal projections of the regio inferior of the hippocampus arise from the same neurons. Brain Res. 197, 207–212. https://doi.org/10.1016/0006-8993(80)90446-1

Szirmai, I., Buzsáki, G., Kamondi, A., 2012. 120 years of hippocampal Schaffer collaterals. Hippocampus 22, 1508–1516. https://doi.org/10.1002/hipo.22001

Takeuchi, T., Duszkiewicz, A.J., Morris, R.G.M., 2014. The synaptic plasticity and memory hypothesis: encoding, storage and persistence. Philos. Trans. R. Soc. B Biol. Sci. 369, 20130288. https://doi.org/10.1098/rstb.2013.0288

Takumi, Y., Ramírez-León, V., Laake, P., Rinvik, E., Ottersen, O., 1999. Different modes of expression of AMPA and NMDA receptors in hippocampal synapses. Nat. Neurosci. 2, 618–24. https://doi.org/10.1038/10172

Teng, E., Squire, L.R., 1999. Memory for places learned long ago is intact after hippocampal damage. Nature 400, 675–677. https://doi.org/10.1038/23276

Thevenaz, P., Ruttimann, U.E., Unser, M., 1998. A pyramid approach to subpixel registration based on intensity. IEEE Trans. Image Process. 7, 27–41. https://doi.org/10.1109/83.650848

Thompson, L.T., Best, P.J., 1990. Long-term stability of the place-field activity of single units recorded from the dorsal hippocampus of freely behaving rats. Brain Res. 509, 299–308. https://doi.org/10.1016/0006-8993(90)90555-p

Tolman, E.C., 1948. Cognitive maps in rats and men. Psychol. Rev. 55, 189–208. https://doi.org/10.1037/h0061626

Trachtenberg, J.T., Chen, B.E., Knott, G.W., Feng, G., Sanes, J.R., Welker, E., Svoboda, K., 2002. Long-term in vivo imaging of experience-dependent synaptic plasticity in adult cortex. Nature 420, 788–794. https://doi.org/10.1038/nature01273

Tsien, J.Z., 2000. Linking Hebb's coincidence-detection to memory formation. Curr. Opin. Neurobiol. 10, 266–273. https://doi.org/10.1016/S0959-4388(00)00070-2

Tzakis, N., Holahan, M.R., 2019. Social Memory and the Role of the Hippocampal CA2 Region. Front. Behav. Neurosci. 13.

Ucar, H., Watanabe, S., Noguchi, J., Morimoto, Y., Iino, Y., Yagishita, S., Takahashi, N., Kasai, H., 2021. Mechanical actions of dendritic-spine enlargement on presynaptic exocytosis. Nature 600, 686–689. https://doi.org/10.1038/s41586-021-04125-7

van Groen, T., Wyss, M., 1988. Species differences in hippocampal commissural connections: Studies in rat, guinea pig, rabbit, and cat. J. Comp. Neurol. 267, 322–334. https://doi.org/10.1002/cne.902670303

Van Harreveld, A., Fifkova, E., 1975. Swelling of dendritic spines in the fascia dentata after stimulation of the perforant fibers as a mechanism of post-tetanic potentiation. Exp. Neurol. 49, 736–749. https://doi.org/10.1016/0014-4886(75)90055-2

Vardalaki, D., Chung, K., Harnett, M.T., 2022. Filopodia are a structural substrate for silent synapses in adult neocortex. Nature 612, 323–327. https://doi.org/10.1038/s41586-022-05483-6

Vicidomini, G., Bianchini, P., Diaspro, A., 2018. STED super-resolved microscopy. Nat. Methods 15, 173–182. https://doi.org/10.1038/nmeth.4593

Virtanen, P., Gommers, R., Oliphant, T.E., Haberland, M., Reddy, T., Cournapeau, D., Burovski, E., Peterson, P., Weckesser, W., Bright, J., van der Walt, S.J., Brett, M., Wilson, J., Millman, K.J., Mayorov, N., Nelson, A.R.J., Jones, E., Kern, R., Larson, E., Carey, C.J., Polat, İ., Feng, Y., Moore, E.W., VanderPlas, J., Laxalde, D., Perktold, J., Cimrman, R., Henriksen, I., Quintero, E.A., Harris, C.R., Archibald, A.M., Ribeiro, A.H., Pedregosa, F., van Mulbregt, P., 2020. SciPy 1.0: fundamental algorithms for scientific computing in Python. Nat. Methods 17, 261–272. https://doi.org/10.1038/s41592-019-0686-2

Wang, H.C., LeMessurier, A.M., Feldman, D.E., 2022. Tuning instability of non-columnar neurons in the salt-and-pepper whisker map in somatosensory cortex. Nat. Commun. 13, 6611. https://doi.org/10.1038/s41467-022-34261-1

Wang, X., Naud, R., 2022. Overwriting the past with supervised plasticity. eLife 11, e76320. https://doi.org/10.7554/eLife.76320

Waters, J., Schaefer, A., Sakmann, B., 2005. Backpropagating action potentials in neurones: measurement, mechanisms and potential functions. Prog. Biophys. Mol. Biol., Biophysics of Excitable Tissues 87, 145–170. https://doi.org/10.1016/j.pbiomolbio.2004.06.009

Wei, Z., Lin, B.-J., Chen, T.-W., Daie, K., Svoboda, K., Druckmann, S., 2020. A comparison of neuronal population dynamics measured with calcium imaging and electrophysiology. PLoS Comput. Biol. 16, e1008198. https://doi.org/10.1371/journal.pcbi.1008198

Wheal, H.V., Lancaster, B., Bliss, T.V.P., 1983. Long-term potentiation in Schaffer collateral

and commissural systems of the hippocampus: In vitro study in rats pretreated with kainic acid. Brain Res. 272, 247–253. https://doi.org/10.1016/0006-8993(83)90570-X

Whitlock, J.R., Heynen, A.J., Shuler, M.G., Bear, M.F., 2006. Learning Induces Long-Term Potentiation in the Hippocampus. Science 313, 1093–1097. https://doi.org/10.1126/science.1128134

Wiegert, J.S., Oertner, T.G., 2013. Long-Term depression triggers the selective elimination of weakly integrated synapses. Proc. Natl. Acad. Sci. U. S. A. 110. https://doi.org/10.1073/pnas.1315926110

Wiegert, J.S., Pulin, M., Gee, C.E., Oertner, T.G., 2018. The fate of hippocampal synapses depends on the sequence of plasticity-inducing events. eLife 7, 1–18. https://doi.org/10.7554/eLife.39151

Williams, S.R., Stuart, G.J., 2003. Role of dendritic synapse location in the control of action potential output. Trends Neurosci. 26, 147–154. https://doi.org/10.1016/S0166-2236(03)00035-3

Wilson, M.A., McNaughton, B.L., 1993. Dynamics of the hippocampal ensemble code for space. Science 261, 1055–1058. https://doi.org/10.1126/science.8351520

Wu, Y., Whiteus, C., Xu, C.S., Hayworth, K.J., Weinberg, R.J., Hess, H.F., De Camilli, P., 2017. Contacts between the endoplasmic reticulum and other membranes in neurons. Proc. Natl. Acad. Sci. U. S. A. 114, E4859–E4867. https://doi.org/10.1073/pnas.1701078114

Xu, T., Yu, X., Perlik, A.J., Tobin, W.F., Zweig, J.A., Tennant, K., Jones, T., Zuo, Y., 2009. Rapid formation and selective stabilization of synapses for enduring motor memories. Nature 462, 915–919. https://doi.org/10.1038/nature08389

Yaeger, C.E., Vardalaki, D., Zhang, Q., Pham, T.L.D., Brown, N.J., Ji, N., Harnett, M.T., 2022. A dendritic mechanism for balancing synaptic flexibility and stability (preprint). Neuroscience. https://doi.org/10.1101/2022.02.02.478840

Yamamoto, C., Matsumoto, K., Takagi, M., 1980. Potentiation of excitatory postsynaptic potentials during and after repetitive stimulation in thin hippocampal sections. Exp. Brain Res. 38, 469–477. https://doi.org/10.1007/BF00237528

Yang, G., Pan, F., Gan, W.-B., 2009. Stably maintained dendritic spines are associated with lifelong memories. Nature 462, 920–924. https://doi.org/10.1038/nature08577

Yang, W., Chini, M., Pöpplau, J.A., Formozov, A., Dieter, A., Piechocinski, P., Rais, C., Morellini, F., Sporns, O., Hanganu-Opatz, I.L., Wiegert, J.S., 2021. Anesthetics fragment hippocampal network activity, alter spine dynamics, and affect memory consolidation. PLOS Biol. 19, e3001146. https://doi.org/10.1371/journal.pbio.3001146

Yang, Y., Wang, X., Frerking, M., Zhou, Q., 2008. Spine Expansion and Stabilization Associated with Long-Term Potentiation. J. Neurosci. 28, 5740–5751. https://doi.org/10.1523/JNEUROSCI.3998-07.2008

Yasuda, R., Hayashi, Y., Hell, J.W., 2022. CaMKII: a central molecular organizer of synaptic plasticity, learning and memory. Nat. Rev. Neurosci. 23, 666–682. https://doi.org/10.1038/s41583-022-00624-2

Yu, X., Zuo, Y., 2011. Spine Plasticity in the Motor Cortex. Curr. Opin. Neurobiol. 21, 169–174. https://doi.org/10.1016/j.conb.2010.07.010

Yuste, R., 2015. The discovery of dendritic spines by Cajal. Front. Neuroanat. 9.

Yuste, R., Denk, W., 1995. Dendritic spines as basic functional units of neuronal integration. Nature 375, 682–684. https://doi.org/10.1038/375682a0

Yuste, R., Majewska, A., Cash, S.S., Denk, W., 1999. Mechanisms of Calcium Influx into Hippocampal Spines: Heterogeneity among Spines, Coincidence Detection by NMDA Receptors, and Optical Quantal Analysis. J. Neurosci. 19, 1976–1987. https://doi.org/10.1523/JNEUROSCI.19-06-01976.1999

Yuste, R., Majewska, A., Holthoff, K., 2000. From form to function: calcium compartmentalization in dendritic spines. Nat. Neurosci. 3, 653–659. https://doi.org/10.1038/76609

Zemla, R., Moore, J.J., Hopkins, M.D., Basu, J., 2022. Task-selective place cells show behaviorally driven dynamics during learning and stability during memory recall. Cell Rep. 41, 111700. https://doi.org/10.1016/j.celrep.2022.111700

Zhang, Haorui, Ben Zablah, Y., Zhang, Haiwang, Jia, Z., 2021. Rho Signaling in Synaptic Plasticity, Memory, and Brain Disorders. Front. Cell Dev. Biol. 9, 729076. https://doi.org/10.3389/fcell.2021.729076

Zhang, K., Ginzburg, I., McNaughton, B.L., Sejnowski, T.J., 1998. Interpreting neuronal population activity by reconstruction: unified framework with application to hippocampal place cells. J. Neurophysiol. 79, 1017–1044. https://doi.org/10.1152/jn.1998.79.2.1017

Zhang, Y., Cudmore, R.H., Lin, D.-T., Linden, D.J., Huganir, R.L., 2015. Visualization of NMDA receptor-dependent AMPA receptor synaptic plasticity in vivo. Nat. Neurosci. 18, 402–407. https://doi.org/10.1038/nn.3936

Zhang, Y., Rózsa, M., Liang, Y., Bushey, D., Wei, Z., Zheng, J., Reep, D., Broussard, G.J., Tsang, A., Tsegaye, G., Narayan, S., Obara, C.J., Lim, J.-X., Patel, R., Zhang, R., Ahrens, M.B., Turner, G.C., Wang, S.S.-H., Korff, W.L., Schreiter, E.R., Svoboda, K., Hasseman, J.P., Kolb, I., Looger, L.L., 2023. Fast and sensitive GCaMP calcium indicators for imaging neural populations. Nature 615, 884–891. https://doi.org/10.1038/s41586-023-05828-9

Zhou, Q., Homma, K.J., Poo, M.M., 2004. Shrinkage of dendritic spines associated with long-term depression of hippocampal synapses. Neuron 44, 749–757. https://doi.org/10.1016/j.neuron.2004.11.011

Zipfel, W.R., Williams, R.M., Webb, W.W., 2003. Nonlinear magic: multiphoton microscopy in the biosciences. Nat. Biotechnol. 21, 1369–1377. https://doi.org/10.1038/nbt899

Ziv, Y., Burns, L.D., Cocker, E.D., Hamel, E.O., Ghosh, K.K., Kitch, L.J., Gamal, A.E., Schnitzer, M.J., 2013. Long-term dynamics of CA1 hippocampal place codes. Nat. Neurosci. 16, 264–266. https://doi.org/10.1038/nn.3329

Zuo, Y., Lin, A., Chang, P., Gan, W.-B., 2005. Development of Long-Term Dendritic Spine Stability in Diverse Regions of Cerebral Cortex. Neuron 46, 181–189. https://doi.org/10.1016/j.neuron.2005.04.001

Appendix

1. Abbreviations

AMPA	α-amino-3-hydroxy-5-methyl-4-isoxazolepropionic acid
B	Basal Nucleus
BAPTA	1, 2-bis(o-amino-phenoxy)-ethane-N, N, N'N'-tetra-acetic acid
BTSP	Behavioral Timescale Synaptic Plasticity
CA	Cornu Ammoni
CaMKII	Calcium-calmodulin-dependent protein kinase II
CASK	CAlcium/calmodulin-dependent Serine Kinase
CE	Central Nucleus
clCA3	Contralateral CA3
CNS	Central Nervous System
CV	Coated Vesicle
DG	Dentate gyrus
EC	Entorhinal cortex
EGTA	Ethylene Glycol Tetra-acetic Acid
EPSCaT	Excitatory Postsynaptic CAlcium Transient
F-actin	Filamentous actin
FOV	Field Of View
GECI	Genetically Encoded Calcium Indicator
GFP	Green Fluorescent Protein
GKAP	Guanylate-Kinase-Associated Protein
GRIP	Glutamate-Receptor-Interacting Protein
IA	Inhibitory Avoidance task
ICM	Intercalated Cell Masses
iGluR	Ionotropic glutamatergic receptor
ilCA1	Ipsilateral CA1
IP_3R	inositol-1,4,5triphosphate receptor
Kali-7	Kalirin-7

LA	Lateral AmygDALA
LTD	Long-Term Depression
LTP	Long-Term Potentiation
MAD	Median Absolute Deviation
mGluR	Metabotropic glutamatergic receptor
MMF	Midazolam, Medetomidine and Fentanyl
NMDA	N-Methyl-D-Aspartate
PFA	Paraformaldehyde
PMCA	Plasma Membrane Calcium ATPase
PSD	PostSynaptic Densities
ROI	Region of interest
RyR	RYanodine-Receptor
SER	Smooth Endoplasmic Reticulum
SERCA	Smooth ER Calcium ATPase
sLTP	Structural Long-Term Potentiation
SPAR	SPine-Associated RapGAP
SST	Somatostatin
STED	STimulated-Emission Depletion
V1	Primary visual area
VSCC	Voltage-Sensitive Calcium Channel
VTA	Ventral Tegmental Area
YFP	Yellow Fluorescent Protein

2. Curriculum vitae

RAIS Cynthia
France
28 years-old
Woman

Education

2019-2024	**PhD in Neuroscience** RG Synaptic Wiring and Information Processing, Center for Molecular Neuroscience, Universitätsklinikum Hamburg-Eppendorf Supervised by J. Simon Wiegert
2016-2018	**Euromediterranean Master of Neuroscience (EMN-Online)** Université de Bordeaux, Bordeaux, France *Semester 1 & 2 : Courses of Cellular Neurobiology, Pharmacology, Bioinformatics*
2015-2016	**Licence 3 of Molecular, Cellular Biology and Physiology** Université de Bordeaux, Bordeaux, France *Courses of cellular neurobiology*
2013-2015	**Classe préparatoire of Biology, Chemistry, Physics and Geology** Lycée Michel de Montaigne, Bordeaux, France *Courses of maths and informatics, biology, physics and chemistry*
2010-2013	**Scientific Baccalaureate with mention Assez Bien** Lycée Nord Bassin, Andernos-les-Bains, France

Professional experience

May-June 2017	**Internship at IMN Mnemosyne** Bordeaux, France *Replication of the article « A euro-computational model of economic decisions » written by Rustichini and Padoa-Schioppa* Supervised by Fabien Benureau and Nicolas Rougier
January-July 2018	**Internship at Institut Pasteur** Paris, France *Role of autoantibodies against nicotinic receptor in the pathology* Supervised by Uwe Maskos

Publications

• Yang W, Chini M, Pöpplau JA, Formozov A, Dieter A, Piechocinski P, **Rais C**, Morellini F, Sporns O, Hanganu-Opatz IL, Wiegert JS (2021). Anesthetics fragment hippocampal network activity, alter spine dynamics, and affect memory consolidation. PLOS Biology 19(4): e3001146

• [Re] « A neuro-computational model of economic decisions », **Rais Cynthia** and Benureau Fabien C. Y., Bordeaux, France - ReScience (*In preparation*)

Attended Conferences

2017	Bordeaux Neurocampus Day
2017	Symposium of Biology of Decision Making
2017	NeuroFrance
2017	Symposium for Neuroscience students of Bordeaux
	Poster presentation
2018	Internal symposium of the Neuroscience Department of the Pasteur Institute of Paris
	Poster presentation
2022	FENS
	Poster presentation
2023	Cosyne
	Poster presentation
2023	Göttingen Meeting of the German Neuroscience Society
	Poster presentation

Formations

• Regulatory course on experimental animals for Designers in rodents and lagomorphs, in France
• Regulatory course for surgery, in France

3. Acknowledgments

Despite the distance separating us, I want to thank my oldest friends, Marie and Baptiste, for taking me on holidays to such beautiful places. I could really forget everything, relax and just follow the plans Marie made for us while listening to the vibrant life of Baptiste. I am looking forward for the next fun trips with you two. I also want to thank Marine, Clémence and Stéphanie for their support over the years.

I also want to thank Dr. Mélody. For a very unknown reason, we made friends. And for an even more obscure reason in my mind, suddenly, we just went on a week-end together. I am glad I can have you as my friend. I am looking forward to the next adventures we will have together.

Finally, I want to express my gratitude to my parents, Régine and Serge, and my sister, Laëtitia, that accepted my choice to live abroad on my own, even if I easily forget everything. Although with complaints, thanks for accepting that most of my time was devoted to work.

4. Eidesstattliche Versicherung

Ich versichere ausdrücklich, dass ich die Arbeit selbständig und ohne fremde Hilfe verfasst, andere als die von mir angegebenen Quellen und Hilfsmittel nicht benutzt und die aus den benutzten Werken wörtlich oder inhaltlich entnommenen Stellen einzeln nach Ausgabe (Auflage und Jahr des Erscheinens), Band und Seite des benutzten Werkes kenntlich gemacht habe.

Ferner versichere ich, dass ich die Dissertation bisher nicht einem Fachvertreter an einer anderen Hochschule zur Überprüfung vorgelegt oder mich anderweitig um Zulassung zur Promotion beworben habe.

Ich erkläre mich einverstanden, dass meine Dissertation vom Dekanat der Medizinischen Fakultät mit einer gängigen Software zur Erkennung von Plagiaten überprüft werden kann.

Unterschrift: ....